The Pennsylvania State University
APPLIED RESEARCH LABORATORY
P.O. Box 30
State College, PA 16804

THERMO-MECHANICAL FATIGUE OF POLYMER MATRIX COMPOSITES

by

L. H. Strait

Technical Report No. TR 94-12
October 1994

Supported by:
Space and Naval Warfare Systems Command

L.R. Hettche, Director
Applied Research Laboratory

Approved for public release; distribution unlimited

REPORT DOCUMENTATION PAGE

OMB No. 0704-0188

1. AGENCY USE ONLY (Leave blank)	2. REPORT DATE	3. REPORT TYPE AND DATES COVERED
	October 1994	

4. TITLE AND SUBTITLE

THERMO-MECHANICAL FATIGUE OF POLYMER MATRIX COMPOSITES

5. FUNDING NUMBERS

N00039-92-C-0100

6. AUTHOR(S)

L. H. Strait

7. PERFORMING ORGANIZATION NAME(S) AND ADDRESS(ES)

Applied Research Laboratory
The Pennsylvania State University
P. O. Box 30
State College, PA 16804

8. PERFORMING ORGANIZATION REPORT NUMBER

TR# 94-12

9. SPONSORING/MONITORING AGENCY NAME(S) AND ADDRESS(ES)

Space and Naval Warfare Systems Command
2451 Crystal Drive
Arlington, VA 22245-5200

10. SPONSORING/MONITORING AGENCY REPORT NUMBER

11. SUPPLEMENTARY NOTES

12a. DISTRIBUTION/AVAILABILITY STATEMENT

12b. DISTRIBUTION CODE

13. ABSTRACT *(Maximum 200 words)*

Thermo-mechanical fatigue occurs when a component is exposed to thermal cycling under mechanical constraint and/or superimposed mechanical loading. Thermo-mechanical loading is an increasingly common service condition for polymer matrix composite materials. Unfortunately, little or no information is available regarding the behavior of polymer composites subject to this loading condition. The present thesis research program was undertaken to evaluate the effects of mechanical constraint on the response of polymer matrix composites during thermal cycling. Analytical and experimental techniques were used to characterize the response of carbon fiber reinforced cyanate ester (IM6/BT3008) and bismaleimide (IM7/5240-4) composites. Cross-ply laminates were subjected to thermal cycles from 24 to 177°C in the unconstrained, fully-constrained and over-constrained conditions. Laminate response, damage mechanisms and residual compressive properties were characterized for each material and degree of constraint.

Predicted ply stress distributions are significantly different for the various degrees of constraint and are highly sensitive to temperature-dependent lamina properties and laminate stress free temperature. Predictions of laminate response correlate well with experimental results. Deviations are apparent at elevated temperature which are attributed to the effects of time-dependent deformation.

14. SUBJECT TERMS	15. NUMBER OF PAGES
thermo-mechanical fatigue, polymer matrix composites, carbon fiber, cyanate ester, bismaleimide	118
	16. PRICE CODE

17. SECURITY CLASSIFICATION OF REPORT	18. SECURITY CLASSIFICATION OF THIS PAGE	19. SECURITY CLASSIFICATION OF ABSTRACT	20. LIMITATION OF ABSTRACT
UNCLASSIFIED	UNCLASSIFIED	UNCLASSIFIED	UNLIMITED

Changes in laminate response are observed during thermal cycling of IM6/BT3008 in the unconstrained and fully-constrained conditions. The changes are attributed to time-dependent deformation in the 90° plies which leads to changes in the ply stress distribution and ultimately to transverse microcracking. Microcracking initiates more rapidly for fully-constrained laminates due to higher 90° ply stresses which result in more time-dependent deformation per cycle. With continued cycling, microcrack densities appear to converge and become equivalent after 1000 cycles. The ply stress distribution in over-constrained laminates is substantially different from those in unconstrained and fully-constrained laminates. Time-dependent deformation in the 90°s plies results in changes in the ply stress distribution but does not significantly alter the laminate response. The microcrack density in over-constrained laminates is equivalent to that in unconstrained and fully-constrained laminates after 1000 cycles. However, extensive fiber/matrix debonding is observed in the over-constrained laminates. This additional damage is accompanied by a small but significant reduction in comprehensive strength.

IM7/5250-4 laminates are unaffected by 1000 thermal cycles in the unconstrained and fully-constrained conditions. A small amount of transverse ply microcracking is observed after 1000 thermal cycles in the over-constrained condition. This damage does not result in a significant reduction in compressive strength. The superior performance of IM7/5250-4 is attributed to the higher glass transition temperature of the bismaleimide resin.

The results of this research indicate that the level of constraint can have a significant effect on the response of polymer matrix composites during thermal cycling. Longer term testing is required to determine if the observed changes in response will ultimately affect the final failure mode and fatigue endurance of the materials.

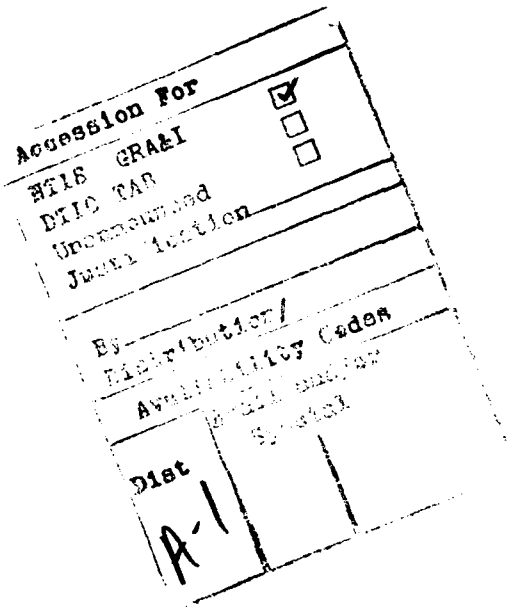

ABSTRACT

Thermo-mechanical fatigue occurs when a component is exposed to thermal cycling under mechanical constraint and/or superimposed mechanical loading. Thermo-mechanical loading is an increasingly common service condition for polymer matrix composite materials. Unfortunately, little or no information is available regarding the behavior of polymer composites subject to this loading condition. The present thesis research program was undertaken to evaluate the effects of mechanical constraint on the response of polymer matrix composites during thermal cycling. Analytical and experimental techniques were used to characterize the response of carbon fiber reinforced cyanate ester (IM6/BT3008) and bismaleimide (IM7/5250-4) composites. Cross-ply laminates were subjected to thermal cycles from 24 to 177 °C in the unconstrained, fully-constrained and over-constrained conditions. Laminate response, damage mechanisms and residual compressive properties were characterized for each material and degree of constraint.

Predicted ply stress distributions are significantly different for the various degrees of constraint and are highly sensitive to temperature-dependent lamina properties and laminate stress free temperature. Predictions of laminate response correlate well with experimental results. Deviations are apparent at elevated temperature which are attributed to the effects of time-dependent deformation.

Changes in laminate response are observed during thermal cycling of IM6/BT3008 in the unconstrained and fully-constrained conditions. The changes are attributed to time-dependent deformation in the 90° plies which leads to changes in the ply stress distribution and ultimately to transverse microcracking. Microcracking initiates more rapidly for fully-constrained laminates due to higher 90° ply stresses which result in more time-dependent deformation per cycle. With continued cycling, microcrack densities appear to converge and become equivalent after 1000 cycles. The ply stress distribution in over-constrained laminates is substantially different from those in unconstrained and fully-constrained laminates. Time-

dependent deformation in the 90° plies results in changes in the ply stress distribution but does not significantly alter the laminate response. The microcrack density in over-constrained laminates is equivalent to that in unconstrained and fully-constrained laminates after 1000 cycles. However, extensive fiber/matrix debonding is observed in the over-constrained laminates. This additional damage is accompanied by a small but significant reduction in compressive strength.

IM7/5250-4 laminates are unaffected by 1000 thermal cycles in the unconstrained and fully-constrained conditions. A small amount of transverse ply microcracking is observed after 1000 thermal cycles in the over-constrained condition. This damage does not result in a significant reduction in compressive strength. The superior performance of IM7/5250-4 is attributed to the higher glass transition temperature of the bismaleimide resin.

The results of this research indicate that the level of constraint can have a significant effect on the response of polymer matrix composites during thermal cycling. Longer term testing is required to determine if the observed changes in response will ultimately affect the final failure mode and fatigue endurance of the materials.

TABLE OF CONTENTS

LIST OF FIGURES

LIST OF TABLES

1.0 INTRODUCTION

Thermo-mechanical fatigue occurs when a structural component is subjected to thermal cycling under mechanical constraint and/or superimposed mechanical loading. Structural components subject to thermo-mechanical loading include aircraft engine components and support structure, heat exchangers, piping, etc. Traditionally, such components have been fabricated from metals or metal alloys and the behavior of these materials under thermo-mechanical loading has been extensively investigated. However, the performance requirements for the next generation of military and commercial aircraft can only be satisfied if substantial reductions in weight are realized. One means of achieving these reductions is through the use of fiber reinforced polymer composites utilizing high temperature matrix materials such as cyanate ester, bismaleimide and polyimide resins. Considerable work has been performed to characterize the effects of temperature on the physical and mechanical properties of these materials and the effects of unconstrained thermal cycling have been documented in the literature. Unfortunately, little or no information is currently available regarding the effects of thermo-mechanical fatigue, i.e. constrained thermal cycling, on polymer matrix composites. The present thesis research program examines the effects of mechanical constraint on the behavior of carbon fiber reinforced cyanate ester (triazine) and bismaleimide composites subjected to thermal cycling.

For organizational purposes, the thesis is divided into 8 chapters. Chapter 1 provides a brief introduction and describes the organization of the document. Chapter 2 presents background information which forms the basis for the research. Included in Chapter 2 is information regarding the structure, properties and processing characteristics of cyanate ester (triazine) resins as well as information regarding thermal and thermo-mechanical loading of

polymer composite materials. The specific objectives of the research and original contributions of the work are outlined in Chapter 3. Complete descriptions of the fibers, resins and prepreg materials included in this study are provided in Chapter 4, along with information on the processing of composite laminates and characterization of laminate physical/mechanical properties. Chapter 5 describes the development of a computer code for predicting laminate response under thermal and thermo-mechanical loading. Ply stress predictions are compared for unconstrained, fully-constrained and over-constrained laminates exposed to thermal cycles from ambient to elevated temperature. Thermal and thermo-mechanical fatigue testing procedures and test results are given in Chapter 6. The results of the tests are compared with the analytical predictions. A summary and conclusions are presented in Chapter 7 and plans for future work are outlined in Chapter 8.

2.0 BACKGROUND

Little or no information is currently available in the literature regarding the effects of thermo-mechanical fatigue on polymer matrix composites. However, the literature does contain related information which forms the basis for the current research program. This background information has been divided into two sections. The first section is concerned with the structure, properties, and processing characteristics of cyanate ester resins relative to the more common epoxy and bismaleimide systems. A cyanate ester-based resin is utilized in the present study. The second section describes thermal and thermo-mechanical loading in general and reviews the information available in the literature regarding unconstrained thermal cycling of polymer matrix composites. Based on this information, potential effects of constrained thermal cycling are discussed.

2.1 CYANATE ESTER RESINS

During the past decade, cyanate ester resins have seen considerable use in printed circuit boards for high-speed computers [1] and as curing agents for epoxy resins [2]. These materials are now making the transition into high performance aerospace applications such as radomes and high-gain antennas [1,3] as well as primary and secondary aircraft/spacecraft structures [1]. Cyanate ester resins exhibit glass transition temperatures in the 190 to 290 °C range which places them between epoxy and bismaleimide systems [1-5]. Asymmetrically structured cyanate ester monomers are available which exhibit viscosities sufficiently low for resin transfer molding and wet filament winding [1,4-5]. Cyanate ester resins generally exhibit higher inherent toughness, lower moisture absorption, and lower dielectric loss than either epoxy or BMI resins [1-5].

2.1.1 Structure and Reactivity

Cyanate esters are bisphenol derivatives of the addition polymerization type which contain the functional group -O-C≡N [1,4-5]. On heating to an appropriate temperature, cyanate esters undergo a cyclotrimerization to form a three-dimensional network containing alternating triazine rings and bisphenol units connected by oxygen atoms (polycyanurate). An example is given in Figure 1 for a cyanate ester resin based on bisphenol-A-dicyanate.

Dicyanate monomers are prepared by reaction of bisphenols with cyanogen chloride in the presence of an HCl acceptor [4]. Because the monomers are derivatives of cyanic acid rather than hydrogen cyanide, they exhibit low toxicity and mutagenicity [2,4]. Cyanate ester prepolymers/polymers exhibit similar characteristics as no secondary reaction products are formed in the cyclotrimerization (addition-type reaction).

Uncatalyzed trimerization rates for commercial dicyanates are very slow (i.e. 90% conversion after 30 hours at 200 °C) owing to their dependence on active hydrogen impurities [4]. Catalysts consisting of coordination metals (i.e. copper) dissolved in nonvolatile hydroxyl compounds (i.e. alkylphenols) are often utilized to reduce the time/temperature required for achieving a satisfactory degree of conversion (i.e. 85%) [4]. Epoxy resins may also be added to dicyanate monomer or prepolymer to reduce the cure time/temperature. Cure temperatures for commercial cyanate ester resin formulations are generally in the 120 to 175 °C range [1-5]. An interesting characteristic of cyanate ester resins is the continued formation of triazine rings at 85-99 percent of final cure [1]. This is not observed in epoxy systems where the polymerization mechanism is ring opening and crosslinking or in bismaleimide systems where aromatic rings are present in the prepolymer but do not form during cure [1,4,6]. In order to ensure full conversion to aromaticity in cyanate ester resins, a free standing postcure at 225 to 250 °C is generally employed [1-5].

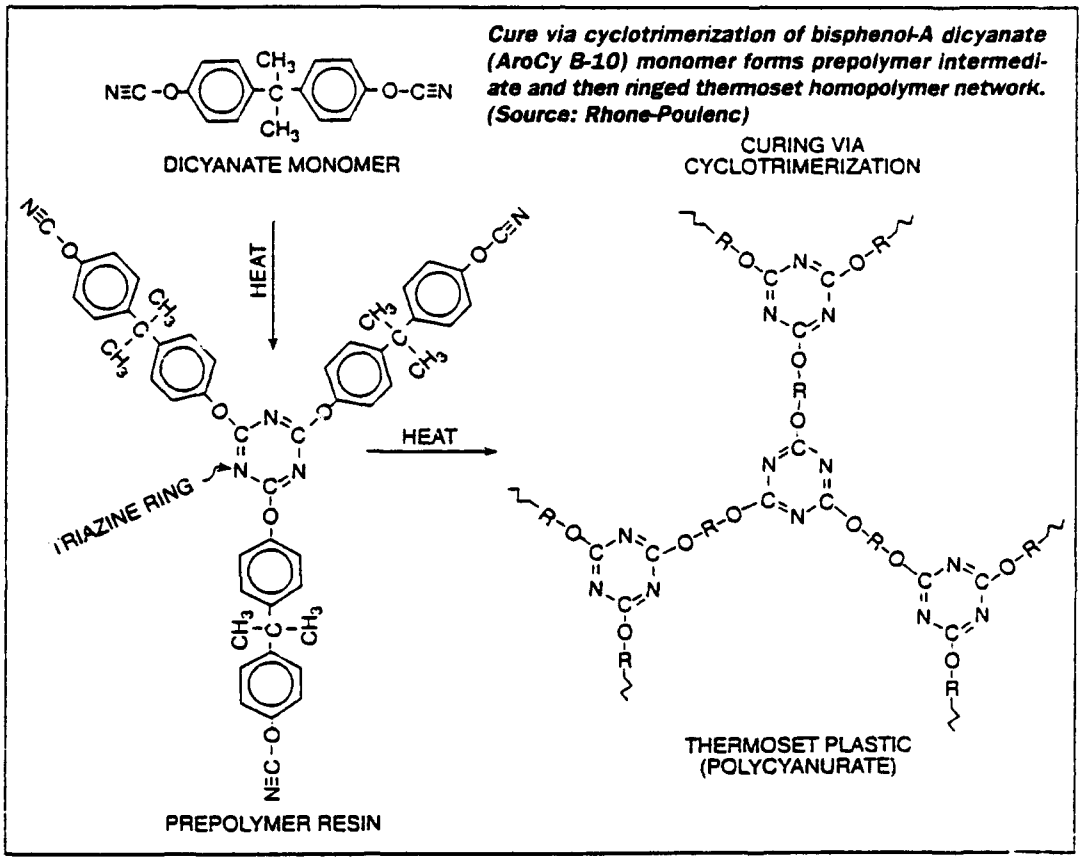

Figure 1. Cyclotrimerization of cyanate ester resin based on bisphenol-A-dicyanate [1].

2.1.2 Structure/Property Relationships

In cyanate ester monomer and prepolymer, the flexibility of the -O- linkages and absence of strong dipoles lead to low viscosity and good flow characteristics [1,4-5]. Low cure temperatures (120 to 175 °C) and moderate to large increases in free volume following gelation result in cure shrinkage of less than 1 percent and low levels of residual stress [1,4-5]. The high density of sterically hindered benzene and triazine rings in cyanate ester networks results in high glass transition temperatures [1,3-5]. Typical values are in the 190 to 290 °C range. The flexible -O- linkages assist in the dissipation of localized residual stresses and contribute to the inherent toughness of the cured resin [1,4-5]. The absence of strong dipoles results in low dielectric constants (2.6-3.1 at 1 MHz and 25 °C) and low moisture uptake (0.6-2.5 wt% for immersion at 100 °C) relative to epoxy and bismaleimide resins [1,3-5].

Neat resin property data have been reported for a cyanate ester resin based on bisphenol-A-dicyanate (CE) relative to a tetrafunctional epoxy (TGMDA/DDS-Epoxy), a methylene dianiline toughened bismaleimide (MDA-BMI) and a o,o'-diallylbisphenol-A toughened bismaleimide (DAB-BMI) [4]. These data are summarized in Table 1. The flexural strength of the CE is equivalent to that of the DAB-BMI and significantly greater (80-130%) than those of the MDA-BMI and TGMDA/DDS-Epoxy. The flexural modulus of the CE is approximately 15% lower than those of the other systems. The flexural strain to failure, Izod impact strength, and critical strain energy release rate (G_{IC}) are significantly higher for the CE relative to the other systems.

Tensile, compressive, and interlaminar shear strength data have been reported for epoxy, cyanate ester (CE), and bismaleimide (BMI) laminates reinforced with E-glass fabric (7781 style weave) [3]. These data are summarized in Table 2. The tensile strength of the CE laminate is 10-20% lower than those of the epoxy and BMI laminates at room temperature. The compressive strength of the CE laminate is 13% higher than that of the

Table 1. Neat resin properties of cyanate ester, epoxy and bismaleimide resins [4].

Property	CE[1]	TGMDA/DDS-Epoxy[2]	MDA-BMI[3]	DAB-BMI[4]
Flexural Strength [MPa]	174	96.5	75.2	176
Flexural Modulus [GPa]	3.1	3.8	3.4	3.7
Flexural Strain to Failure [%]	7.7	2.5	2.2	5.1
Izod Impact [N-m/cm]	0.37	0.21	0.16	0.27
G_{IC} [N-m/cm]	0.036	0.018	0.018	0.022

[1]Cyanate ester based on bisphenol-A-dicyanate.
[2]Tetrafunctional epoxy.
[3]Methylene dianiline toughened bismaleimide.
[4]O,o'-diallylbisphenol-A toughened bismaleimide.

Table 2. Properties of E-glass (7781 style weave) reinforced laminates in warp direction [3].

Property	Temperature [°C]	CE[1]	Epoxy[2]	BMI[3]
Tensile Strength [MPa]	23	358	400	441
	93	---	310	---
	175	324	---	420
Compression Strength [MPa]	23	490	434	579
	93	---	331	---
	175	372	---	---
	232	379	---	393
SBS Strength [MPa]	23	56	55	72
	175	48	--	65

[1]BASF 5575-2 cyanate ester.
[2]Unspecified epoxy.
[3]Unspecified bismaleimide.

epoxy laminate but 15% lower than that of the BMI laminate at room temperature. However, the compressive strengths of the CE and BMI laminates are similar at 232 °C. The interlaminar shear strength of the CE laminate is equivalent to that of the epoxy laminate but 22% lower than that of the BMI laminate at room temperature. At 175 °C, the interlaminar shear strength of the CE laminate is 26% lower than that of the BMI laminate. The epoxy laminate has no appreciable interlaminar shear strength at this temperature.

2.1.3 Cyanate Ester/Bismaleimide Resin Blends

Cyanate ester (CE) resins can be blended with bismaleimide (BMI) resins [8]. Polymerization of CE/BMI resins takes place by: (1) formation of triazine rings by cyclotrimerization of -O-C≡N groups, (2) formation of BMI networks by addition polymerization of maleimide double bonds, and (3) formation of triazine-imidazole rings [8-10]. Epoxy modifiers may also be added to CE/BMI formulations leading to the formation of oxazole rings [2,4,8]. Examples of these individual reactions are given in Figure 2. A reactivity model for a CE/BMI resin based on bisphenol-A-dicyanate and 4,4'-bismaleimidodiphenylmethane (no epoxy modifier) is given in Figure 3.

CE/BMI resins generally exhibit improved processability, toughness, and moisture resistance relative to BMI homopolymers [1-5,7-11]. Moderate reductions in elevated temperature performance are also observed. The improved processability is a result of the lower viscosities and cure temperatures of CE resins relative to BMI resins. The improved toughness and reduced temperature performance are attributed to the flexible -O- linkages in CE/BMI networks compared to BMI networks. The increased moisture resistance is a result of the decrease in polar C=O groups in CE/BMI blends relative to BMI homopolymers.

The limited data available in the literature regarding the mechanical properties of structural composites based on CE/BMI resins indicate that mechanical properties and

Formation of triazine rings by cyclotrimerization of -O-C≡N groups:

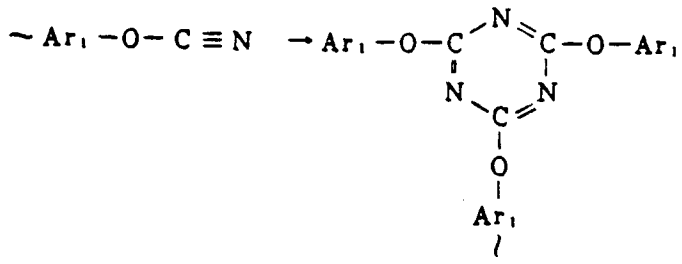

Formation of bismaleimide networks by addition polymerization of maleimide double bonds:

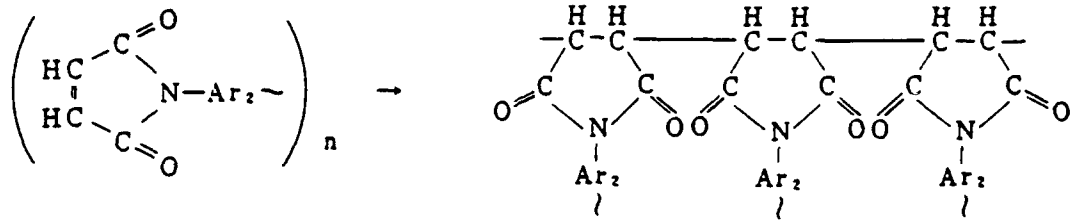

Formation of triazine-imidazole rings:

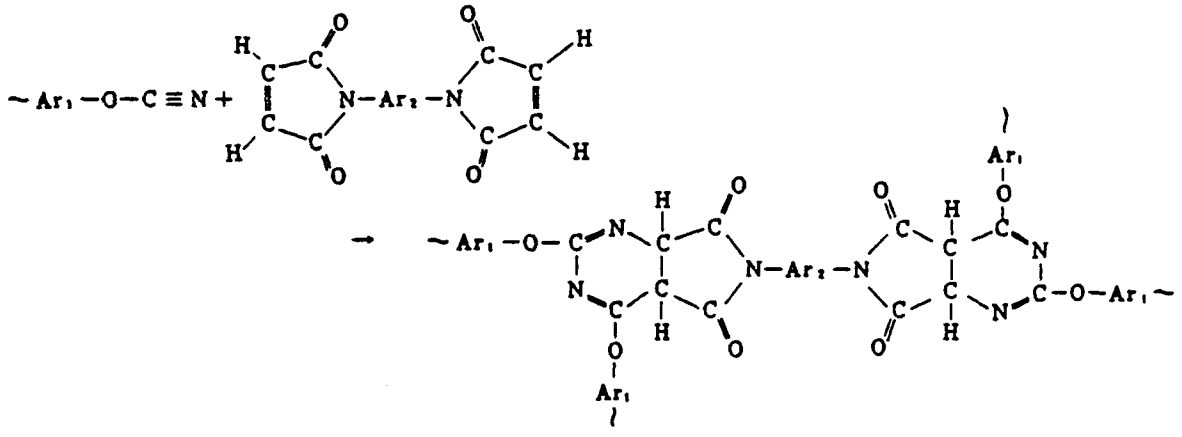

Formation of oxazole rings (mechanism active only with epoxy modifiers):

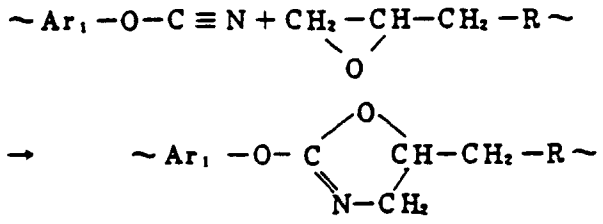

Figure 2. Polymerization reactions in cyanate ester/bismaleimide resins [8].

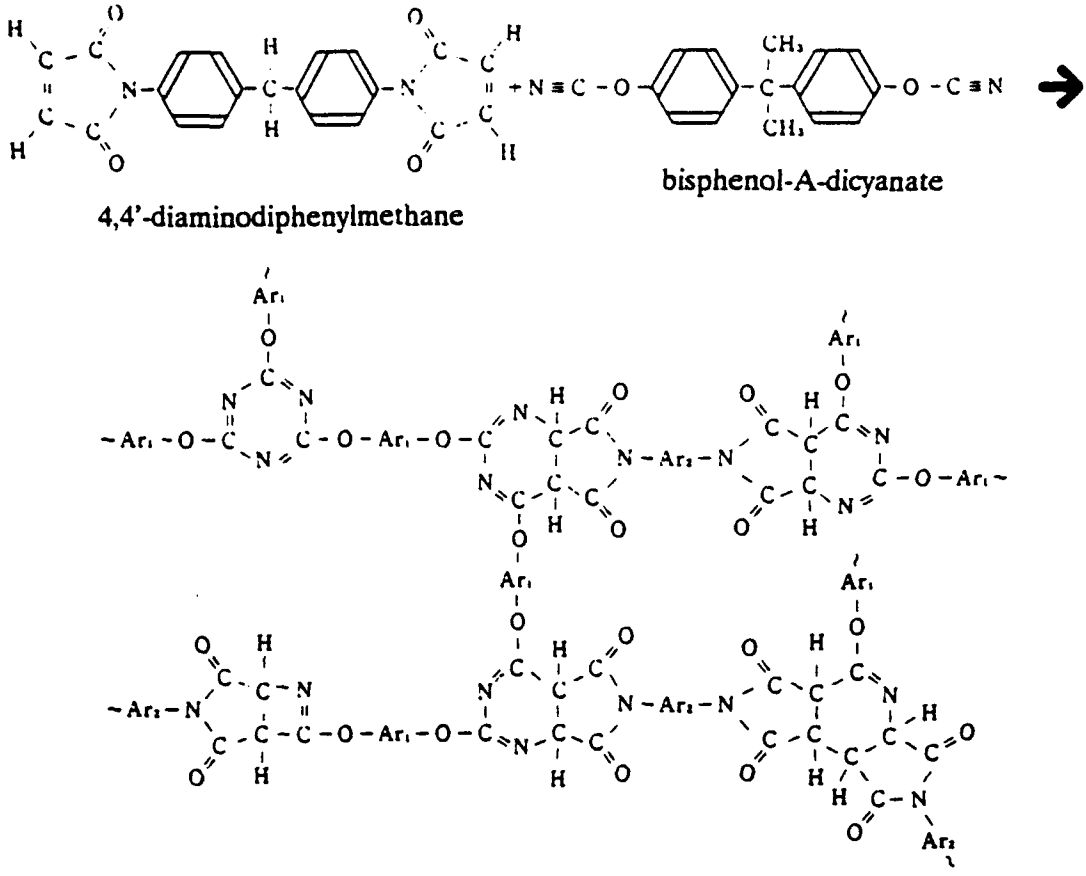

Figure 3. Reactivity model for cyanate ester/bismaleimide resin (no epoxy modifier) [8].

property retention at elevated temperature are highly dependent on the specific resin formulation [8]. Flexural and interlaminar shear strength data have been reported for 8 ply CE/BMI laminates reinforced with carbon fabric (8 harness satin weave). Flexural strengths ranged from 731 to 873 MPa at 25 °C with 56-100% retention at 200 °C depending on the resin formulation. Interlaminar shear strengths ranged from 52 to 72 MPa at 25 °C with 55-91% retention at 200 °C depending on the resin formulation.

2.2 THERMAL AND THERMO-MECHANICAL LOADING

Thermal cycling is a common loading condition in aircraft engine components and support structure, heat exchangers, piping, etc. Such components have traditionally been fabricated from metals and metal alloys. Consequently, a large body of literature is available on the behavior of these materials under thermal and thermo-mechanical loading. Metals and metal alloys generally exhibit little or no degradation due to thermal cycling if the material is allowed to expand and contract freely. However, constrained thermal cycling results in fatigue damage roughly comparable to that observed for isothermal fatigue loading [12].

While excellent results have been achieved with metal alloys, the drive for improvements in the performance characteristics of military and commercial aircraft has raised interest in polymer composites for engine components and support structure. Many such components see significant thermal excursions under varying degrees of mechanical constraint. The unconstrained case has received considerable attention in the literature [13-25]. These studies have shown that thermal loading can result in transverse ply cracking and delamination accompanied by changes in thermal expansion behavior and mechanical properties. Unfortunately, little or no information is currently available regarding the effects of constrained thermal cycling on this class of materials.

2.2.1 Parallel Bar Models

The effects of thermal and thermo-mechanical loading are often visualized using parallel bar models. An example of a parallel bar model for a homogeneous (i.e. metal or alloy) sample is given in Figure 4. The model consists of two bars, each of which is characterized by its cross-sectional area (A_i), modulus of elasticity (E_i), and thermal expansion coefficient (α_i). Bar 1 is the sample, while bar 2 determines the degree of constraint. To model a test, the bars are each subjected to a temperature excursion (ΔT_i). For the purpose of this discussion, E_1 and E_2 are assumed to be of the same order of magnitude. If $A_1 >> A_2$ and $\Delta T_2 = 0$, bar 1 may expand or contract freely under ΔT_1 and is considered to be in a condition of zero constraint. Under zero constraint, bar 1 remains unstressed regardless of ΔT_1. If $A_1 << A_2$ and $\Delta T_2 = 0$, bar 1 cannot expand or contract under ΔT_1 and is considered to be fully-constrained. Under full constraint, bar 1 experiences an axial stress equal to $E_1 \alpha_1 \Delta T_1$. An over-constrained condition occurs when bar 1 is forced to expand or contract by bar 2. If $A_1 << A_2$, bar 1 will be over-constrained when α_1 and α_2 are of opposite sign and ΔT_1 and ΔT_2 are of the same sign, or vice versa. For the over-constrained case, the axial stress in bar 1 is equal to $E_1(\alpha_1 \Delta T_1 - \alpha_2 \Delta T_2)$. If $A_1 \approx A_2$, various conditions of partial constraint are possible depending on the relative values of α_i, ΔT_i, and E_i.

Parallel bar models may also be applied to thermal and thermo-mechanical loading of continuous fiber reinforced polymer composites. Unidirectional composites subject to thermal excursions without constraint can be modelled as shown in Figure 5. One bar represents the fibers and the second bar the matrix. For most carbon fiber reinforced thermosets, A_f and A_m may be assumed to be similar since useful materials generally have fiber volume fractions between 0.40 and 0.60. Therefore, heating or cooling a unidirectional composite results in a condition of partial constraint between the fibers and matrix. The longitudinal thermal expansion coefficient of the fibers (α_f) is generally small and negative while the thermal expansion coefficient of the matrix (α_m) is relatively large and positive.

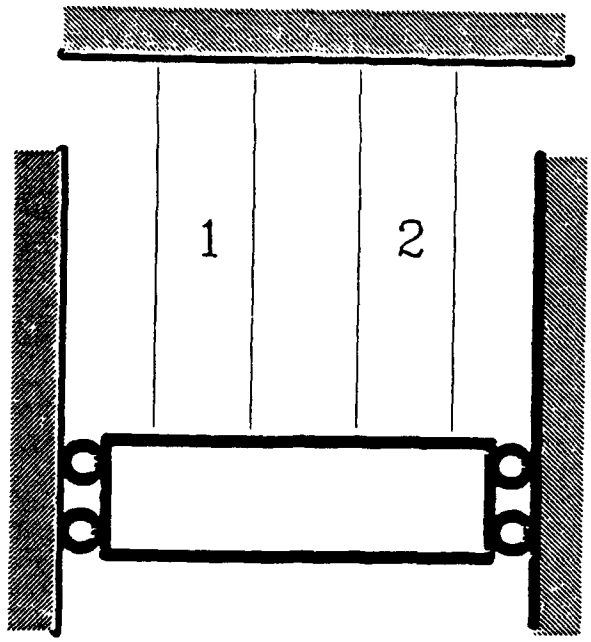

Figure 4. Parallel bar model (general).

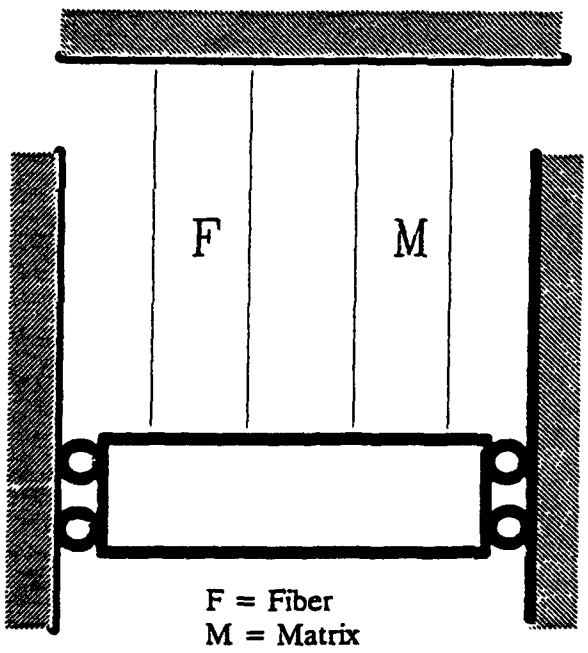

Figure 5. Parallel bar model for unconstrained unidirectional composite (lamina).

Heating the composite leads to the development of tensile stresses (axial direction) in the fibers and compressive stresses (axial direction) in the matrix. These stresses are in equilibrium and the net stress on the composite is zero.

Unidirectional composites are rarely utilized in structural applications due to their poor transverse properties. Rather, laminates are constructed which contain plies with the fibers oriented at various angles (θ) relative to the reference direction (0°). Laminates can be modelled using parallel bar models such as that shown in Figure 6. Each bar represents one ply of a given orientation. The axes of the bars are oriented at 0°. The cross-sectional areas of the bars (A_i) are assumed equal since all plies are considered to have been cut from the same material albeit at different orientations. Therefore, heating or cooling the laminate results in conditions of partial constraint between plies of different orientations with the degree of constraint dependent on the relative values of θ. The thermal expansion coefficient of each ply in the reference direction is also dependent on θ. For carbon fiber reinforced thermosets, ply thermal expansion coefficients are typically in the range from -1.5 μ/°C (fibers oriented 0°) to 50 μ/°C (fibers oriented 90°). Heating the laminate leads to the development of tensile stresses in plies with fibers oriented at or near 0° and compressive stresses in plies with fibers oriented at larger angles to the reference direction. These stresses are in equilibrium and the net stress on the composite is zero. Partial constraint is also present within each ply as described in the previous paragraph.

Up to this point, the discussion has focused on describing the behavior of polymer composites subject to thermal loading in the unconstrained condition using parallel bar models. Parallel bar models can also be used to describe the behavior of laminates subject to thermal loading in the constrained condition. In such cases, the composite is visualized as a series of bars connected in parallel to form bar 1 (see Figure 7). Bar 1 is connected in parallel with bar 2 which determines the degree of constraint on the laminate. As in the unconstrained case, partial constraint is also present between plies of different orientations and within each ply. However, the constraint on the laminate imposed by bar 2 also results

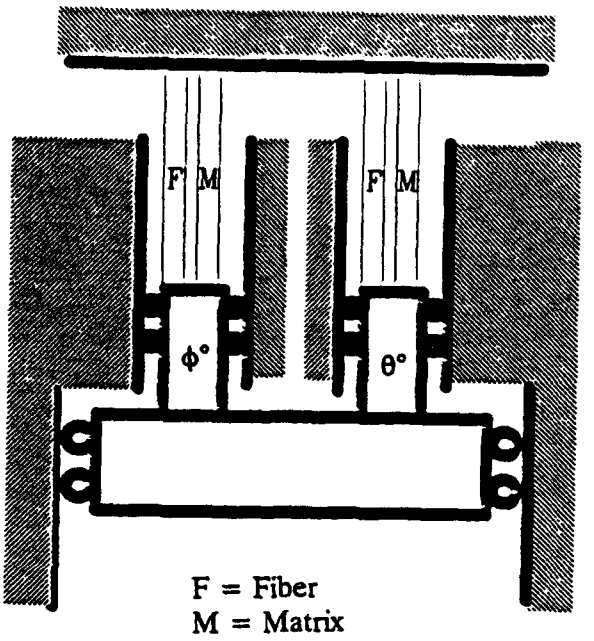

Figure 6. Parallel bar model for unconstrained laminate (2 ply orientations).

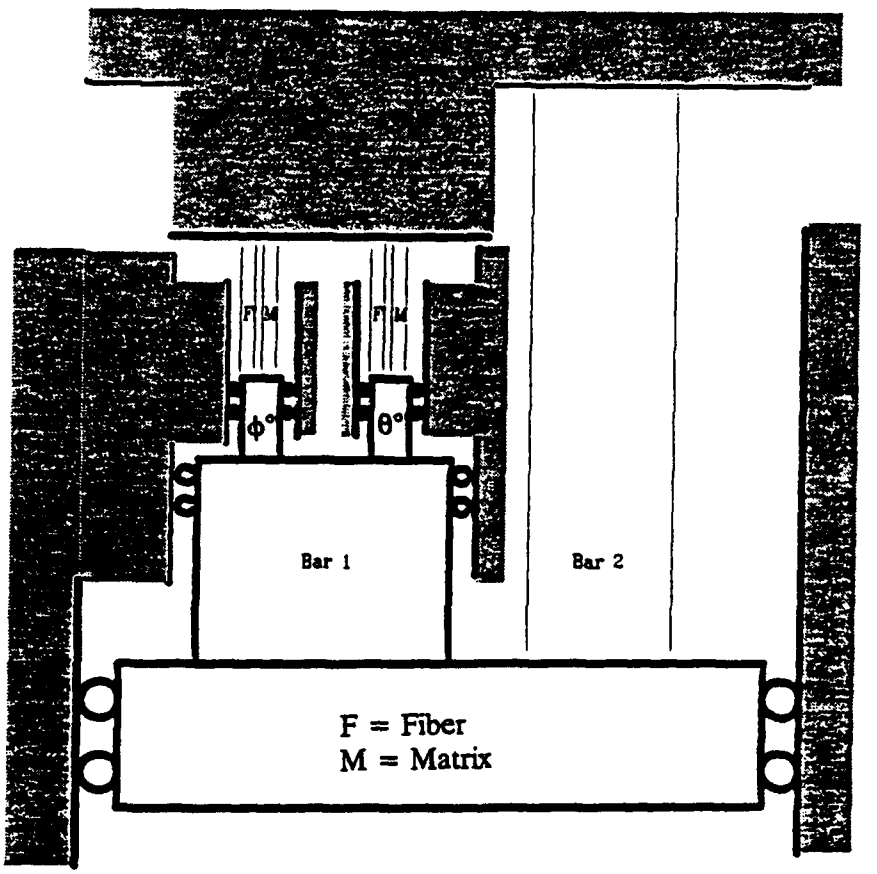

Figure 7. Parallel bar model for constrained laminate (2 ply orientations).

in a net stress on the composite which is not present in the unconstrained case. This in turn leads to higher ply stresses as well as higher fiber and matrix stresses via superposition.

It is apparent from the preceding discussion that defining the degree of constraint is considerably more complicated for composite materials relative to metals or alloys. Varying degrees of constraint may exist within composite materials at the constituent (fiber and matrix) and ply levels. Varying degrees of external constraint may also be applied at the laminate level. Throughout this document, all references to degree of constraint are understood to refer to external constraint on the laminate unless otherwise specified. Thermal cycling without external constraint is referred to as unconstrained cycling in spite of the fact that constraint may be present at the constituent and ply levels within the laminate. Thermal cycling with rigid external constraint is referred to as fully-constrained thermal cycling. Finally, thermal cycling with a superimposed mechanical strain is referred to as over-constrained thermal cycling.

2.2.2 Residual Stresses

The above discussion of thermal and thermo-mechanical loading of polymer composites via parallel bar models was simplified by assuming that no residual stresses were present at either the lamina or laminate level. However, carbon fiber reinforced thermosets will exhibit significant levels of residual stress when the temperature of the laminate deviates from its stress free temperature [26-27]. The stress free temperature (T_{SFT}) of a laminate is determined by the cure cycle. It is the temperature at which the resin gels and forms a semi-rigid network structure [26]. Prior to gelation, the resin behaves as a viscoelastic fluid and stresses developed due to resin cure shrinkage or thermal expansion mismatch are rapidly dissipated. After gelation, the resin behaves as an elastic solid and residual stresses begin to develop due to the thermal expansion mismatch between constituent materials and between plies of different orientations. On cooling to ambient temperature (T_{AMB}) following cure,

the laminate will exhibit levels of residual stress which are a function of the temperature difference (T_{SFT} - T_{AMB}), the constituent and ply thermal expansion coefficients, and the constituent and ply elastic constants.

Constituent and lamina residual stresses can be calculated from micromechanical models and classical laminate theory, respectively [27]. For carbon fiber reinforced thermosets, reasonable results may be achieved by assuming the constituent materials behave elastically between the stress free temperature and ambient [26,28]. However, the accuracy of the results is improved by including temperature-dependent material properties [29] and effects of moisture [30] in the analysis. Further improvements are also possible by incorporating viscoelastic effects into the analysis [30-31].

From the previous discussion, it is apparent that significant levels of residual stress exist in composite laminates at ambient temperature. Obviously, residual stresses will influence the response of the laminate to the thermal and thermo-mechanical loading conditions described in Section 2.2.1. Figure 8 provides an illustration of this effect. Ply stresses (axial direction) are given as a function of temperature for a $[0/90]_{ns}$ carbon/bismaleimide laminate subjected to thermal cycles from 25 to 205 °C under zero constraint and full constraint. For the fully-constrained case, the constraint was applied at ambient temperature after cool-down from the processing temperature. The laminate stress free temperature was assumed to be the same as the final cure temperature (205 °C). Ply stresses were predicted using classical laminate theory [32] and assuming elastic behavior in the temperature range of interest.

In addition to illustrating the effect of the residual stress state, Figure 8 also emphasizes the effect of the constraining force on the ply stresses. Plies oriented at 90° to the bar axis experience a higher stress amplitude in the fully-constrained condition. These plies also experience an axial compressive stress at 205 °C which is absent in the unconstrained case. Plies oriented parallel to the bar axis (0°) experience a lower stress amplitude but a higher mean stress and a large axial compressive stress at 205 °C which was

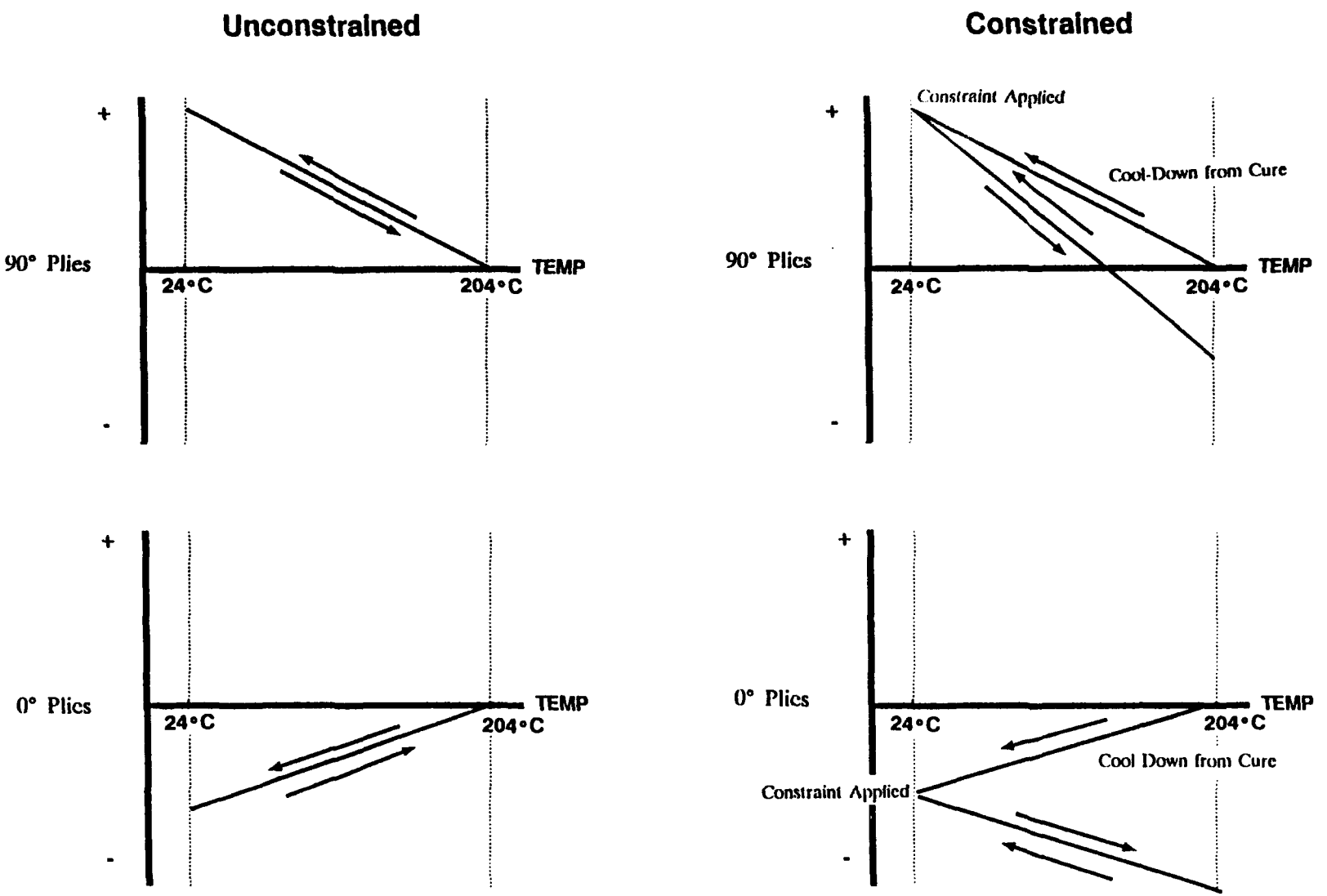

Figure 8. Ply stresses (axial direction) as a function of temperature for $[0/90]_{ns}$ carbon/bismaleimide laminate.

absent in the unconstrained case. It should be emphasized that these results do not consider the effects of temperature on the physical/mechanical properties of the material. Furthermore, even if such effects are minimal for the material in question, the predicted ply stresses will be accurate only for the initial thermal cycles. Changes in laminate mechanical properties and thermal expansion behavior resulting from matrix yielding, microcracking and other damage will alter the ply stresses during the course of the test.

2.2.3 Damage Mechanisms

The development of transverse tensile stresses in the plies of laminates during cool-down from the processing temperature was discussed in the previous section. Microcracking in the transverse plies due to residual thermal stresses has been reported by a number of investigators [27]. Microcracking is particularly problematic for composites based on high temperature resins (i.e. bismaleimide, polyimide, etc.) which cure at high temperatures and exhibit rigid network structures [33-35]. Even when residual stresses are insufficient to cause microcracking, they can reduce transverse ply failure strains by a significant margin [36-38]. Residual thermal stresses can also contribute to the initiation of free edge delaminations [39-40].

Unconstrained thermal cycling has been shown to induce microcracking in the transverse plies of polymer matrix composites [7,15-24]. Fiber splitting has also been reported in some materials [17]. Crack densities are generally observed to increase with the number of cycles until a saturation value is achieved [17,22-23]. Delaminations initiated by transverse ply microcracks have been reported [17,19,22] and propagation of delaminations under subsequent thermal cycling has been observed in some materials [17]. In general, composites based on polyimides are highly susceptible to damage resulting from thermal cycling [19-20,23]. Other common resin systems listed in order of increasing microcrack resistance are bismaleimides, epoxies, cyanate esters, and semicrystalline thermoplastics (i.e.

polyetheretherketone) [7,16]. Second phase toughening mechanisms have not been shown to be particularly effective for improving the microcrack resistance of epoxy-based composites [16]. Toughening by the introduction of flexible segments into the epoxy network has been shown to improve resistance to microcracking [16], presumably by dissipating localized residual stresses. This finding is consistent with the higher microcrack resistance of composites based on cyanate ester resins which contain many flexible -O- linkages [7,16,22]. Cure conditions have been shown to affect microcrack resistance in composites based on polyimides [20]. Reduced microcracking has been observed for polyimide-based systems cured at lower temperatures [20].

As indicated previously, no data are available in the literature regarding constrained thermal cycling of polymer composites. However, it is possible to predict potential damage mechanisms relative to the unconstrained case based on the predicted ply stresses (see Section 2.2.2). The transverse tensile stresses in the 90° plies at ambient temperature are similar in the fully-constrained and unconstrained conditions. Therefore, microcracking and delamination as observed in the unconstrained case would be expected under full constraint. However, increased levels of microcracking and delamination may be observed in the constrained condition due to the increased stress amplitude. Furthermore, under full constraint the 0° and 90° plies are subject to axial compressive stresses at 205 °C. These stresses may lead to matrix yielding or compressive failure due to temperature-induced reductions in mechanical properties. Significant reductions in mechanical properties have been observed for cyanate ester and bismaleimide-based composites in this temperature range [3,4,11]. Even polyimide-based systems show considerable nonlinearity at such temperatures [25]. Changes in laminate mechanical properties and thermal expansion behavior resulting from matrix yielding, microcracking and other damage will alter the ply stresses and additional damage mechanisms may become active during the course of the test.

2.2.4 Residual Mechanical Properties

Damage induced by unconstrained thermal cycling has been shown to affect both the mechanical properties and thermal expansion behavior of polymer composite laminates [13-14,16,18-20,22-24]. In particular, polyimide-based composites are particularly susceptible to the effects of thermal cycling. Significant reductions in flexural strength (41%), compressive strength (22%), and interlaminar shear strength (41%) have been reported for quasi-isotropic layups of Celion 6000 carbon/PMR-15 polyimide after 500 cycles from -156 to 316 °C [19]. Substantial reductions in compressive strength (60%) and interlaminar shear strength (55%) have been observed for carbon fabric/PMR-15 cross-ply laminates subjected to 1500 cycles from -54 to 232 °C [20]. A 50% reduction in compressive strength has also been reported for a cross-ply layup of Celion 3000 carbon (8H satin fabric)/PMR-15 after 5000 cycles from -18 to 232 °C [23]. The tensile strength of the latter cross-ply layup was not affected [23].

The mechanical properties of epoxy-based composites appear to be less sensitive to the effects of thermal cycling although less extensive property data are available for these materials. Available data show reductions in tensile strength and modulus of less than 5% for a variety of materials and thermal cycles [16,22,24]. However, significant reductions in tensile strength (16-28%) and tensile modulus (13-14%) have been reported for a $[0_4/\pm40/\pm70]_s$ layup of Hercules HMS carbon/Fiberite 934 epoxy and various hybrid layups of HMS/T300 carbon fabric/934 [24]. A 60% reduction in compressive strength and an 11% reduction in compressive modulus have been reported for unidirectional HMS graphite/Epon 828 epoxy composites after 500 cycles from -54 to 149 °C [18]. Thermal expansion coefficients for carbon/epoxy angle-ply laminates can be reduced considerably by thermal cycling [13-14,22,24]. At high crack densities, the expansion coefficient of the laminate often approaches that of unidirectional material.

Mechanical property data are not available for cyanate ester or bismaleimide-based composites following unconstrained thermal cycling. No data on the effects of constrained

thermal cycling are available for any polymer-based system. However, based on the discussion of damage mechanisms in Section 2.2.3, it is reasonable to expect property reductions equal to or greater than those observed in the unconstrained condition. Property reductions in the constrained condition could be considerably greater if matrix yielding or localized compressive failure occurs in the 0° plies at elevated temperature.

3.0 PROBLEM STATEMENT

Thermo-mechanical loading is an increasingly common service condition for polymer matrix composites. Unfortunately, little or no information is currently available regarding the behavior of polymer composites subject to this loading condition. The present thesis research program examines the effects of mechanical constraint on the behavior of carbon fiber reinforced cyanate ester (triazine) and bismaleimide (BMI) composites subjected to thermal cycling.

Prepreg consisting of IM6 carbon fiber tows in a triazine resin was fabricated by wet filament winding. Unidirectional and cross-ply laminates were layed-up and molded in an autoclave. Prepreg consisting of IM7 carbon fibers in a BMI resin was purchased commercially. Cross-ply laminates were layed-up and molded in an autoclave. Lamina properties were generated for the triazine system as a function of temperature from 24 to 177 °C. The temperature-dependent lamina properties were used to predict the ply stresses in cross-ply laminates during thermal cycling in the unconstrained, fully-constrained and over-constrained conditions. The ply stress data were used to explain the laminate response and damage mechanisms observed experimentally.

The triazine and BMI cross-ply laminates were subjected to 1000 thermal cycles from 24 to 177 °C in the unconstrained, fully-constrained and over-constrained conditions. The tests were performed using an Instron servohydraulic test frame. A condition of zero constraint was achieved by performing the test in load control and requiring that zero load be maintained during thermal cycling. Laminate strain was recorded as a function of temperature during the test. A condition of full constraint was achieved by performing the test in strain control and requiring that zero strain be maintained during thermal cycling. Load was monitored as a function of temperature during the test. An over-constrained

condition was achieved by performing the test in strain control and imposing the following condition:

$$\epsilon_{lam} = \alpha_{Al}(T - 24) \tag{3.1}$$

where ϵ_{lam} is the laminate strain, α_{Al} is the coefficient of thermal expansion of 6061-T6 aluminum and T is the temperature in °C. Load was monitored as a function of temperature during the test.

The laminate response was monitored as a function of the number of thermal cycles for each material and degree of constraint. Damage mechanisms were characterized for each material and degree of constraint. Residual compressive strength and modulus were measured for each material and degree of constraint.

The results of this research provide insight into the effects of mechanical constraint on the behavior of polymer matrix composites subjected to thermal cycling. This work is particularly significant given the current interest in polymer composite materials for military and commercial aircraft engine components and support structure. To the author's knowledge, this study constitutes the first treatment of thermo-mechanical fatigue in polymer matrix composite materials published in the open literature.

4.0 MATERIALS

Two materials are included in the present study. The first is a carbon fiber reinforced cyanate ester (triazine) resin designated IM6/BT3008. IM6/BT3008 laminates were fabricated from fiber and resin obtained separately. The second material is a carbon fiber reinforced bismaleimide resin designated IM7/5250-4. IM7/5250-4 laminates were fabricated from prepreg material. Details of the materials and fabrication procedures are provided below.

4.1 FIBERS, RESINS AND PREPREGS

4.1.1 Hercules IM6 Carbon Fiber

IM6 is a continuous, intermediate modulus, PAN-based carbon fiber produced in 12K tows by Hercules Inc., Wilmington, Delaware. The fiber used in this study (lot 685-3N) was treated with type G sizing and packaged in 0.45 kg spools. The certified properties for lot 685-3N are given in Table 3.

4.1.2 Mitsubishi BT3008 Cyanate Ester (Triazine) Resin

BT3008 is a two-component, thermosetting resin produced by Mitsubishi Gas Chemical Company Inc., Tokyo, Japan. It is a proprietary blend containing a cyanate ester (triazine) resin, an epoxy resin and a reactive diluent. The material is supplied in two-components designated A and B. Part A contains triazine resin (bisphenol-A-dicyanate) and diluent (hexanedioldimethacrylate). Part B contains epoxy resin (unspecified) and diluent (hexanedioldimethacrylate). The rheological and cure characteristics of the resin were evaluated for mix ratios (A:B) of 60:40 and 70:30 parts by weight. The results of the evaluation and selected neat resin data reported by the manufacturer are summarized in Table

4. Details are provided in Appendix A. Pot life and mechanical properties are similar for the two mix ratios. Based on its higher glass transition temperature, the 70:30 mix ratio was selected for fabrication of composite laminates.

Table 3. Certified properties for IM6 12K tows (lot 685-3N) [41].

Property	Value
Tensile Strength [MPa]	4490
Tensile Modulus [GPa]	290
Tensile Elongation [%]	1.56
Interlaminar (Short Beam) Shear Strength [MPa]	124
Density [g/cm^3]	1.741
Size Type	G
Size Content [% by weight]	0.9

Table 4. Properties for BT3008 resin with 60:40 and 70:30 mix ratios.

Property	Mix Ratio (A:B)	
	60:40	70:30
Resin Viscosity at 60 °C [cP]	130	130
Pot Life for Filament Winding at 60 °C[1] [hr.]	5.0	4.0
Cured Resin Density[2] [g/cm^3]	1.16	1.16
Glass Transition Temperature (T_g) by DSC [°C]	202	218
Glass Transition Temperature (T_g) by TMA[2] [°C]	215	221
Tensile Strength (σ_t) at 24 °C[2] [MPa]	66.7	65.7
Tensile Modulus (E_t) at 24 °C[2] [GPa]	3.14	3.34

[1]Pot life defined as time to reach viscosity of 1000 cP.
[2]Data provided by Mitsubishi Gas Chemical Company [42].

4.1.3 BASF IM7/5250-4 Carbon Fiber Reinforced Bismaleimide Prepreg

5250-4 is a bismaleimide resin produced by BASF Structural Materials Inc., Anaheim, California. Selected neat resin data reported by the manufacturer are given in Table 5. For the present study, prepreg consisting of IM7 12K tows in 5250-4 resin (batch 20157-00) was obtained from BASF. The resin content of the prepreg was reported at 33 percent by weight.

4.2 LAMINATE FABRICATION

4.2.1 IM6/BT3008 Laminates

4.2.1.1 Wet Filament Winding of Prepreg Material

Sheets of unidirectional IM6/BT3008 prepreg were prepared using a McClean Anderson WD60 four axis filament winder. A schematic of the filament winding operation is given in Figure 9. Five IM6 12K tows were drawn from 0.45 kg spools through a resin bath containing BT3008 resin (70:30 mix ratio) maintained at 60 °C. At this point, the tension on the tow was approximately 11 to 13 N. Once impregnated with resin, the tows were drawn through close tolerance orifices (CTO's) to accurately control the resin content. A CTO diameter of 0.813 mm was selected which resulted in a tow resin content of 39.9 ± 1.0 percent by weight. After leaving the CTO's the tows were fed through a series of tensioning pulleys which increased the tension on the tows to approximately 27 N. Finally, the tows were drawn though a series of combs and columnated at a delivery eye in close proximity to the mandrel. The delivery eye forced the tows to spread out prior to their placement on the mandrel, thereby preventing gaps in the prepreg. The tows were wound on an 86 cm diameter rotating mandrel covered with release film. The carriage index rate was 8.64 mm per revolution. After winding, the prepreg was covered with a second layer of release film and cut from the

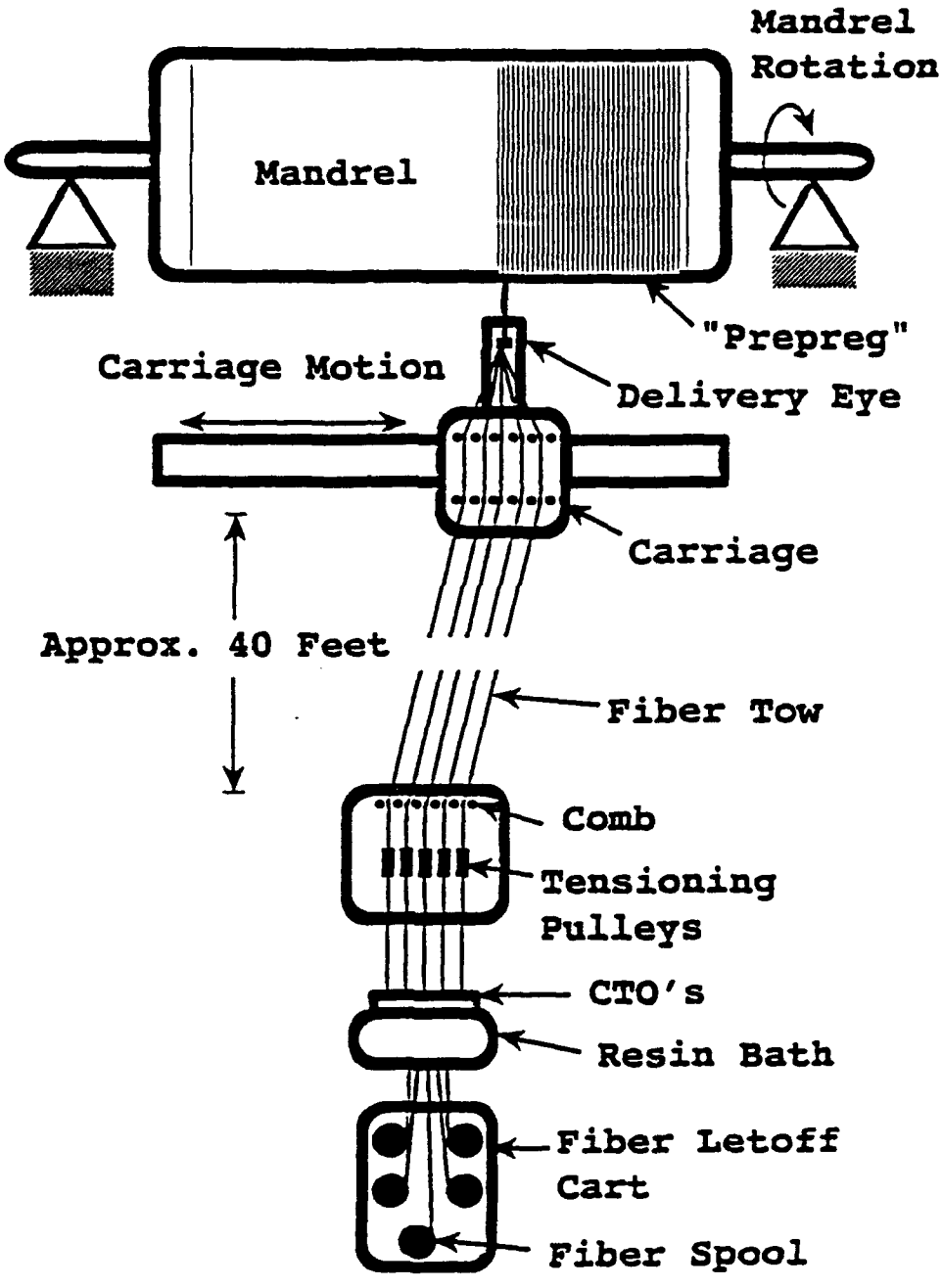

Figure 9. Schematic of wet filament winding operation.

mandrel. The resulting prepreg sheets measured approximately 270 x 137 cm. Ply patterns were cut from the prepreg sheets, sealed in polypropylene and stored in a freezer at -17 °C.

Table 5. Properties for 5250-4 resin [43].

Property	Value
Cured Resin Density [g/cm^3]	1.25
Glass Transition Temperature (T_g) by TMA [°C]	300
Tensile Strength (σ_t) at 24 °C [MPa]	103
Tensile Modulus (E_t) at 24 °C [GPa]	4.6

4.2.1.2 Layup

The ply patterns were removed from the freezer and allowed to warm to room temperature prior to removal of the polypropylene packaging material. Panels were layed-up on glass-covered tables. Each laminate was layed-up individually and each ply was checked-off on a router sheet as it was added to the laminate. This ensured that each laminate received the proper number of plies and that each ply was placed at the correct orientation. Three $[0]_{12}$ laminates measuring 61.0 x 61.0 cm, one $[0/90]_{3S}$ laminate measuring 30.5 x 30.5 cm, and two $[0/90]_{3S}$ laminates measuring 61.0 x 15.2 cm were layed-up for use in this study.

4.2.1.3 Autoclave Cure

Each laminate was vacuum-bagged and cured in a Baron model BAC-37 autoclave. A schematic of the vacuum bag assembly is given in Figure 10. The vacuum bag assembly was supported on a 6.35 mm thick aluminum caul plate. The caul plate was covered with a layer

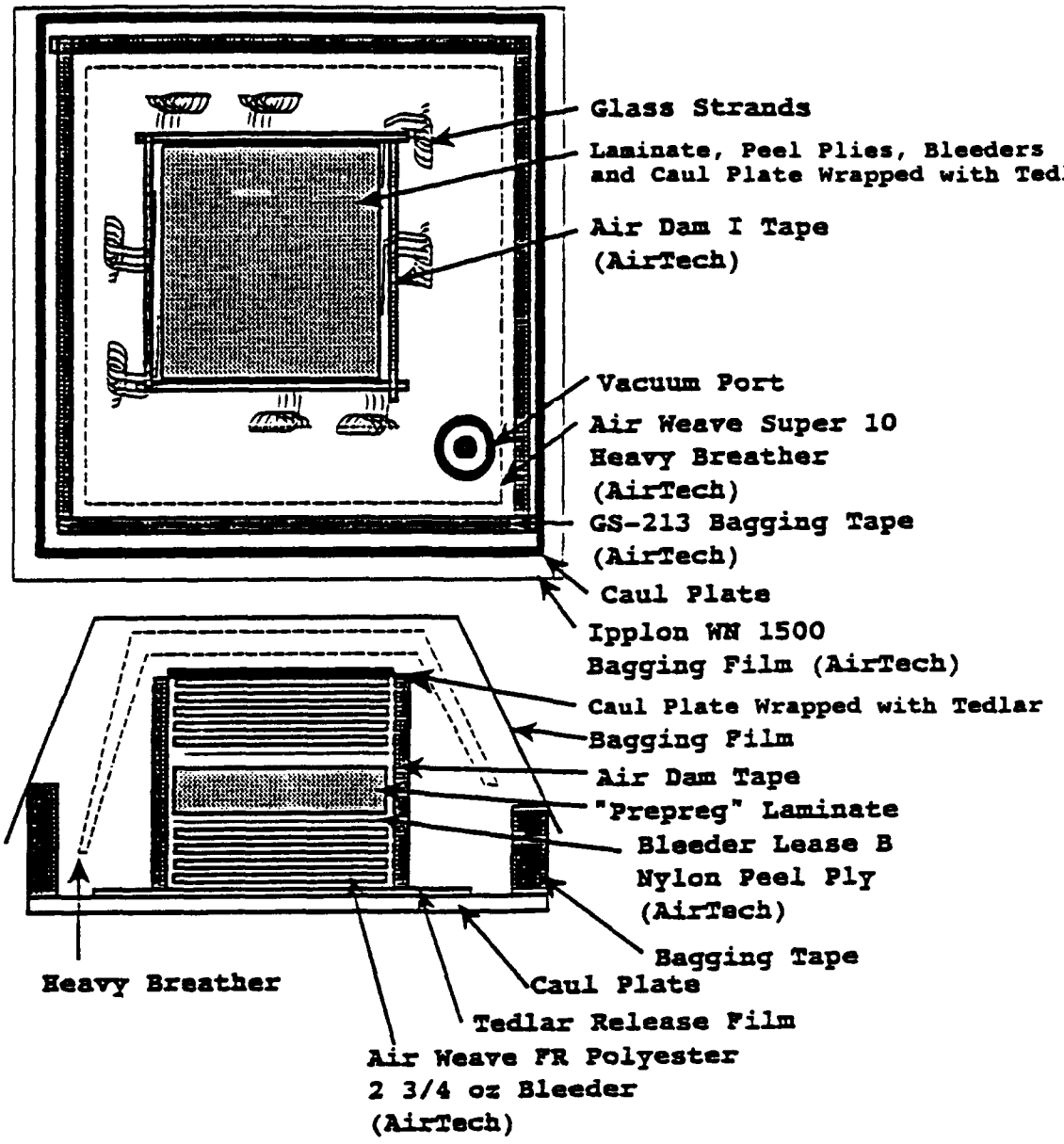

Figure 10. Schematic of vacuum bag assembly.

of Tedlar release film which extended to within 2.54 cm of the edges of the plate. One ply of 93.3 g/m^2 nonwoven polyester bleeder material was used for every three plies of prepreg. Half of the bleeder plies were placed on top of the tedlar release film followed by two layers of porous teflon, the laminate, two layers of porous teflon, and the remaining half of the bleeder plies. The edges of the laminate were enclosed by 12.7 mm wide strips of air dam tacked-down against the Tedlar release film. Bundles of 8 glass fiber tows were placed at the corners of the laminate and at the midpoint of each edge. Each bundle extended approximately 7.62 cm along the edge of the laminate inside the air dam then passed through the air dam to the outer area of the vacuum bag. The purpose of the glass tows was to provide pathways for gases to vent from the edges of the laminate. A 3.18 mm thick aluminum caul plate with dimensions equivalent to those of the laminate was covered with a layer of Tedlar release film and placed over the top of the bleeder plies. Two plies of Air Weave Super 10 heavy breather material were placed over the entire assembly and tacked-down against the air dam. The heavy breather material was trimmed back approximately 2.54 cm from the edges of the caul plate. Strips of GS-213 bagging tape were tacked-down to the caul plate around the perimeter of the heavy breather. A sheet of Ipplon WN-1500 bagging film was placed over the caul plate and sealed with the bagging tape. Prior to sealing the final edge of the bag, a vacuum port was installed at a location away from the laminate.

The laminate was vacuum debulked at 711 mm-Hg for a minimum of 30 min. prior to the start of the cure cycle. Since the BT3008 resin system was known to exhibit a relatively strong exotherm during cure, a cycle with multiple temperature ramps/holds was utilized to increase the molecular weight of the resin slowly and prevent overheating. Failure to control the exotherm can result in high void contents due to volatilization of monomer and low molecular weight polymer. Details of the IM6/BT3008 cure cycle are given in Table 6. This cycle resulted in a moderate exotherm at the completion of the ramp to 120 °C. The laminate temperature generally peaked at 140-145 °C approximately 10-15 min. into the hold segment then gradually returned to the set point over a 30 min. period. At the completion

Table 6. Autoclave cure cycle for IM6/BT3008 laminates.

Segment	1	2	3	4	5	6	7	8	9	10	11	12	13
Type: R=Ramp H=Hold	R	H	R	R	H	R	H	R	H	R	H	R	R
Time [min.]	---	60	---	---	120	---	120	---	120	---	250	---	---
Temp. [°C]	80	80	80	120	120	150	150	180	180	200	200	121	65
Temp. Rate [°C/min.]	2.8	---	---	2.8	---	2.8	---	2.8	---	2.8	---	2.8	2.8
Press. [kPa]	0	0	414	414	414	414	414	414	414	414	414	414	0
Press. Rate [kPa/min.]	---	---	13.8	---	---	---	---	---	---	---	---	---	13.8
Vacuum [mm-Hg]	711	711	711	711	711	711	711	711	711	711	711	711	0

of the cure cycle, the vacuum bag assembly was removed from the autoclave and permitted to cool to ambient. The laminate was carefully debagged and all bleeder plies were removed along with the outer plies of porous teflon. The inner plies were left in place to protect the surface of the laminate during machining. However, the corners of the peel ply were turned up temporarily to allow measurement of the laminate thickness. The overall thickness and cured ply thickness for each laminate are given in Table 7.

Table 7. Overall thickness and cured ply thickness for IM6/BT3008 laminates.

Panel	Dimensions [cm]	Layup	Laminate Thickness[1] [mm]	Cured Ply Thickness[2] [mm]
UNI-A	61.0 x 61.0	$[0]_{12}$	2.972 ± 0.051	0.248
UNI-B	61.0 x 61.0	$[0]_{12}$	2.972 ± 0.025	0.248
UNI-C	61.0 x 61.0	$[0]_{12}$	2.819 ± 0.051	0.235
XPLY-A	30.5 x 30.5	$[0/90]_{3S}$	2.896 ± 0.051	0.241
XPLY-B	61.0 x 15.2	$[0/90]_{3S}$	2.870 ± 0.025	0.239
XPLY-C	61.0 x 15.2	$[0/90]_{3S}$	2.845 ± 0.051	0.237

[1]Average of four measurements made 2.54 cm in from corners of panel.
[2]Based on average thickness.

4.2.2 IM7/5250-4 Laminates

4.2.2.1 Layup

The prepreg was removed from the freezer and allowed to come to room temperature prior to removal of the packaging material. Ply patterns were cut from the prepreg and panels were layed-up on glass-covered tables. Each laminate was layed-up individually and

each ply was checked-off on a router sheet as it was added to the laminate. This ensured that each laminate received the proper number of plies and that each ply was placed at the correct orientation. One $[(0/90)_3/0]_S$ laminate measuring 61.0 x 61.0 cm and one $[0/90]_{4S}$ laminate measuring 30.5 x 30.5 cm were layed-up for use in this study.

4.2.2.2 Autoclave Cure

Each laminate was vacuum-bagged and cured in a Baron model BAC-37 autoclave. The bagging procedures were equivalent to those used for the IM6/BT3008 laminates (Section 4.2.1.3) with the exception of the number of bleeder plies. For the IM7/5250-4 laminates, one ply of 93.3 g/m^2 nonwoven polyester bleeder material was used for every five plies of prepreg.

Each laminate was vacuum debulked at 711 mm-Hg for a minimum of 30 min. prior to the start of the cure cycle. The laminates were cured in accordance with the manufacturer's recommended autoclave cure cycle and free standing oven postcure [43]. Details of the IM7/5250-4 cure cycle are given in Table 8. No significant exotherm was observed using this procedure. At the completion of the cure cycle, the vacuum bag assembly was removed from the autoclave and permitted to cool to ambient. The laminate was carefully debagged and all bleeder plies were removed along with the outer plies of porous teflon. The inner plies were left in place to protect the surface of the laminate during postcure and machining. Postcure was conducted in an air-circulating oven. The laminate was heated to 243 °C at 3 °C per min., held at 243 °C for 360 min., then cooled to 49 °C or lower at 3 °C per min. prior to removal from the oven. After postcure, the corners of the peel ply were turned up temporarily to allow measurement of the laminate thickness. The overall thickness and cured ply thickness for each laminate are given in Table 9.

Table 8. Autoclave cure cycle for IM7/5250-4 laminates.

Segment	1	2	3	4	5	6	7	8
Type: R=Ramp H=Hold	R	R	H	R	R	H	R	R
Time [min.]	---	---	45	---	---	360	---	---
Temperature [°C]	25	121	121	121	177	177	120	65
Temp. Rate [°C/min.]	---	2.8	---	---	2.8	---	2.8	2.8
Pressure [kPa]	103	103	103	586	586	586	586	0
Press. Rate [kPa/min.]	13.8	---	---	13.8	---	---	---	13.8
Vacuum [mm-Hg]	711	711	711	711	711	711	711	0

Table 9. Overall thickness and cured ply thickness for IM7/5250-4 laminates.

Panel	Dimensions [cm]	Layup	Laminate Thickness[1] [mm]	Cured Ply Thickness[2] [mm]
XPLY-A	61.0 x 61.0	$[(0/90)_3/0]_S$	1.764 ± 0.035	0.126
XPLY-B	30.5 x 30.5	$[0/90]_{5S}$	2.521 ± 0.029	0.126

[1]Average of four measurements made 2.54 cm in from corners of panel.
[2]Based on average thickness.

4.2.3 Laminate Machining

A variety of test specimens were required for characterization of the materials (Section 4.3) as well as thermo-mechanical fatigue testing (Section 6.0). Unless otherwise specified, test specimens were cut from the panels using a diamond saw with water spray mist to minimize heat buildup in the laminate. In order to remove moisture introduced during the machining process, the specimens were heated in an oven at 50 °C for 24 hr. in the presence of a desiccant then cooled in a desiccator. All specimens were stored in a desiccator prior to testing.

4.3 MATERIAL PROPERTIES

A thorough characterization of physical and mechanical properties was performed for the IM6/BT3008 system. Fiber volume and void content were measured for each panel. Mechanical strengths, elastic constants and thermal expansion coefficients were evaluated as a function of temperature from 24 to 177 °C. The stress free temperature of the composite was also determined. The IM7/5250-4 system was not characterized although limited data was obtained from the literature.

4.3.1 IM6/BT3008

4.3.1.1 Fiber Volume and Void Content

Fiber volume measurements were performed according to ASTM D3171-76, "Test Method for Fiber Content of Resin-Matrix Composites by Matrix Digestion". Specimens measuring 1.9 x 1.9 cm (nominal) were cut from each IM6/BT3008 panel. A 1.2 g sample of IM6 fiber was taken from a spool to allow correction of the data for changes in fiber weight by the digesting medium. Resin digestion was accomplished in nitric acid (ACS reagent grade, 70% concentration) at 65 °C. Complete digestion required approximately 30 hours. No significant change in weight was noted for the IM6 fiber sample after accounting for the sizing content. Void content calculations were performed according to ASTM D2734-70, "Test Method for Void Content of Reinforced Plastics". Void content calculations required the fiber, resin and composite densities. Composite density measurements were performed on each fiber volume specimen prior to digestion. Density measurements were performed according to ASTM D792-66, "Test Methods for Specific Gravity and Density of Plastics by Displacement". Fiber and resin densities were obtained from the suppliers.

Fiber volumes and void contents for the IM6/BT3008 panels are given in Table 10. Fiber volume fractions averaged 0.664 ± 0.001 for the $[0]_{12}$ panels and 0.648 ± 0.003 for the $[0/90]_{3S}$ panels. Void contents averaged 0.009 ± 0.005 for the $[0]_{12}$ panels and 0.005 ± 0.003 for the $[0/90]_{3S}$ panels. These results are typical for structural composite laminates in the aerospace industry and indicate that the fabrication procedures outlined in Section 4.2.1 are suitable for producing well-consolidated IM6/BT3008 laminates.

Table 10. Fiber volume fractions and void contents for IM6/BT3008 laminates.

$[0]_{12}$ Laminates		
Panel	Fiber Volume Fraction	Void Content
UNI-A	0.664	0.003
UNI-B	0.663	0.010
UNI-C	0.665	0.014
Average	0.664 ± 0.001	0.009 ± 0.005

$[0/90]_{3S}$ Laminates		
Panel	Fiber Volume Fraction	Void Content
XPLY-A	0.646	0.004
XPLY-B	0.651	.008
XPLY-C	0.646	0.002
Average	0.648 ± 0.003	0.005 ± 0.003

4.3.1.2 Mechanical Strengths and Elastic Constants

Mechanical strengths and elastic constants were determined for the IM6/BT3008 $[0]_{12}$ laminates at temperatures of 24, 93, 121, 150 and 177 °C. The tests were performed according to the relevant ASTM and SACMA standard test methods listed in Table 11. Tensile and compressive test coupons required bonded end tabs. The end tabs were machined from the IM7/5250-4 panel designated XPLY-A and bonded to the coupons using film adhesive. FM 87-1 film adhesive was used for specimens tested at 24, 93 and 121 °C while HT 424 film adhesive was used for specimens tested at 150 and 177 °C. Both adhesives are produced by the American Cyanamid Company, Wayne, New Jersey.

Table 11. Mechanical properties and corresponding test methods.

Property	Test Method	Comments
0° Tensile Strength (σ_{t11})	SACMA SRM 4-88	
0° Tensile Modulus (E_{t11})	SACMA SRM 4-88	Chord: 0.1 - 0.6 % Strain.
Poisson's Ratio (ν_{12})	SACMA SRM 4-88	Chord: 0.1 - 0.6 % Strain.
90° Tensile Strength (σ_{t22})	SACMA SRM 4-88	
90° Tensile Modulus (E_{t22})	SACMA SRM 4-88	Chord: 0.1 - 0.3 % Strain.
Poisson's Ratio (ν_{21})	SACMA SRM 4-88	Chord: 0.1 - 0.3 % Strain.
0° Compressive Strength (σ_{c11})	ASTM D3410	
0° Compressive Modulus (E_{c11})	ASTM D3410	Chord: 0.1 - 0.3 % Strain.
90° Compressive Strength (σ_{c22})	ASTM D3410	
90° Compressive Modulus (E_{c22})	ASTM D3410	Chord: 0.1 - 0.3 % Strain.
In-Plane Shear Strength (S_{12})	Iosipescu Shear[1]	
In-Plane Shear Modulus (G_{12})	Iosipescu Shear[1]	Chord: 0.1 - 0.3 % Strain.
Interlaminar Shear Strength (S_{31})	ASTM D2344	

[1]Details available in reference [47].

Mechanical strengths and elastic constants for the IM6/BT3008 $[0]_{12}$ laminates are given in Table 12. The results are as expected for this class of materials with three notable exceptions. First, the translation of fiber tensile strength and modulus (based on rule of mixtures and fiber tow test data) are somewhat lower than expected, i.e. 75% and 76% respectively at 24 °C. Translation of tensile strength is typically 80-85% and translation of tensile modulus typically approaches 100% in carbon fiber reinforced epoxy and bismaleimide systems [43-45]. It should be noted, however, that the tow test results used in the rule of mixtures calculations were lot mean averages. Results for individual spools may vary significantly within a given lot. Furthermore, the filament winding process introduces some fiber waviness into the prepreg material. Fiber waviness would be expected to cause reductions in the tensile strength and modulus of the composite. Finally, no attempt was made to optimize the fiber sizing for the BT3008 resin system as is customary in many prepreg systems. Reduced interfacial strength would also be expected to cause reductions in the tensile strength and modulus of the composite.

The second anomaly in the data involved the minor Poisson's ratio (ν_{21}). The value of ν_{21} measured at 177 °C does not satisfy the reciprocity condition, specifically:

$$\nu_{21} = (E_{22}/E_{11})\nu_{12} \tag{4.1}$$

where E_{11} and E_{22} are the elastic moduli in the longitudinal and transverse directions respectively and ν_{12} is the major Poisson's ratio. Agreement is reasonable at the lower temperatures, however, as shown in Figure 11. This result was attributed to difficulties associated with utilizing bonded strain gauges at elevated temperatures, particularly when the strains to be measured were very small. To compensate for this deficiency in the data, the thermal and thermo-mechanical analyses reported in Section 5.0 were conducted using values of ν_{21} calculated according to equation (4.1).

Table 12. Mechanical properties of IM6/BT3008 as a function of temperature.

Property	Temperature [°C]				
	24	93	121	149	177
σ_{t11} [MPa]	2230 ± 140	2100 ± 30	2100 ± 120	2040[1]	> 1430[1,2]
E_{t11} [GPa]	147 ± 7	147 ± 9	146 ± 7	144 ± 8	132 ± 9
ν_{12}	0.313 ± 0.008	0.320 ± 0.011	0.321 ± 0.016	0.286 ± 0.016	0.314 ± 0.003
σ_{t22} [MPa]	39.0 ± 1.2	42.9 ± 3.4	41.3 ± 2.0	29.3 ± 3.4	17.3 ± 2.1
E_{t22} [GPa]	8.34 ± 0.28	7.24 ± 0.28	6.62 ± 0.07	6.00 ± 1.40	2.97 ± 0.00
ν_{21}	0.016 ± 0.001	0.019 ± 0.002	0.015 ± 0.001	0.012 ± 0.002	0.014[1]
σ_{c11} [MPa]	1320[1]	862 ± 41	669 ± 55	559 ± 28	317 ± 55
E_{c11} [GPa]	N/A[3]	N/A[3]	141 ± 2	141 ± 1	143[1]
σ_{c22} [MPa]	181 ± 14	160 ± 24	133 ± 10	91.0 ± 6.9	53.1 ± 4.8
E_{c22} [GPa]	N/A[3]	N/A[3]	7.51 ± 0.23	6.24 ± 0.63	3.33 ± 0.24
S_{12} [MPa]	96.5 ± 7.6	91.0 ± 4.1	77.9 ± 2.1	69.6 ± 2.1	46.2 ± 2.1
G_{12} [GPa]	6.77 ± 0.16	4.79 ± 0.23	4.79 ± 0.40	3.89 ± 0.65	1.79 ± 0.08

[1]One test only.
[2]Adhesive shear failure at tab.
[3]Insufficient material available for these tests.

Finally, the 0° compressive strengths reported in Table 12 are lower than expected, i.e. 59% of the tensile strength at 24 °C versus 70% reported in the literature for carbon fiber reinforced epoxy [46] and bismaleimide [43] systems. Based on analysis of the back-to-back strain gauge data and examination of the failed specimens, this result is attributed to bending stresses induced by deformation of the IM7/5250-4 end tabs. At high loads, the serrated reverse-wedge grips in the Wyoming Modified IITRI fixture indent the tabs on one side of the specimen and apply a bending moment to the gauge section. The resultant bending stresses result in premature failure of the coupon. Insufficient material was available to repeat these tests. Fortunately, the 0° compressive modulus, 90° compressive strength and 90° compressive modulus data were unaffected as these measurements required relatively low loads which did not result in deformation of the end tab material.

4.3.1.3 Coefficients of Thermal Expansion

Coefficient of thermal expansion (CTE) measurements were performed on the IM6/BT3008 laminates using a quartz-rod dilatometer and a strain-gauge technique. Neither method produced accurate and reproducible results due in part to the small laminate CTE values. Therefore, the composite CTE values were analytically determined using fiber and resin CTE data obtained from the literature. The longitudinal (0°) and transverse (90°) CTE's were computed for the $[0]_{12}$ layup and the 0° CTE was computed for the $[0/90]_{3S}$ layup. All CTE values were computed as a function of temperature from 24 to 177 °C. Details of the analytical method are provided below.

The longitudinal and transverse CTE's for the IM6/BT3008 $[0]_{12}$ layup were computed using the following expressions derived by Schapery [48]:

$$\alpha_{11} = (1/E_{11})(\alpha_f E_f V_f + \alpha_m E_m V_m) \qquad (4.2)$$

$$\alpha_{22} = (1 + \nu_f)\alpha_f V_f + (1 + \nu_m)\alpha_m V_m - \alpha_{11}\nu_{12} \quad (4.3)$$

where α_f and α_m are the CTE's of the fibers and matrix, E_f and E_m are the elastic moduli of the fibers and matrix, V_f and V_m are the volume fractions of fibers and matrix, E_{11} is the elastic modulus of the composite in the longitudinal direction, and ν_{12} is the major Poisson's ratio of the composite. The values of V_f, V_m, E_{11} and ν_{12} were measured for the composite as described in Sections 4.3.1.1 and 4.3.1.2. Temperature-dependent CTE data for IM6 carbon fiber was obtained from Tsai and Daniel [49]. E_f and ν_f were assumed constant with temperature. E_f was obtained from Hercules Inc. [41] and an approximate value for ν_f was obtained from the literature [50-51]. Temperature-dependent elastic modulus and CTE data for BT3008 resin were obtained from Mitsubishi Gas Chemical Corporation Inc. [42]. No information regarding Poisson's ratio was available for BT3008 resin. Temperature-dependent Poisson's ratio data for 934 epoxy resin were available in the literature [51] and were utilized in this analysis. Available mechanical property data for 934 and BT3008 were sufficiently similar and Poisson's ratio effects sufficiently small to justify this substitution. Temperature-independent properties were substituted directly into the Schapery equations. Polynomials were fit to all temperature-dependent data to permit each property to be determined at all temperatures in the range of interest. Table 13 provides a summary of all property data used to calculate α_{11} and α_{22} for IM6/BT3008 $[0]_{12}$. The resulting temperature-dependent values of α_{11} and α_{22} are presented graphically in Figures 12 and 13.

The temperature-dependent 0° CTE for the IM6/BT3008 $[0/90]_{3S}$ layup was calculated using a computer code based on classical laminate theory (see Section 5.1.1). Input to the code consisted of the temperature-dependent mechanical property data described in Section 4.3.1.2 and the temperature-dependent lamina CTE data described in the preceding paragraph. Polynomials were fit to all temperature-dependent data to permit each property to be determined at all temperatures in the range of interest. Table 13 along with Figures 12 and 13 provide a summary of all property data used to calculate the 0° CTE for

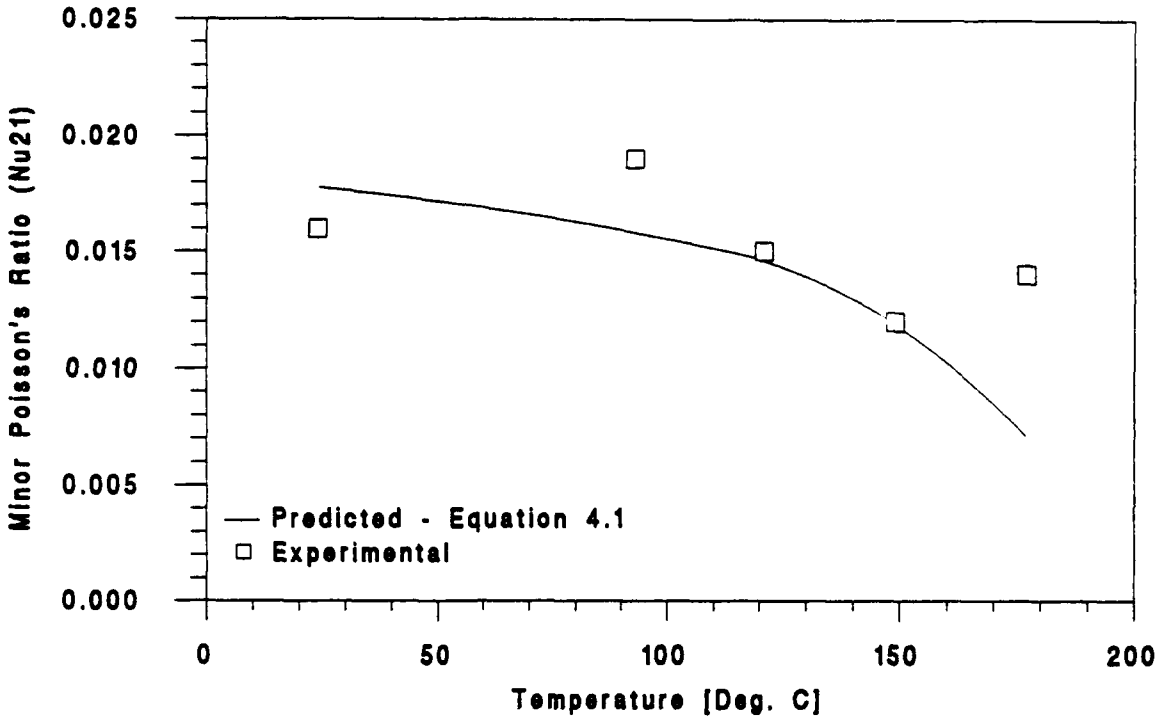

Figure 11. Minor Poisson's ratio (ν_{21}) for IM6/BT3008 $[0]_{12}$.

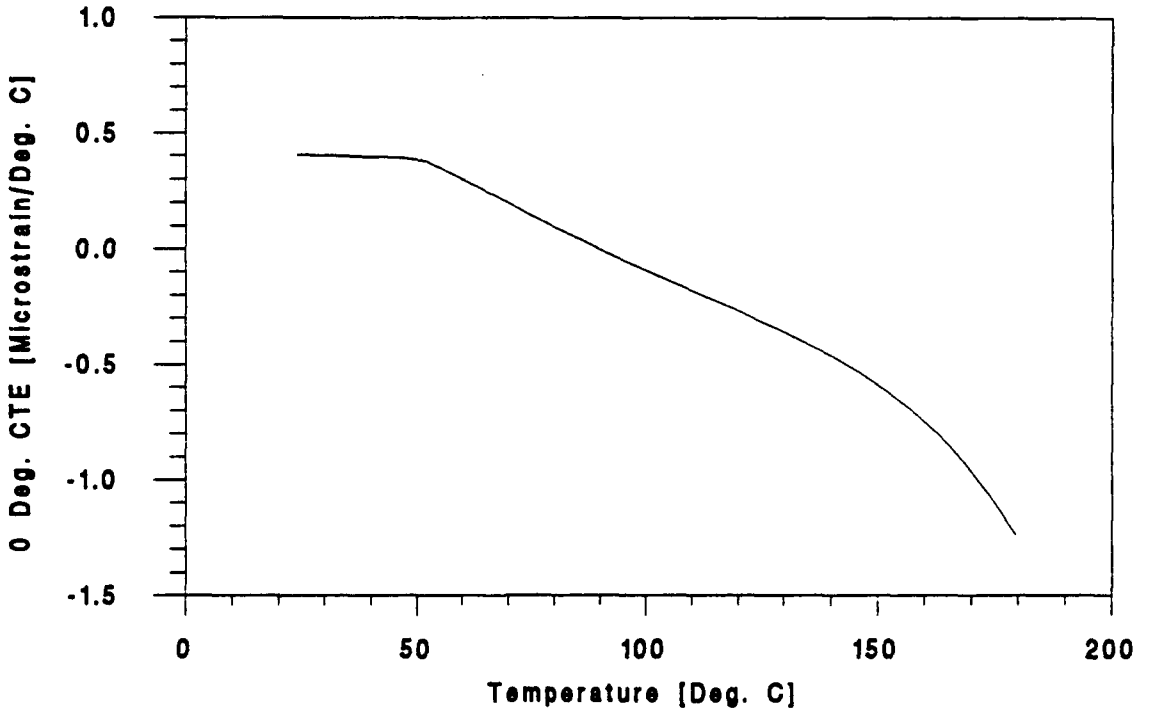

Figure 12. Longitudinal (0°) CTE for IM6/BT3008 $[0]_{12}$ from equation 4.2.

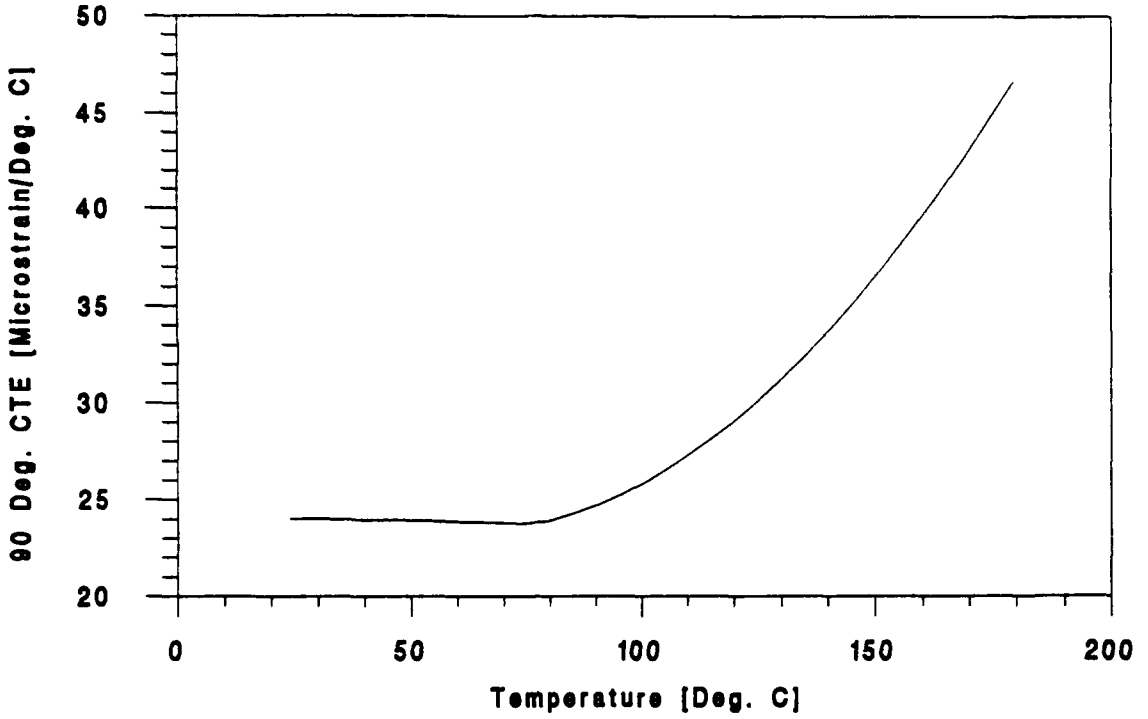

Figure 13. Transverse (90°) CTE for IM6/BT3008 $[0]_{12}$ from equation 4.2.

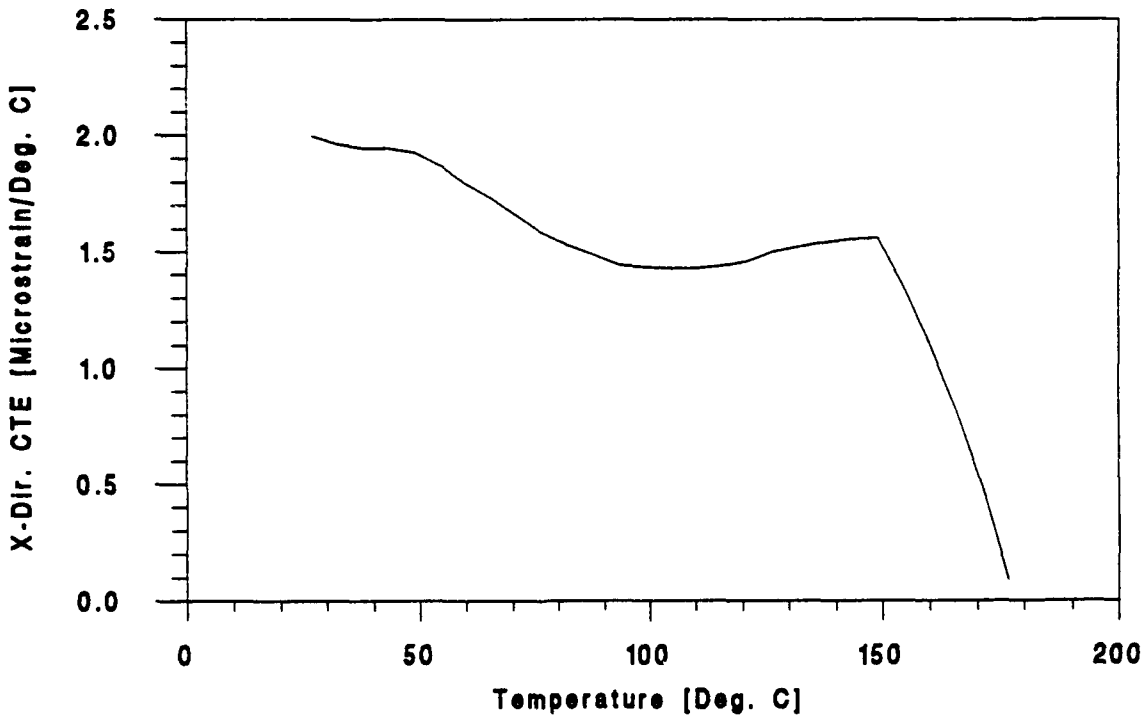

Figure 14. 0° CTE for IM6/BT3008 $[0/90]_{3S}$ from classical laminate theory.

Table 13. Property data used to calculate coefficients of thermal expansion (CTE's) for IM6/BT3008.

Property	Temperature [°C]	Value
Fiber CTE [μ/°C]	T ≤ 49.9	$\alpha_f = 0.00$
	T > 49.9	$\alpha_f = 3.926E\text{-}2 + 8.134E\text{-}3T - 2.551E\text{-}4T^2 + 1.740E\text{-}6T^3 - 4.220E\text{-}9T^4$
Matrix CTE [μ/°C]	T ≤ 76.8	$\alpha_m = 52.76$
	T > 76.8	$\alpha_m = 6.542E+1 - 4.554E\text{-}1T + 3.783E\text{-}3T^2$
Fiber Elastic Modulus [GPa]	All	$E_f = 290.1$
Matrix Elastic Modulus [GPa]	All	$E_m = 3.528E+0 - 1.123E\text{-}2T + 1.710E\text{-}4T^2 - 1.052E\text{-}6T^3$
Fiber Volume Fraction	All	$V_f = 0.664$
Matrix Volume Fraction	All	$V_m = 0.336$
Composite 0° Elastic Modulus [GPa]	T ≤ 93.9	$E_{11} = 146.9$
	T > 93.9	$E_{11} = 1.503E+2 - 2.033E\text{-}1T + 2.887E\text{-}3T^2 - 1.265E\text{-}5T^3$
Composite 90° Elastic Modulus [GPa]	T ≤ 94.9	$E_{22} = 8.727E+0 - 1.599E\text{-}2T$
	T > 94.9	$E_{22} = 1.073E+1 - 1.351E\text{-}1T + 1.625E\text{-}3T^2 - 6.244E\text{-}6T^3$
Composite Major Poisson's Ratio	All	$\nu_{12} = 3.189E\text{-}1 - 7.139E\text{-}5T$
Composite Shear Modulus [GPa]	T ≤ 92.1	$G_{12} = 7.462E+0 - 2.878E\text{-}2T$
	T > 92.1	$G_{12} = 9.498E+0 - 1.487E\text{-}1T + 1.572E\text{-}3T^2 - 5.538E\text{-}6T^3$

IM6/BT3008 $[0/90]_{3S}$. The resulting temperature-dependent CTE data is presented graphically in Figure 14.

The coefficient of thermal expansion of the $[0]_{12}$ laminate in the 0° direction decreased with temperature from 0.404 μ/°C at 24 °C to -1.149 μ/°C at 177 °C (see Figure 12). The coefficient of thermal expansion of the $[0]_{12}$ laminate in the 90° direction increased with temperature from 23.93 μ/°C at 24 °C to 45.82 μ/°C at 177 °C (see Figure 13). The coefficient of thermal expansion of the $[0/90]_{3S}$ laminate in the 0° direction decreased with temperature from 2.034 μ/°C at 24 °C to 0.088 μ/°C at 177 °C (see Figure 14). These results show good agreement with published data for carbon/epoxy and carbon/bismaleimide laminates available in the literature [24,52-54].

4.3.1.4 Stress Free Temperature

Stress free temperature (T_{SFT}) measurements were performed on the IM6/BT3008 $[0/90]_{3S}$ laminates. Three specimens measuring 13.97 x 1.27 cm were machined from the laminates with the long dimension oriented at 0°. The thickness of the specimens was reduced by surface grinding on one side until a layup of [0/90/0/90/0/90/90] was achieved. The resulting asymmetry in the layup caused significant out-of-plane warpage in the specimens. To remove any moisture introduced during machining, the specimens were heated in an oven at 50 °C for 24 hr. in the presence of a desiccant then cooled in a desiccator. The T_{SFT} was determined by placing the specimens in an air-circulating oven and heating them at 2.8 °C per minute. During heating, the specimens were observed through a viewing port in the door of the oven. As the temperature of the samples increased, the out-of-plane warpage was reduced. Between 121 and 127 °C, the specimens became flat indicating a T_{SFT} of approximately 124 °C. Heating of the specimens continued to 177 °C. As expected, the out-of-plane warpage of the specimens increased once again but in the opposite direction. The specimens were then cooled to 24 °C at 2.8 °C per minute. The behavior of the specimens during cooling was consistent with that during heating. Based on these results, a T_{SFT} of 124 °C was assumed for all of the IM6/BT3008 laminates. This value is consistent with the exotherm observed at approximately 120 °C during cure of the IM6/BT3008 panels.

4.3.2 IM7/5250-4

Physical and mechanical properties were not characterized for the IM7/5250-4 system in the present study. However, limited mechanical property data for IM7/5250-4 were obtained from BASF Structural Materials, Inc. [43]. These data are presented in Table 14. A comparison of Tables 14 and 12 indicates that the mechanical properties of the IM7/5250-4 system are superior to those of the IM6/BT3008 system at 24 °C. While some inherent improvement was expected for the IM7/5250-4 system, it is likely that fiber waviness induced in the IM6/BT3008 by the wet filament winding process is responsible for much of this difference. As expected, the higher T_g of the 5250-4 resin (see Section 4.1) results in improved property retention at elevated temperature for IM7/5250-4 relative to IM6/BT3008.

Coefficient of thermal expansion (CTE) data for IM7/5250-4 obtained from BASF Structural Materials, Inc. [43] are presented in Table 15. Unfortunately, no temperature range was reported for the measurements. A comparison of Table 15 and Figure 13 indicates that the transverse (90°) CTE reported for IM7/5250-4 falls within the range calculated for IM6/BT3008 in the present study (see Section 4.3.1.3). However, a comparison of Table 15 and Figure 12 indicates that the longitudinal (0°) CTE reported for IM7/5250-4 is well below the range calculated for IM6/BT3008 in the present study (see Section 4.3.1.3). This discrepancy may be the result of less than optimal interfacial bonding in the IM6/BT3008 system. This proposition is consistent with the lower than expected translation of fiber tensile strength and modulus for IM6/BT3008 (see Section 4.3.1.2). As indicated previously, no attempt was made to optimize the fiber sizing for the BT3008 resin system as is customary in many commercial prepreg systems.

Table 14. Mechanical property data for IM7/5250-4 [43].

Property[1]	Test Method	Temperature [°C]		
		24	177	232
σ_{t11} [MPa]	ASTM D3039	2618	2550	2550
E_{t11} [GPa]	ASTM D3039	162	162	N/A[2]
σ_{t22} [MPa]	ASTM D3039	66	N/A[2]	N/A[2]
E_{t22} [GPa]	ASTM D3039	9.7	N/A[2]	N/A[2]
σ_{c11} [MPa]	ASTM D3410	1820	1310	N/A[2]
E_{c11} [GPa]	ASTM D3410	158	158	N/A[2]
σ_{c22} [MPa]	ASTM D695[3]	248	N/A[2]	N/A[2]
E_{c22} [GPa]	ASTM D695[3]	9.7	N/A[2]	N/A[2]
S_{12} [MPa]	ASTM D3518	103	N/A[2]	N/A[2]
G_{12} [GPa]	ASTM D3518	5.9	N/A[2]	N/A[2]

[1]Properties determined at fiber volume fraction of 0.60.
[2]Data not available.
[3]Modified version of standard test method.

Table 15. Coefficient of thermal expansion (CTE) data for IM7/5250-4 [43].

Property	Value
Longitudinal (0°) CTE [μ/°C]	-1.62
Transverse (90°) CTE [μ/°C]	30.06

5.0 THERMO-MECHANICAL ANALYSIS

Limited analytical work was performed to predict the response of IM6/BT3008 laminates to unconstrained, fully-constrained and over-constrained thermal cycling from 24 to 177 °C. The predictions were based on classical laminate theory and the temperature-dependent lamina physical/mechanical properties presented in Section 4.3.1. Predicted quantities include the laminate strain, constraining force and ply stresses as a function of temperature. Detailed results are presented for the $[0/90]_{3S}$ layup. These results are compared with experimental data in Section 6.0. Results of parametric studies are presented to demonstrate the sensitivity of the analysis with respect to the temperature-dependence of the lamina properties, the nonlinear stress-strain response and the laminate stress free temperature. Finally, several additional cases are presented for illustrative purposes. These cases include variations in the layup and variations in the temperature at which the constraint is applied.

5.1 ANALYTICAL METHODS

5.1.1 Computer Code Generation

A computer code was generated to perform the thermo-mechanical analysis. The code is based on classical laminate theory and is written in FORTRAN and compiled/executed on an 80386 personal computer. The basic structure of the program is similar to that of GENLAM [55]. However, the program has been modified to include temperature-dependent lamina physical/mechanical properties and nonlinear stress-strain response. Input to the program includes the degree of constraint, the upper (T_{MAX}) and lower (T_{MIN}) bounds of the thermal cycle, the laminate stress free temperature (T_{SFT}), the laminate stacking sequence or layup, the temperature-dependent lamina physical/mechanical properties for the composite,

and the nonlinear stress-strain response where applicable. Temperature-dependent lamina properties are entered as polynomials (i.e. $E_{11} = C_0 + C_1T + C_2T^2 + \ldots$). Nonlinear stress-strain response is considered only for resin dominated properties such as transverse modulus (E_{22}) and shear modulus (G_{12}). In such cases, stress-strain curves at various temperatures in the range of interest are fitted to polynomials (i.e. $\sigma_{22} = C_0 + C_1\epsilon_{22} + C_2\epsilon_{22}^2 + \ldots$). The corresponding moduli are determined by differentiation (i.e. $E_{22} = C_1 + C_2\epsilon_{22} + C_3\epsilon_{22}^2 + \ldots$). Linear interpolation is used to determine the response at intermediate temperatures.

The code begins its calculations at T_{SFT} and steps the temperature down to T_{MIN} in 5.6 °C increments. This imparts the correct residual stress distribution in the laminate at the start of the thermal cycle. For most of the cases considered here, the laminate is unconstrained during this portion of the cycle. The temperature-dependent lamina physical/mechanical properties are determined at the midpoint of each temperature interval. The properties dependent on nonlinear stress-strain response are determined at the midpoint of each temperature interval and at the corresponding lamina strain. For each temperature step in the unconstrained condition, the code outputs the laminate strains in the reference coordinate system (X and Y) and the ply stresses in the principal material directions (1 and 2). In the present study, the X-direction is set parallel to the 0° plies in the laminate (see Figure 15). Upon reaching the constraint temperature (T_{CON}), the code applies the appropriate boundary conditions to the laminate. For most of the cases considered here, T_{CON} corresponds to T_{MIN} and the constraint is applied by fixing the laminate strain in the X-direction (i.e. $\epsilon_{XX} = 0$ for full-constraint). After the temperature reaches T_{MIN}, the code steps the temperature up to T_{MAX} in 5.6 °C increments. Lamina physical/mechanical properties are determined as described previously. For each temperature step in the constrained condition, the code outputs the laminate strains (ϵ_{XX} and ϵ_{YY}), constraining force per unit width (N_{XX}) and ply stresses (σ_{11}, σ_{22} and τ_{12}).

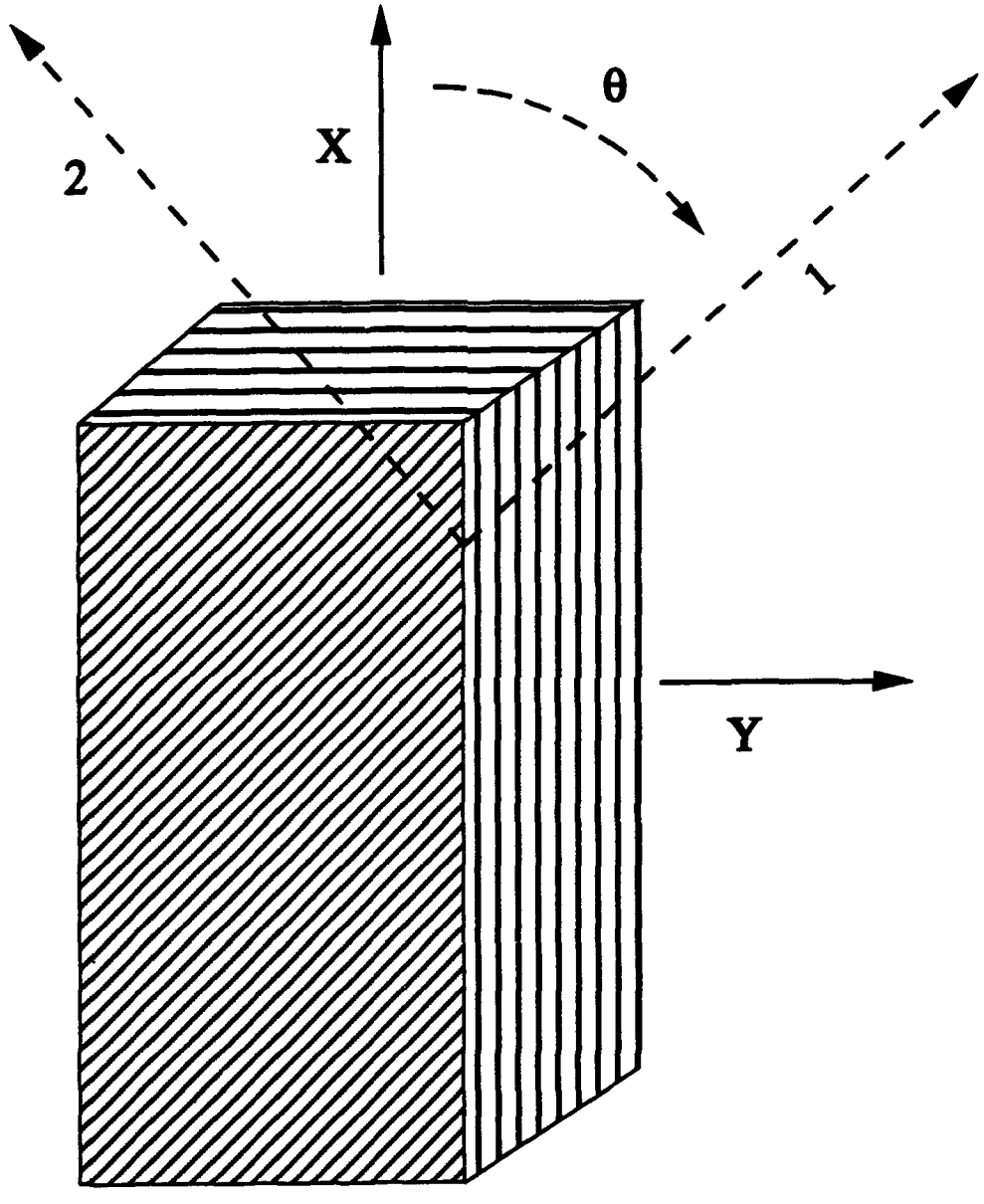

Figure 15. Coordinate systems utilized in thermo-mechanical analysis.

5.1.2 Baseline Analysis

After the computer code was generated, debugged and verified against GENLAM [55], a baseline analysis was performed for an IM6/BT3008 $[0/90]_{3S}$ laminate (T_{SFT} = 124 °C) subject to unconstrained and fully-constrained thermal cycling from 24 to 177 °C. For the fully-constrained condition, the following boundary condition was imposed on the laminate at the constraint temperature (T_{CON} = 24 °C):

$$\epsilon_{XX} = 0 \tag{5.1}$$

where ϵ_{XX} is the laminate strain in the X-direction. Results of the baseline analysis are presented in Section 5.2.1.

5.1.3 Parametric Studies

After the baseline analysis was completed, a series of parametric studies were performed to determine the sensitivity of the analysis with respect to the temperature-dependence of the lamina properties, the nonlinear stress-strain response and the laminate stress free temperature. The temperature-dependence of the lamina properties and laminate stress free temperature were expected to have a significant impact on the ply stress predictions. The nonlinear stress-strain response was expected to have a relatively minor effect on the ply stress predictions for the $[0/90]_{3S}$ laminate due to the absence of shear strains in the plies. However, nonlinear stress-strain response was expected to play a greater role in determining the ply stresses in laminates containing a large percentage of off-axis plies in which shear strains are present.

5.1.3.1 Nonlinear Stress-Strain Response

To illustrate the effects of nonlinear stress-strain response, the baseline analysis was repeated without introducing the strain dependence of the transverse and shear moduli of the lamina. Alternatively, chord moduli from 0.1 to 0.3 percent strain were entered as polynomials (i.e. $E_{22} = C_0 + C_1T + C_2T^2 + \ldots$). Results for the parametric study concerning nonlinear stress-strain response are presented in Section 5.2.2.1.

5.1.3.2 Temperature-dependent Properties

To demonstrate the effects of the temperature-dependent lamina mechanical properties, the baseline analysis was repeated using only the lamina property data generated at 24 °C (see Section 4.3.1). It is important to note that no changes were made to the temperature-dependent lamina CTE's. It should also be noted that the nonlinear stress-strain response, while minimal, was considered in the determination of the transverse and shear moduli at 24 °C. Results for the parametric study concerning temperature-dependent properties are presented in Section 5.2.2.2.

5.1.3.3 Stress Free Temperature

To illustrate the effects of the laminate stress free temperature (T_{SFT}), the baseline analysis was repeated with T_{SFT} set at 179 °C rather than 124 °C. All other parameters were consistent with the original baseline analysis. It should be noted that the choice of 179 °C was not arbitrary. Initially, the maximum cure temperature (T_{CURE}) was to be used for this calculation since it is often assumed that $T_{SFT} = T_{CURE}$. However, for the IM6/BT3008 material, T_{CURE} was 200 °C while mechanical property data was determined only up to 177 °C. A lower value of T_{SFT} (179 °C) was chosen to avoid errors resulting from extrapolating

the mechanical property data beyond the upper bound of the available test results. Results for the parametric study concerning stress free temperature are presented in Section 5.2.2.3.

5.1.4 Additional Cases of Interest

5.1.4.1 Alternative Layups

Significant changes in response to both unconstrained and constrained thermal cycling can be expected with changes in layup. While a complete treatment of alternative layups is well beyond the scope of this thesis, two cases of practical importance are considered. The first case illustrates the effects of varying the ratio of 90° plies to 0° plies in a cross-ply laminate subject to unconstrained and fully-constrained thermal cycles from 24 to 177 °C. The analysis was performed for IM6/BT3008 laminates with stacking sequences of $[0/90_m]_S$ where m = ⅓, ½, 1, 2 and 3. The second case illustrates the effects of off-axis plies in a laminate subject to unconstrained and fully-constrained thermal cycles from 24 to 177 °C. This analysis was performed for an IM6/BT3008 laminate with a $[0/90/\pm45]_S$ layup. For both cases, all parameters with the exception of the layup were consistent with the baseline analysis. Results for the two cases involving alternative layups are presented in Section 5.2.3.1.

5.1.4.2 Over-Constrained Cycling

The baseline analysis examined the fully-constrained case with the constraint temperature (T_{CON}) set at 24 °C. This case is representative of a structure for which the composite sub-components are manufactured separately and attached in a secondary operation which takes place at ambient temperature and provides a precise fit-up with no gaps or pre-stress. The composite sub-components exhibit residual stresses imposed during

cool-down from the processing temperature due to the mismatch in CTE between the constituents and between plies of different orientations (see Section 2.2.2). No external constraint is present at ambient temperature. On heating, the composite expands/contracts against the surrounding structure which remains fixed due to large thermal mass or active cooling systems. The resulting stresses are superimposed on the residual stresses which are locked-in by the constraint. An alternative case of practical importance is the over-constrained case with T_{CON} set at 24 °C. This case is representative of structures similar to those of the baseline case but lacking large thermal mass or active cooling systems. In such cases, the composite sub-components are forced to expand/contract by the surrounding structure which is typically composed of a metal alloy with a relatively large CTE. A very large difference in CTE between the metal alloy and composite can result in ply stresses which approach the static strength of the lamina.

To illustrate the effects of over-constrained thermal cycling, an analysis was performed for an IM6/BT3008 $[0/90]_{3S}$ laminate subject to over-constrained thermal cycling from 24 to 177 °C. The parameters used in the analysis were similar to those used for the baseline case including T_{CON} which remained at 24 °C. However, the full-constraint condition ($\epsilon_{XX} = 0$) imposed at T_{CON} in the baseline analysis was replaced by an over-constrained condition defined as follows:

$$\epsilon_{XX} = \alpha_{CON}(T - T_{CON}) \tag{5.2}$$

where ϵ_{XX} is the laminate strain in the X-direction, α_{CON} is the CTE of the material applying the constraint and T is the temperature at the midpoint of the current temperature interval. It should be emphasized that this constraint condition assumes that the structure imposing the constraint is much stiffer than the composite sub-component due to a larger cross-section and/or higher modulus material. Two variations of this case are presented, one for a Ti-6Al-4V structure with a composite sub-component and one for an 6061-T6 Al structure with a

composite sub-component. CTE data for these materials relative to the IM6/BT3008 composite are given in Table 16. The results for the over-constrained cases are presented in Section 5.2.3.2.

Table 16. Coefficient of thermal expansion (CTE) data for various materials.

Material	CTE [μ/°C]	
	24 °C	177 °C
6061-T6 Aluminum[1]	23.6	23.6
Titanium - 6% Aluminum - 4% Vanadium (Ti-6Al-4V)[1]	9.5	9.5
IM6/BT3008 $[90]_n$	23.93	45.82
IM6/BT3008 $[0]_n$	0.404	-1.149

[1]Data from reference [56].

5.1.4.3 Constraint Temperature

The temperature at which the constraint is applied can have a significant impact on the ply stresses generated during thermal cycling. To illustrate the effect of T_{CON}, an analysis was performed for an IM6/BT3008 $[0/90]_{3S}$ laminate subject to over-constrained thermal cycling from 24 to 177 °C. The parameters used for the analysis were similar to those used for the over-constrained analysis described in Section 5.1.4.2. In this case, however, T_{CON} was set at the stress free temperature of the laminate (124 °C). This case is representative of a structure for which the composite sub-components are cured in-situ with the surrounding structure. Two variations of this case are presented, one for a Ti-6Al-4V structure with co-cured composite sub-components and one for an 6061-T6 Al structure with co-cured composite sub-components. The results for these cases are presented in Section 5.2.3.3.

5.2 ANALYTICAL RESULTS

The results of the analytical studies are presented in the following sections. Emphasis is placed on the ply stresses as a function of temperature during the first thermal cycle. The laminate strain (unconstrained cycling) and constraining force (fully-constrained and over-constrained cycling) are compared with experimental data in Section 6.0 to validate the analyses. As indicated previously, every effort has been made to account for changes in lamina physical/mechanical properties with temperature and for nonlinear stress-strain response where applicable. However, the analysis does not account for time-dependent deformation (creep and stress relaxation), matrix yielding, microcracking or other damage which may accumulate during the first or subsequent cycles.

5.2.1 Baseline Analysis

The baseline analysis was performed for an IM6/BT3008 $[0/90]_{3S}$ laminate (T_{SFT} = 124 °C) subject to unconstrained and fully-constrained thermal cycling from 24 to 177 °C. The 0° ply stresses in the X-direction are given as a function of temperature in Figure 16 for both the unconstrained and fully-constrained cases. The 90° ply stresses in the X-direction are given in Figure 17. As expected the effects of full-constraint are greater for the 0° plies which carry a larger portion of the load. The 0° plies in the unconstrained laminate experience stresses in the range from -17.2 to 10.5 MPa while the 0° plies in the fully-constrained laminate experience stresses in the range from -17.2 to -23.2 MPa. The 90° plies in the unconstrained laminate experience stresses in the range from 17.2 to -10.5 MPa while the 90° plies in the fully-constrained laminate experience stresses in the range from 17.2 to -12.0 MPa. The Y-direction ply stresses in the fully-constrained laminate are within 4% of those in the unconstrained laminate. The small difference can be attributed to Poisson effects.

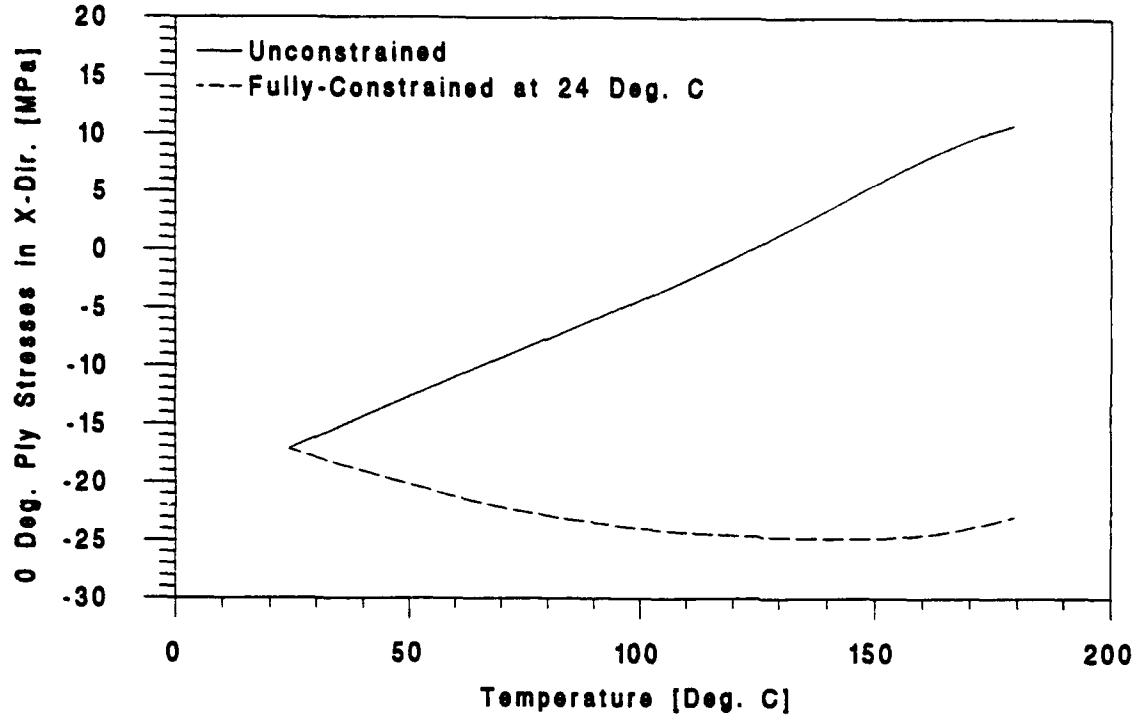

Figure 16. 0° ply stresses in X-direction during unconstrained and fully-constrained thermal cycling of IM6/BT3008 $[0/90]_{3S}$.

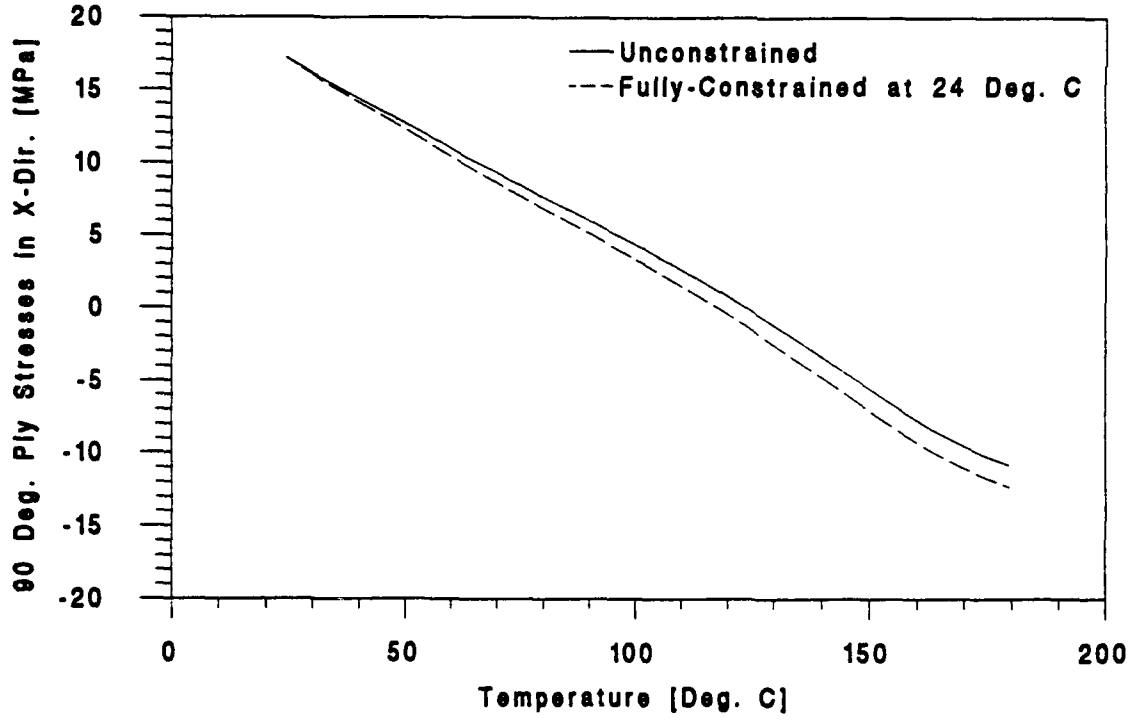

Figure 17. 90° ply stresses in X-direction during unconstrained and fully-constrained thermal cycling of IM6/BT3008 $[0/90]_{3S}$.

At first glance, the changes in the X-direction ply stresses with full-constraint may appear insignificant relative to the ply strengths reported in Section 4.3.1.2. The 0° ply stress in the constrained laminate at 177 °C is -23.2 MPa versus a 0° compressive strength of at least -317 MPa. The 90° ply stress in the constrained laminate at 177 °C is -12.0 MPa versus a 90° compressive strength of -53.1 MPa. However, three additional points should be considered. First, it is not a static failure that is of concern here but rather the development of fatigue damage in the material over an extended service life. Second, the effects of time-dependent deformation (creep and/or stress relaxation) may lead to changes in the ply stress distribution over time. These effects are of particular concern for the 90° plies in the constrained laminate where the stress level at 177 °C is approximately 23% of the strength. Finally, the ply stresses presented here do not take into account any external service loads applied to the laminate. Superposition of stresses resulting from such loads could further reduce the safety factors for ply failure.

5.2.2 Parametric Studies

5.2.2.1 Nonlinear Stress-Strain Response

To illustrate the effects of nonlinear stress-strain response, the baseline analysis was repeated without introducing the strain dependence of the lamina transverse and shear moduli. The 0° ply stresses in the X-direction calculated with and without the nonlinear stress-strain response are given as a function of temperature in Figure 18. The 90° ply stresses in the X-direction calculated with and without the nonlinear stress-strain response are given in Figure 19. As expected, the effects of nonlinear stress-strain response are minimal for the $[0/90]_{3S}$ laminate in the unconstrained and fully-constrained conditions. The error in the ply stress predictions introduced by omitting the nonlinear stress-strain response is less than 5% for the unconstrained laminate and less than 4% for the constrained laminate. It

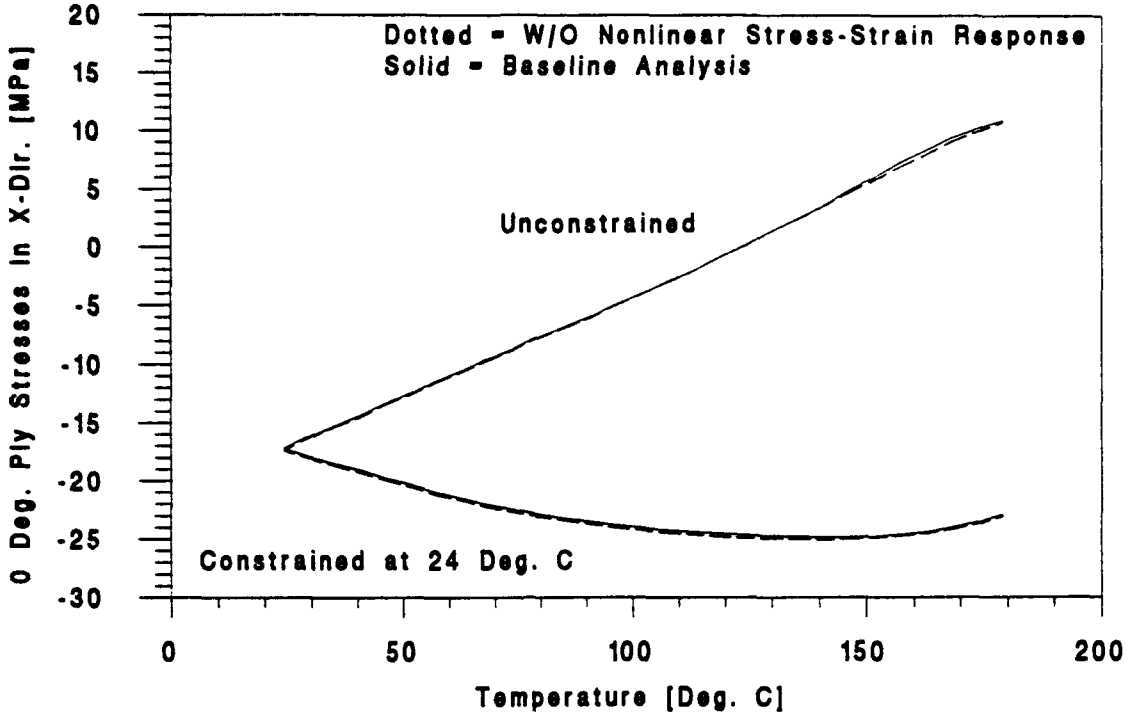

Figure 18. Effects of nonlinear stress-strain response on 0° ply stresses in X-direction during thermal cycling.

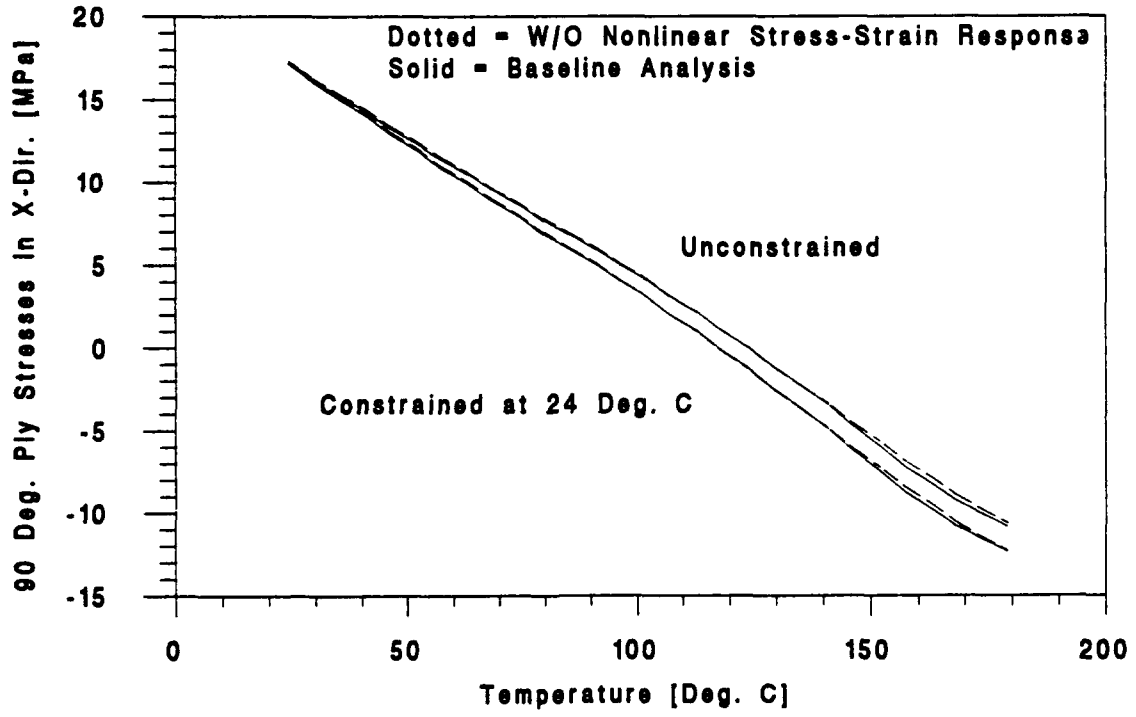

Figure 19. Effects of nonlinear stress-strain response on 90° ply stresses in X-direction during thermal cycling.

useful to note that although the error in the predictions is small, it is nonconservative in some cases.

5.2.2.2 Temperature-Dependent Properties

To demonstrate the effects of temperature-dependent lamina mechanical properties, the baseline analysis was repeated using only the lamina mechanical property data generated at 24 °C. No changes were made to the temperature-dependent lamina CTE's. Nonlinear stress-strain response was considered in the determination of the transverse and shear moduli at 24 °C. The 0° and 90° ply stresses in the X-direction calculated with and without the temperature-dependent lamina properties are given as a function of temperature in Figures 20 and 21, respectively. As expected, the temperature-dependence of the lamina properties has a significant impact on the ply stress predictions. For unconstrained and fully-constrained laminates at 24 °C, the error in the 0° and 90° ply stress predictions introduced by omission of temperature-dependent properties from the model is 13%. For the unconstrained laminate at 177 °C, the error in the 0° and 90° ply stress predictions is 49%. For the fully-constrained laminate at 177 °C, the error in the 0° ply stress predictions is 20% and the error in the 90° ply stress predictions is 51%. In all cases, the error in the ply stress predictions is conservative.

5.2.2.3 Stress Free Temperature

To illustrate the effects of laminate stress free temperature (T_{SFT}), the baseline analysis was repeated with T_{SFT} set at 179 °C rather than 124 °C. All other parameters were consistent with the original baseline analysis. The 0° and 90° ply stresses in the X-direction calculated with T_{SFT} set at 124 and 179 °C are given as a function of temperature in Figures 22 and 23 respectively. As expected, the stress free temperature has a significant impact on

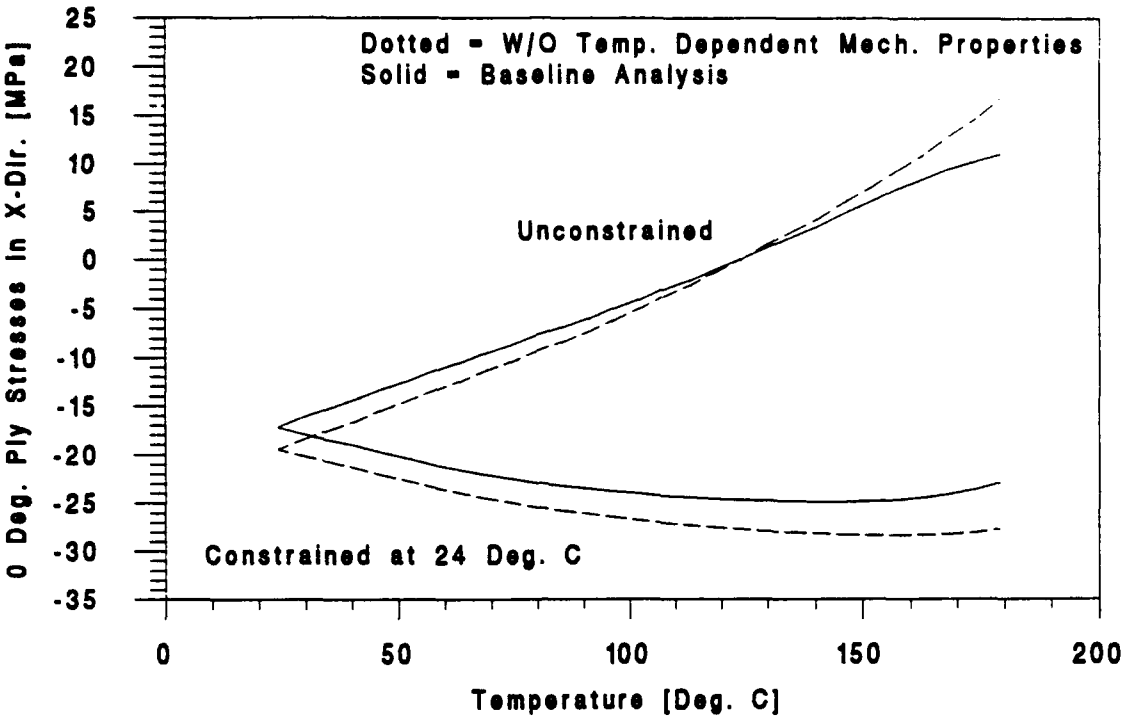

Figure 20. Effects of temperature-dependent properties on 0° ply stresses in X-direction during thermal cycling.

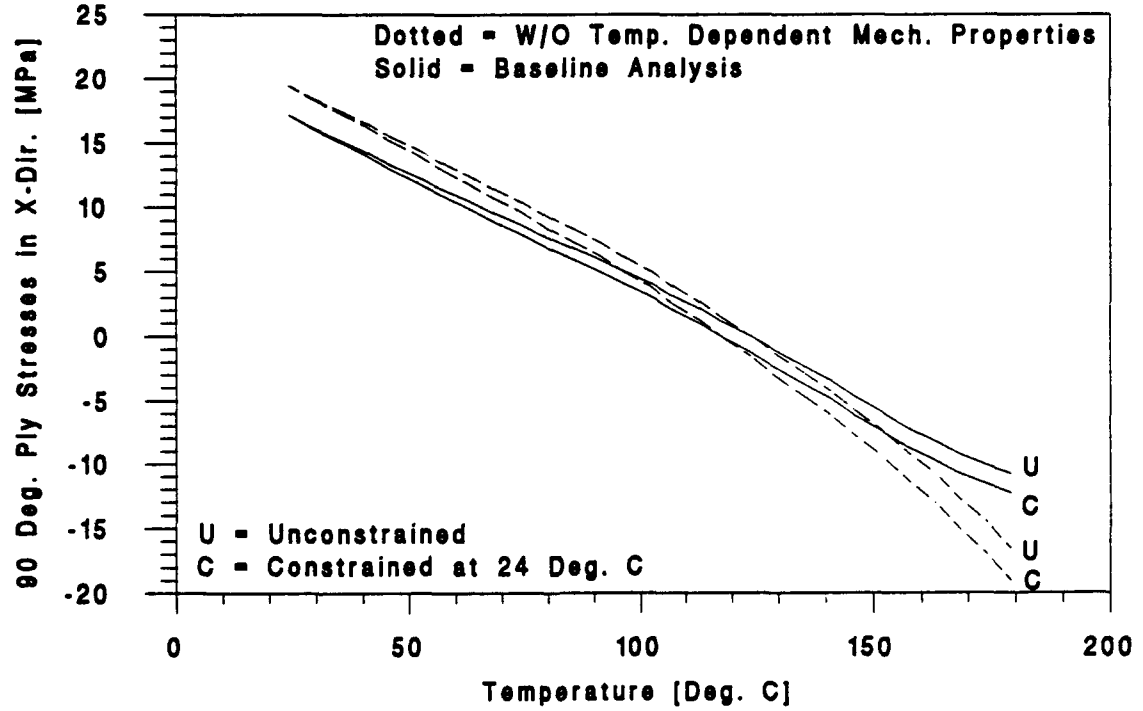

Figure 21. Effects of temperature-dependent properties on 90° ply stresses in X-direction during thermal cycling.

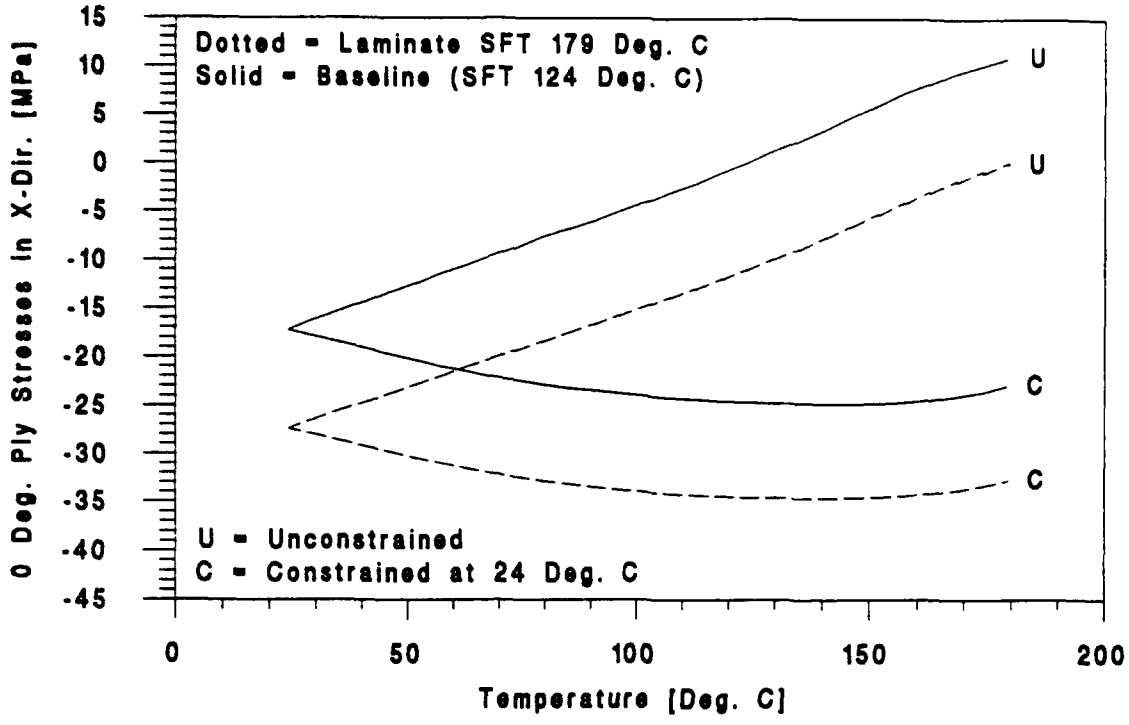

Figure 22. Effects of stress free temperature on 0° ply stresses in X-direction during thermal cycling.

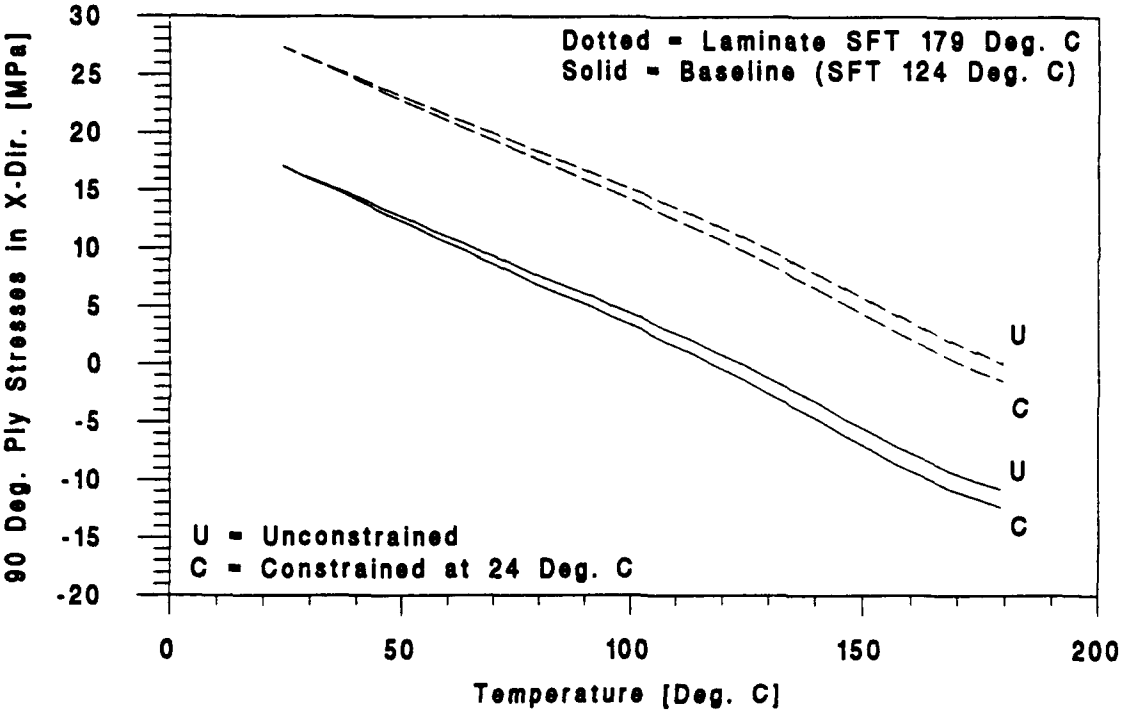

Figure 23. Effects of stress free temperature on 90° ply stresses in X-direction during thermal cycling.

the ply stress predictions. For unconstrained and fully-constrained laminates at 24 °C, the error in the 0° and 90° ply stress predictions resulting from overestimating T_{SFT} is 59%. For the unconstrained laminate at 177 °C, the error in the 0° and 90° ply stress predictions is 107%. For the fully-constrained laminate at 177 °C, the error in the 0° ply stress predictions is 42% and the error in the 90° ply stress predictions is 91%.

It is apparent from this analysis that assuming a stress free temperature higher than the actual value can result in a substantial overprediction of the tensile stresses present in the 90° plies at 24°C. Increasing T_{SFT} from 124 to 179 °C increases the predicted value of the 90° ply stress at 24 °C from 17.2 to 27.4 MPa. The 90° tensile strength of IM6/BT3008 is 39 MPa at 24 °C. Thus the 55 °C increase in T_{SFT} increases the 90° ply stress from 44% to 70% of the static strength. Had the stress free temperature been set at the cure temperature (200 °C) as is often the case when T_{SFT} is not known, the predicted value of the 90° ply stress would have been even higher. Such assumptions could be defended on the basis of conservatism in design. However, inflation of safety factors to this degree may result in over-design and structural inefficiency to the extent that the composite is deemed unsuitable for the application, when in fact it is perfectly adequate.

5.2.3 Additional Cases of Interest

5.2.3.1 Alternative Layups

It is instructive to consider the response of layups other than the $[0/90]_{3S}$ baseline when they are exposed to thermal cycling in the unconstrained and fully-constrained conditions. Two cases of practical importance are presented here. The first case illustrates the effects of varying the ratio of 90° plies to 0° plies in a cross-ply laminate. The analysis was performed for IM6/BT3008 laminates with stacking sequences of $[0/90_m]_S$ where m = ⅓, ½, 1, 2 and 3. All parameters with the exception of the layup were consistent with the

baseline analysis. The 0° and 90° ply stresses in the X-direction for each layup are given as a function of temperature in Figures 24 and 25 respectively. As expected, the ply stresses change considerably with the value of m. In general, the differences between ply stresses in unconstrained and fully-constrained laminates increase with m. In most cases, the extrema in the ply stress values also increase with m. For example, in both unconstrained and fully-constrained laminates at 24 °C, the 0° ply stress in the X-direction increases from -5.77 MPa for m = ⅓ to -47.6 MPa for m = 3. In unconstrained laminates at 177 °C, the 0° ply stress in the X-direction increases from 3.51 MPa for m = ⅓ to 29.6 MPa for m = 3. In fully-constrained laminates at 177 °C, the 0° ply stress in the X-direction increases from -11.1 MPa for m = ⅓ to -53.9 MPa for m = 3 and the 90° ply stress in the X-direction increases from -11.2 MPa for m = ⅓ to -13.5 MPa for m = 3. However, the opposite trend is observed in several cases. In unconstrained and fully-constrained laminates at 24 °C, the 90° ply stress in the X-direction decreases from 17.3 MPa for m = ⅓ to 15.9 MPa for m = 3. For the unconstrained laminates at 177 °C, the 90° ply stress in the X-direction decreases from -10.5 MPa for m = ⅓ to -9.85 MPa for m = 3. While the changes in the X-direction ply stresses with m may appear small relative to the ply strengths reported in Section 4.3.1.2, one must consider the arguments put forth in Section 5.2.1 with respect to fatigue endurance limits, time-dependent deformation and superposition of stresses due to service loads.

The second case illustrates the effects of off-axis plies in a laminate. This analysis was performed for an IM6/BT3008 laminate with a $[0/90/\pm45]_S$ layup. All parameters with the exception of the layup were consistent with the baseline analysis. The results of the analysis for the $[0/90/\pm45]_S$ layup are somewhat unexpected. For unconstrained cycling, the ply stresses in the $[0/90/\pm45]_S$ laminate were identical to those in the $[0/90]_{3S}$ laminate (see Section 5.2.1). For fully-constrained cycling, the ply stresses in the $[0/90/\pm45]_S$ laminate are equal or slightly lower than those in the $[0/90]_{3S}$ laminate with the exception of the 90° ply stress in the Y-direction. A small shear stress is also developed in the $[0/90/\pm45]_S$ laminate which is absent in the $[0/90]_{3S}$ laminate. Specifically, the ply stresses in the $[0/90/\pm45]_S$ and

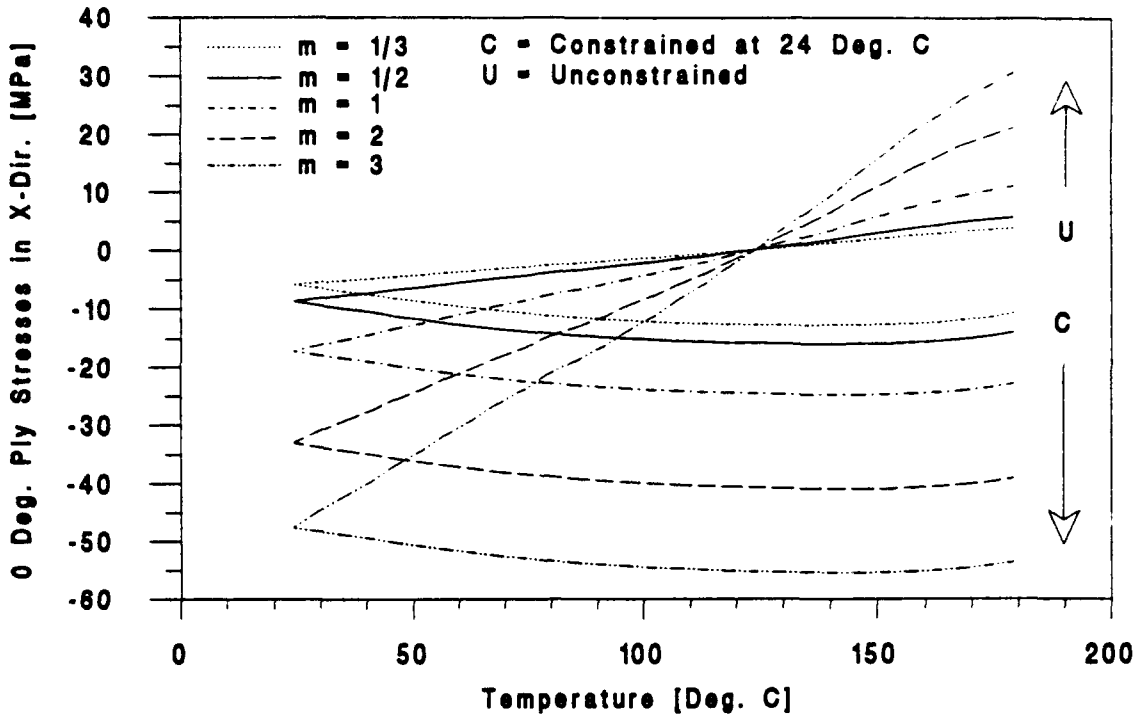

Figure 24. 0° ply stresses in X-direction during unconstrained and fully-constrained thermal cycling of IM6/BT3008 $[0/90_m]_S$.

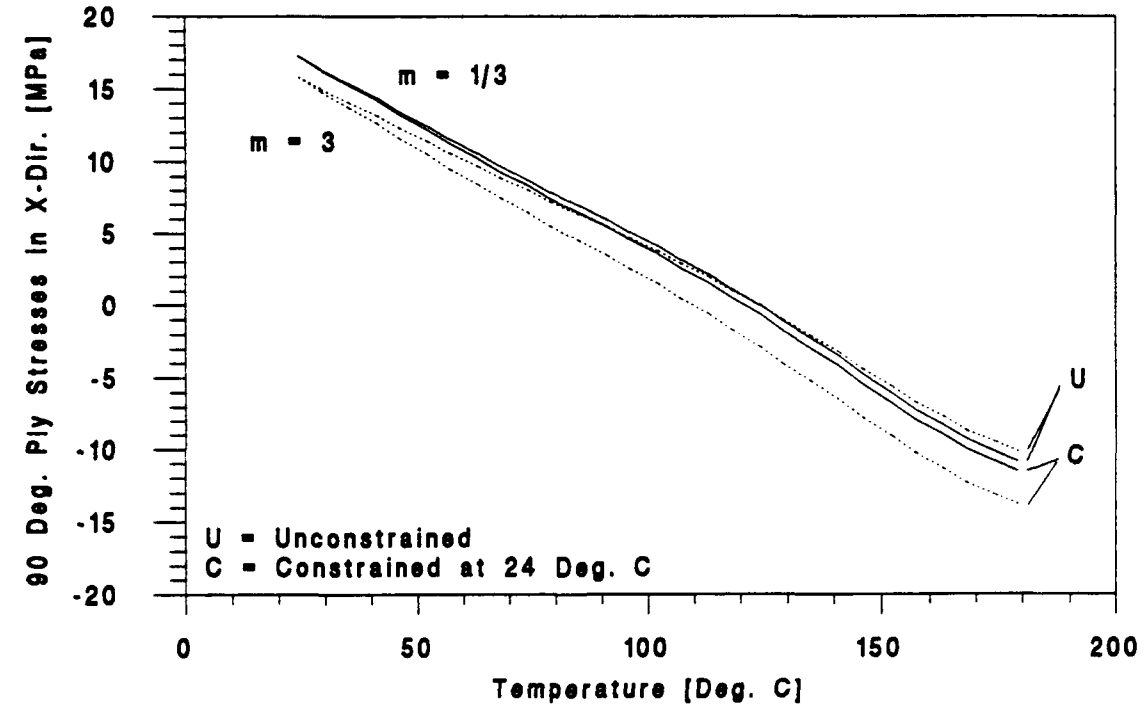

Figure 25. 90° ply stresses in X-direction during unconstrained and fully-constrained thermal cycling of IM6/BT3008 $[0/90_m]_S$.

$[0/90]_{3S}$ laminates are equal at 24 °C where the constraint is applied. At 177 °C, the 0° ply stress in the X-direction is 1% lower in the $[0/90/\pm45]_S$ laminate compared to the $[0/90]_{3S}$ laminate while the 90° ply stress in the X-direction is 2% lower. The 0° ply stress in the Y-direction is 6% lower in the $[0/90/\pm45]_S$ laminate compared to the $[0/90]_{3S}$ laminate. The 90° ply stress in the Y-direction is 121% higher but is still less than 2% of the longitudinal tensile strength at this temperature. The longitudinal and transverse stresses in the ±45° plies of the $[0/90/\pm45]_S$ laminate are lower than those in either the 0° or 90° plies in the $[0/90]_{3S}$ laminate. The in-plane shear stress in the ±45° plies increases from 0 MPa at 24 °C to 1.81 MPa at 177 °C. The lamina in-plane shear strength of IM6/BT3008 at 177 °C is 46.2 MPa. Based on these results, the response of $[0/90/\pm45]_S$ laminates to unconstrained and fully-constrained cycling from 24 to 177 °C is expected to be similar to that of $[0/90]_{3S}$ laminates in the absence of superimposed service loads.

5.2.3.2 Over-Constrained Cycling

To illustrate the effects of over-constrained thermal cycling, an analysis was performed for an IM6/BT3008 $[0/90]_{3S}$ laminate. The parameters used in the analysis were similar to those used for the baseline case. However, the full-constraint condition defined in Equation 5.1 was replaced by the over-constrained condition defined in Equation 5.2. As noted previously, two variations of this analysis were performed, one using a value of α_{CON} corresponding to Ti-6Al-4V and one using a value of α_{CON} corresponding to 6061-T6 Al.

The 0° and 90° ply stress predictions for the $[0/90]_{3S}$ layup subject to thermal cycling in the unconstrained, fully-constrained and over-constrained conditions are presented in Figures 26 and 27 respectively. As expected, the ply stresses developed with a 6061-T6 Al constraint are more severe than those with a Ti-6Al-4V constraint due to the higher coefficient of thermal expansion of 6061-T6 Al. For the 6061-T6 Al constraint, the 0° ply stress in the X-direction ranges from -17.2 MPa at 24 °C to 501 MPa at 177 °C. The 90°

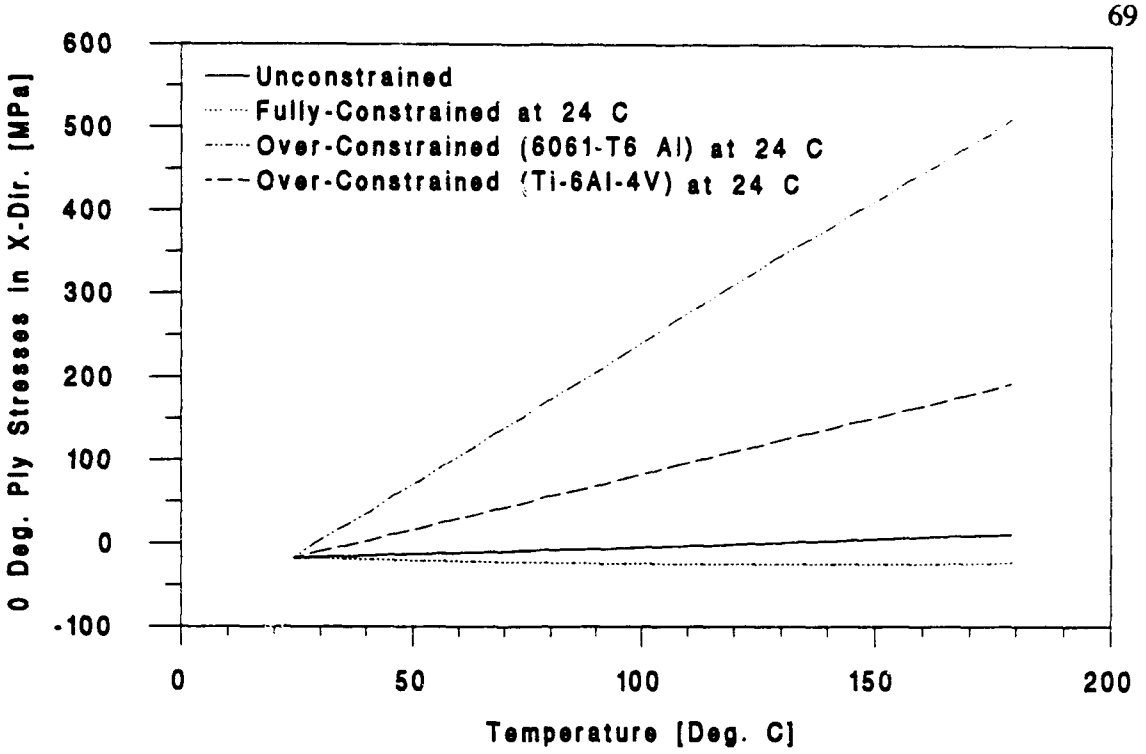

Figure 26. 0° ply stresses in X-direction during over-constrained thermal cycling of IM6/BT3008 $[0/90]_{3S}$.

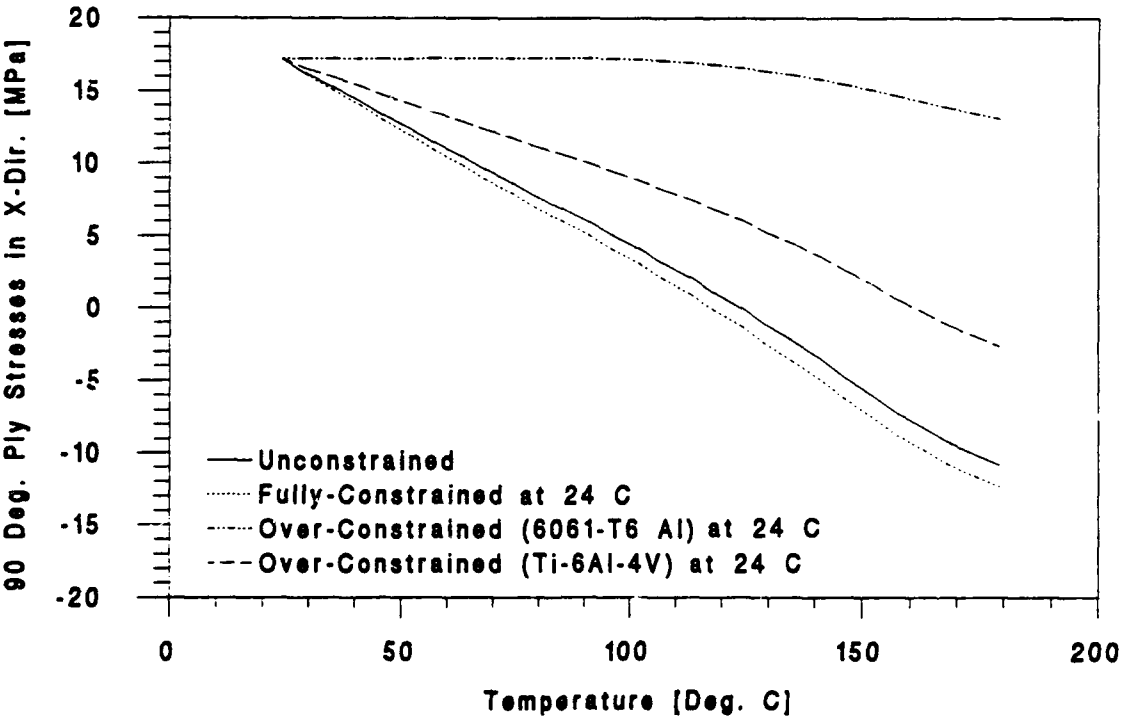

Figure 27. 90° ply stresses in X-direction during over-constrained thermal cycling of IM6/BT3008 $[0/90]_{3S}$.

ply stress in the X-direction varies from 17.2 MPa at 24 °C to 13.3 MPa at 177 °C. Significant nonlinearity is observed in the 90° ply stress at elevated temperature. The 90° ply stress at 177 °C is 77% of the transverse tensile strength. An exact value for the longitudinal tensile strength was not obtained for the IM6/BT3008 material (see Section 4.3.1). However, based on the available data, the 0° ply stress at 177 °C may be as much as 35% of the longitudinal tensile strength. These results indicate that over-constrained cycling with a 6061-T6 Al constraint (T_{CON} = 24 °C) represents a very severe service condition relative to unconstrained or fully-constrained cycling. Fortunately, the ply stresses developed during thermal cycling in the over-constrained condition can be reduced by increasing T_{CON} to the stress free temperature of the laminate (see Section 5.2.3.3). In actual structures, this can be achieved by in-situ curing of the composite subcomponents (see Section 5.1.4.3).

5.2.3.3 Constraint Temperature

To illustrate the effect of T_{CON}, an analysis was performed for an IM6/BT3008 $[0/90]_{3S}$ laminate subject to over-constrained thermal cycling with T_{CON} set at the stress free temperature of the laminate (124 °C). All other parameters were similar to those used for the over-constrained cases in Section 5.1.4.2. The 0° and 90° ply stresses in the X-direction for over-constrained cycling of the $[0/90]_{3S}$ laminate with T_{CON} at 24 and 124 °C are given in Figure 28 and 29 respectively. These results show that for the 6061-T6 Al constraint, the extrema in the 90° ply stress decrease as a percentage of the lamina strength with an increase in T_{CON} from 24 to 124 °C. With T_{CON} at 24 °C, the 90° ply stress in the X-direction is 44% of the transverse tensile strength at 24 °C and 77% of the transverse tensile strength at 177 °C. With T_{CON} at 124 °C, the 90° ply stress in the X-direction is 2% of the transverse tensile strength at 24 °C and 7% of the transverse compressive strength at 177 °C. Increasing T_{CON} from 24 to 124 °C also decreases the 0° ply stress in the X-direction by

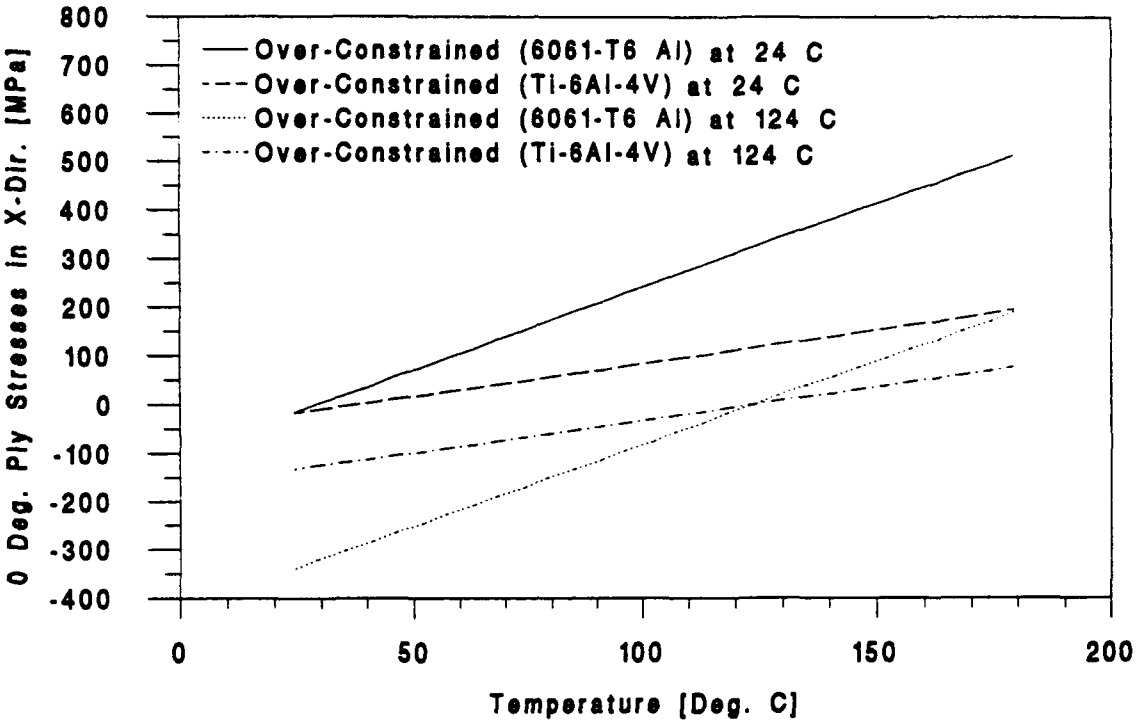

Figure 28. Effects of constraint temperature on 0° ply stresses in X-direction during thermal cycling.

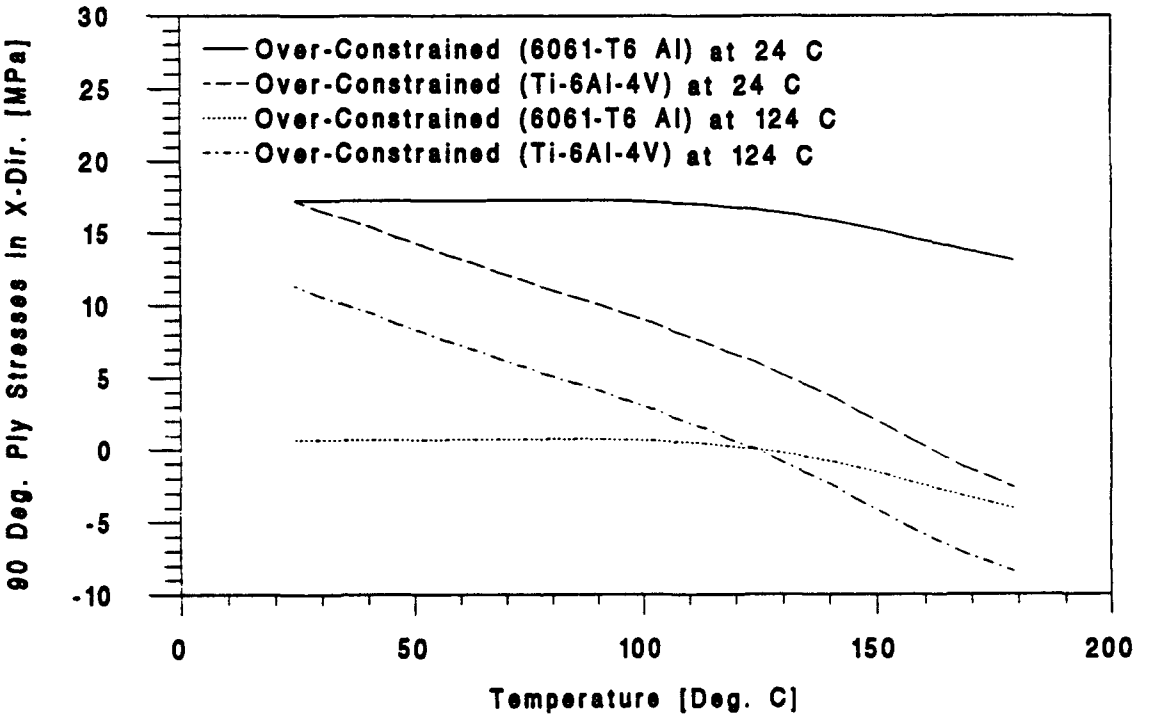

Figure 29. Effects of constraint temperature on 90° ply stresses in X-direction during thermal cycling.

65% at 177 °C. The 0° ply stress in the X-direction increases by a factor of 19 at 24 °C but even with the increase it is only 26% of the longitudinal compressive strength. These results suggest that in-situ curing should be considered as a means for reducing ply stresses and increasing fatigue life in composite sub-components which will experience over-constrained thermal cycling.

6.0 THERMO-MECHANICAL FATIGUE TESTING

Thermal and thermo-mechanical fatigue tests were conducted on IM6/BT3008 $[0/90]_{3S}$ and IM7/5250-4 $[0/90]_{5S}$ laminates. Thermal fatigue tests consisted of unconstrained thermal cycling from 24 to 177 °C. Thermo-mechanical fatigue tests consisted of fully-constrained and over-constrained thermal cycling from 24 to 177 °C. Details of the test methods and test results are provided below.

6.1 EXPERIMENTAL METHODS

6.1.1 Specimen Preparation

The specimen utilized for the thermal and thermo-mechanical fatigue tests was based on the compression test specimen described in ASTM D3410. A schematic of the test specimen is provided in Figure 30. This specimen was selected for its ability to accommodate tensile or compressive loads during thermo-mechanical tests. The specimens were fabricated according to the procedures outlined in the following paragraph.

Coupons measuring 13.97 x 1.27 cm were machined from the IM6/BT3008 $[0/90]_{3S}$ and IM7/5250-4 $[0/90]_{5S}$ laminates. The coupons were oriented with the long dimension at 0°. End tabs were machined from the IM6/5250-4 $[0/90)_3/0]_S$ panel. The end tabs were oriented with the long dimension at 0°. Machining was performed according to the procedures outlined in section 4.2.3. The end tabs were bonded to the specimens with American Cyanamid HT 424 film adhesive. After end tab bonding, one edge of each specimen was polished using 220, 320, 500, 800, 1000, 1200, 2400 and 4000 grit Al_2O_3 papers and 1 μm Al_2O_3 suspension on polishing cloth. Polishing was necessary to permit examination of the gauge section with an optical microscope prior to and following thermal and thermo-mechanical cycling. After polishing, the length and width of each specimen were measured

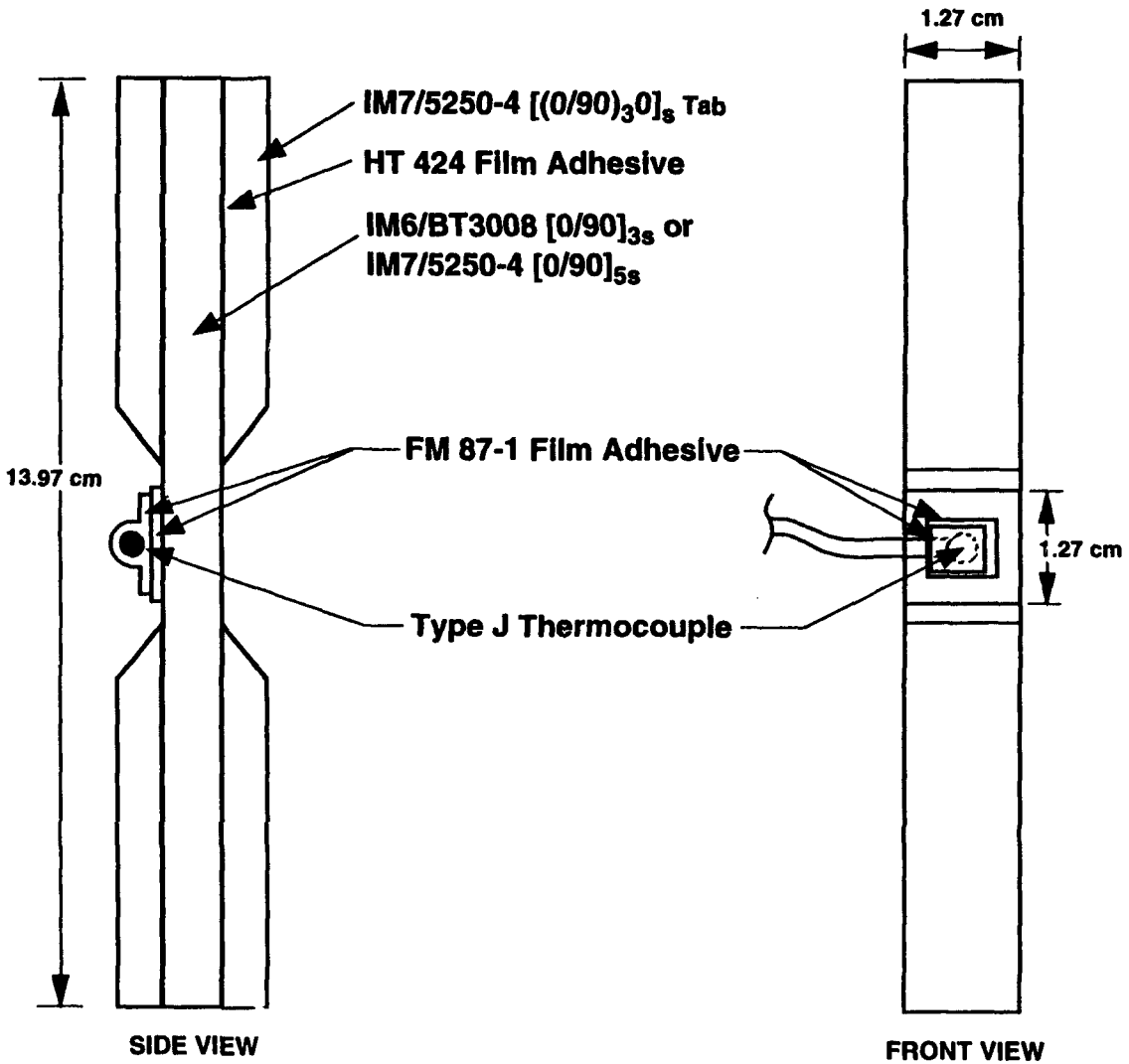

Figure 30. Thermo-mechanical fatigue test specimen.

to the nearest 0.0025 mm at the center of the gauge section. A type J thermocouple was bonded to each specimen at the center of the 1.27 x 1.27 cm gauge section. Bonding was accomplished in two steps. First two plies of American Cyanamid FM 87-1 film adhesive were applied to the specimen and fully cured. These plies were necessary to electrically isolate the thermocouple from the conductive composite. Next, the thermocouple was bonded to the specimen using two additional plies of FM 87-1.

6.1.2 Test Equipment

Thermal and thermo-mechanical fatigue tests were conducted on an Instron 8500 servohydraulic test frame equipped with hydraulic grips and a dynamic extensometer. Heating of the sample gauge section was accomplished using 120 VAC, 7.75 kW/m^2, silicone rubber heating tapes from Cole Parmer Instrument Company, Chicago, Illinois. These tapes are subject to a maximum temperature limit of 260 °C. Cooling was accomplished with 69 kPa forced air. Data acquisition and control of the temperature, load and strain set points were accomplished with an 80386 25 MHz personal computer equipped with a Keithley Metrabyte DAS-16 data acquisition and control board, a set of CP Clare 10 amp solid state relays (OFA 1210-2), and a non-inverting amplifier with a ±15 VDC power supply. A schematic showing a sample loaded in the test fixture is given in Figure 31. A schematic describing the operation of the test equipment is provided in Figure 32.

To start the test, the operator inputs the level of constraint, constraint temperature (T_{CON}), the number of cycles to complete (N_{CYC}), the maximum temperature for the cycle (T_{MAX}), the minimum temperature for the cycle (T_{MIN}) and the four-character prefix for the output files. At the start of the first cycle, the computer opens a text file (i.e. CYCL0001.OUT) for output. The thermal cycle begins at T_{MIN}. The computer closes the heating relay and begins to monitor the heat tape temperature (T_{TAPE}), sample temperature (T_{SAM}), load (P) and strain (ε). The load (unconstrained cycling) or strain (constrained

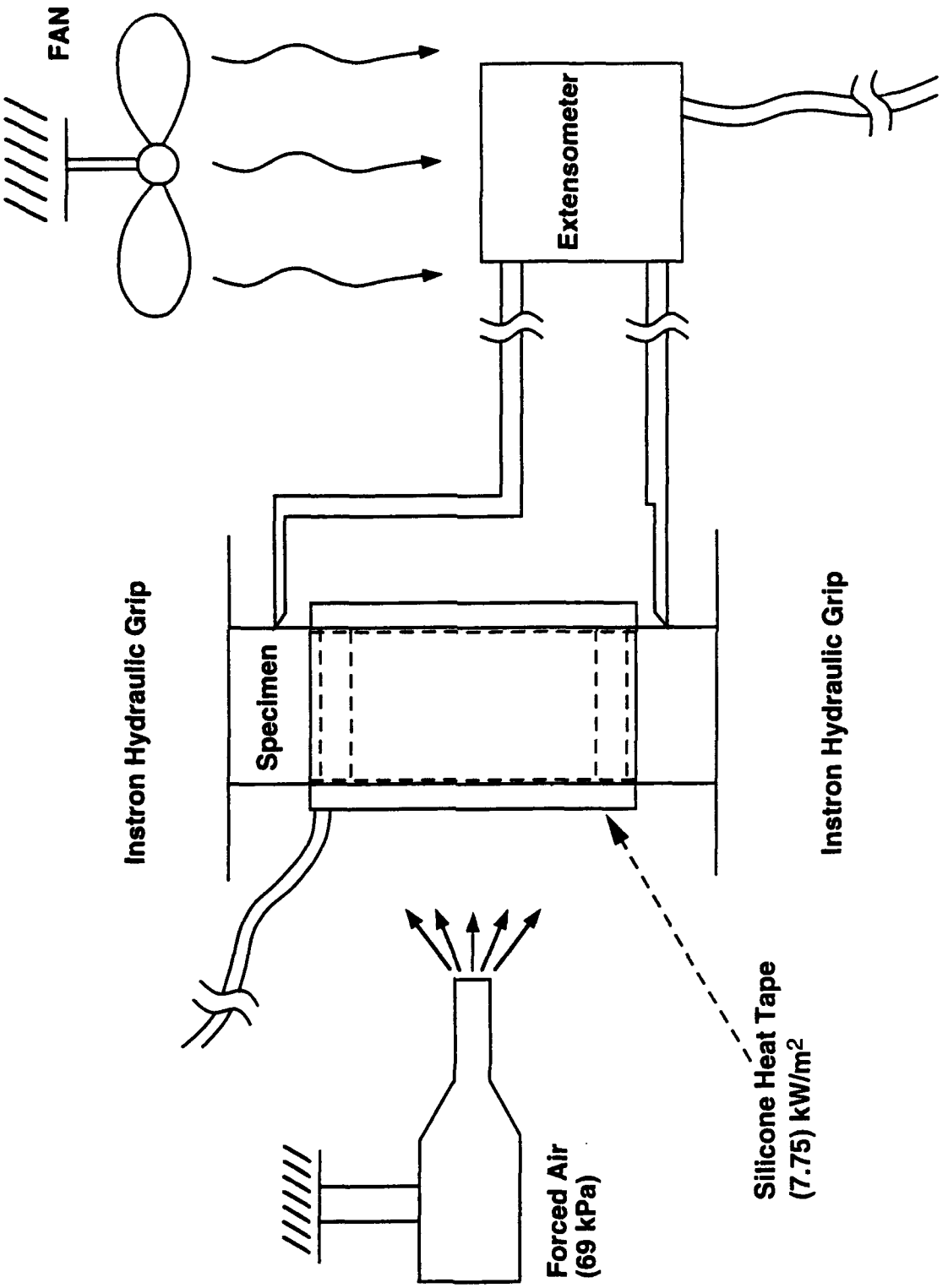

Figure 31. Thermo-mechanical fatigue test fixture.

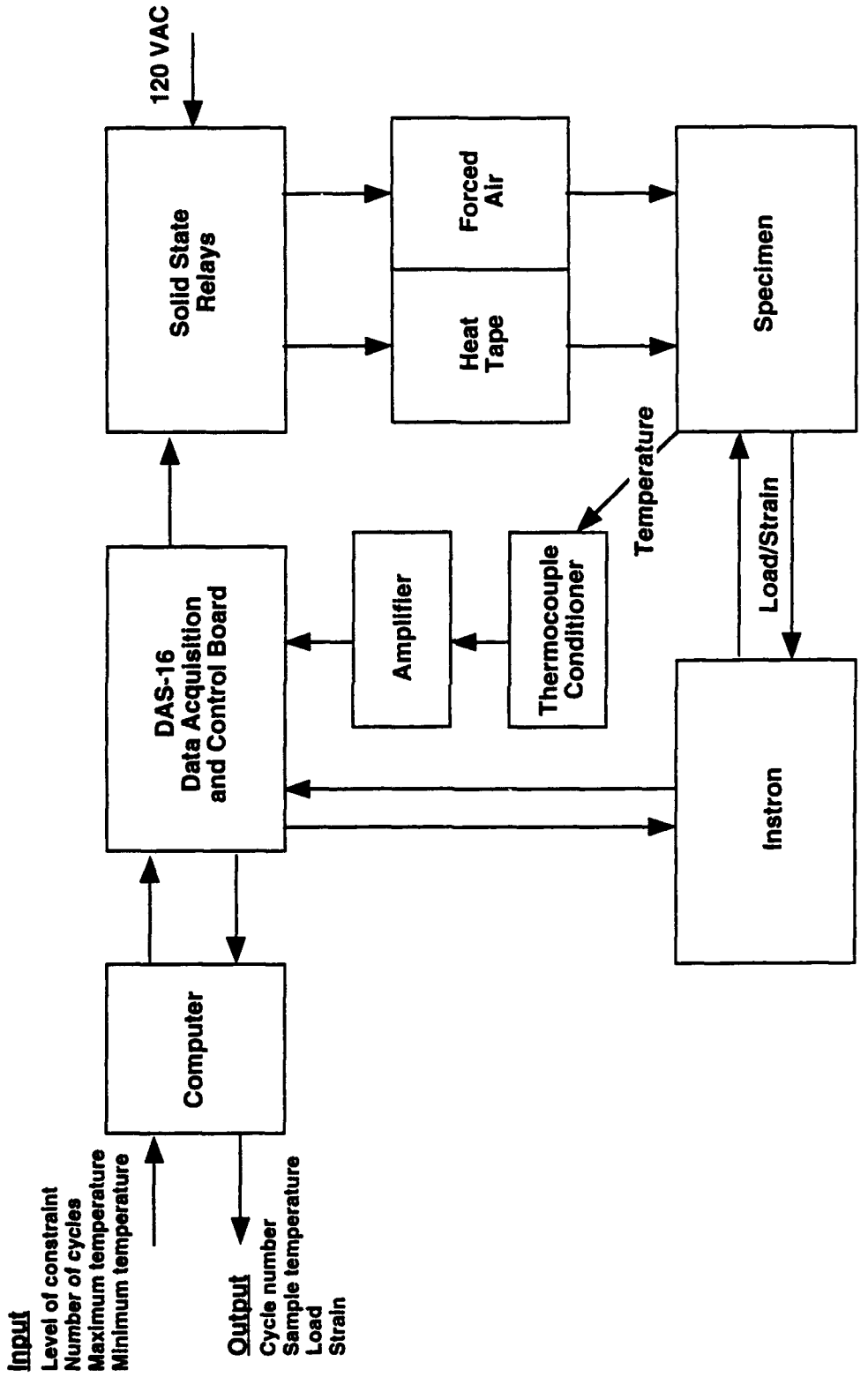

Figure 32. Thermo-mechanical fatigue test equipment.

cycling) is compared with the set point and a feedback signal is output to the Instron to adjust the reading. T_{TAPE}, T_{SAM}, P and e readings are written to the text file when $T_{SAM} = T_{MIN}$ and at 5 °F increments on T_{SAM} thereafter. The heating rate is controlled by the parameters K1 and K2:

$$K1 = T_{SAM} + (T_{SAM} / 2.5) \tag{6.1}$$

$$K2 = T_{SAM} + [(T_{SAM} / 2.5) - 5] \tag{6.2}$$

While $T_{TAPE} < K1$, the heating relay remains closed. When $T_{TAPE} > K1$, the heating relay is opened and it remains open until $T_{TAPE} < K2$ at which point it closes again. This sequence repeats itself until the $T_{SAM} = T_{MAX}$. When $T_{SAM} > T_{MAX}$, the heating relay opens and the cooling relay closes. Data continues to be written to the output file at 5 °F increments on T_{SAM}.

6.1.3 Preliminary Tests

A series of preliminary tests were performed to verify the specimen design and test equipment and to establish detailed procedures for performing unconstrained, fully-constrained and over-constrained tests. The resulting test methods are discussed individually in Section 6.1.4.1 through 6.1.4.3.

A preliminary test was also performed to characterize the temperature gradient in the sample during thermal cycling and to verify that the location selected for bonding the thermocouple was appropriate. An IM6/BT3008 sample was selected and instrumented with several type J thermocouples. Thermocouple #1 was bonded to the surface of the sample in the center of the gauge section. This was the location proposed for all coupons in the test matrix. Thermocouple #2 was bonded to the surface of the sample at the top of the gauge section adjacent to the edge of the tab. Additional thermocouples were embedded in the

sample at the center of the gauge section (#3), at the top of the gauge section (#4) and 1.27 cm above the top of the gauge section (#5). The sample was loaded into the test fixture as shown in Figure 31 and was subjected to ten thermal cycles from 24 to 177 °C. Readings from all thermocouples were recorded at 15 second intervals. Readings for thermocouples #1 through #4 in the gauge section were within a ±2.8 °C range over the 24 to 177 °C interval for all cycles. The reading for thermocouple #5 outside the gauge section lagged by approximately 28 °C. These results indicated that the temperature variation in the gauge section was minimal and that a single thermocouple bonded to the surface at the center of the gauge section was adequate to determine the sample temperature.

Three additional tests were performed to ensure that the temperature cycle was consistent throughout each test and between tests. A different sample was used for each test to evaluate the effects of small variations in the test setup. Data from the three tests (A, B, and C) are given in Figure 33. Little or no variation in the temperature cycle was apparent between cycles in a given test. However, small but significant variations in the temperature cycle were observed between tests. These were attributed to slight differences in the clearance between the heat tape and the individual samples. The most important aspect of the temperature cycle is the asymmetry in the heating and cooling rates. In all cases, the heating rate is significantly lower than the cooling rate, particularly at the upper end of the thermal cycle. The effect of the asymmetry in the heating and cooling rates on the test results is discussed in detail in Section 6.2.

6.1.4 Test Procedures

6.1.4.1 Unconstrained Thermal Cycling

Unconstrained thermal cycling was performed in load control. A load set point of 0 kN was maintained while the sample temperature was cycled between 24 and 177 °C. This

case is identical to the unconstrained case discussed in Sections 5.1.2 and 5.2.1. The laminate strain was monitored as a function of sample temperature for comparison with analytical predications.

6.1.4.2 Fully-Constrained Thermal Cycling

Fully-constrained thermal cycling was performed in strain control. A strain set point of 0 microstrain (μ) was maintained while the sample temperature was cycled between 24 and 177 °C. This case is identical to the fully-constrained case discussed in Sections 5.1.2 and 5.2.1. The load on the laminate was monitored as a function of sample temperature for comparison with analytical predictions.

6.1.4.3 Over-Constrained Thermal Cycling

Over-constrained thermal cycling was performed in strain control. A strain set point of:

$$e_{XX} = 23.6E\text{-}6(T - 24) \tag{6.3}$$

was maintained while the sample temperature was cycled between 24 and 177 °C. This case is identical to the over-constrained case discussed in Sections 5.1.4.2 and 5.2.3.2 where the constraining material is 6061-T6 Al. The load on the laminate was monitored as a function of sample temperature for comparison with analytical predictions.

6.1.4.4 Damage Characterization

After cycling, the polished edge of each coupon was cleaned by wiping carefully with 1,1,1-trichloroethane and was examined using an optical microscope. The presence of matrix

cracks, fiber/matrix disbonds, delaminations and other damage was recorded for comparison with the predicted ply stresses.

6.1.4.5 Residual Mechanical Properties

After damage characterization, the residual compressive strength and modulus of each coupon was measured. The compression tests were performed in a Wyoming modified IITRI test fixture. Strain measurement was accomplished with bonded strain gauges. The method of attachment of the thermocouple precluded the use of back-to-back strain gauges. A single gauge was bonded to the surface of each coupon at the center of the gauge section on the face opposite the thermocouple. Results of preliminary tests performed on coupons without thermocouples indicated that bending effects were negligible below 0.5 percent strain. All modulus measurements were performed using a chord from 0.1 to 0.3 percent strain.

6.2 EXPERIMENTAL RESULTS

6.2.1 IM6/BT3008

6.2.1.1 Unconstrained Thermal Cycling

Experimental values of laminate strain as a function of sample temperature (cycle 1) are given in Figure 34 for a typical IM6/BT3008 sample in the unconstrained condition. The data is compared with the prediction from the baseline analysis (Section 5.1.2). The correlation between the predicted and experimental laminate strains is good during heating to approximately 121 °C at which point the strain begins to drop off from the predicted values. The deviation between the predicted and experimental strain increases with temperature to the upper limit of the cycle (177 °C). On cooling, hysteresis is apparent in

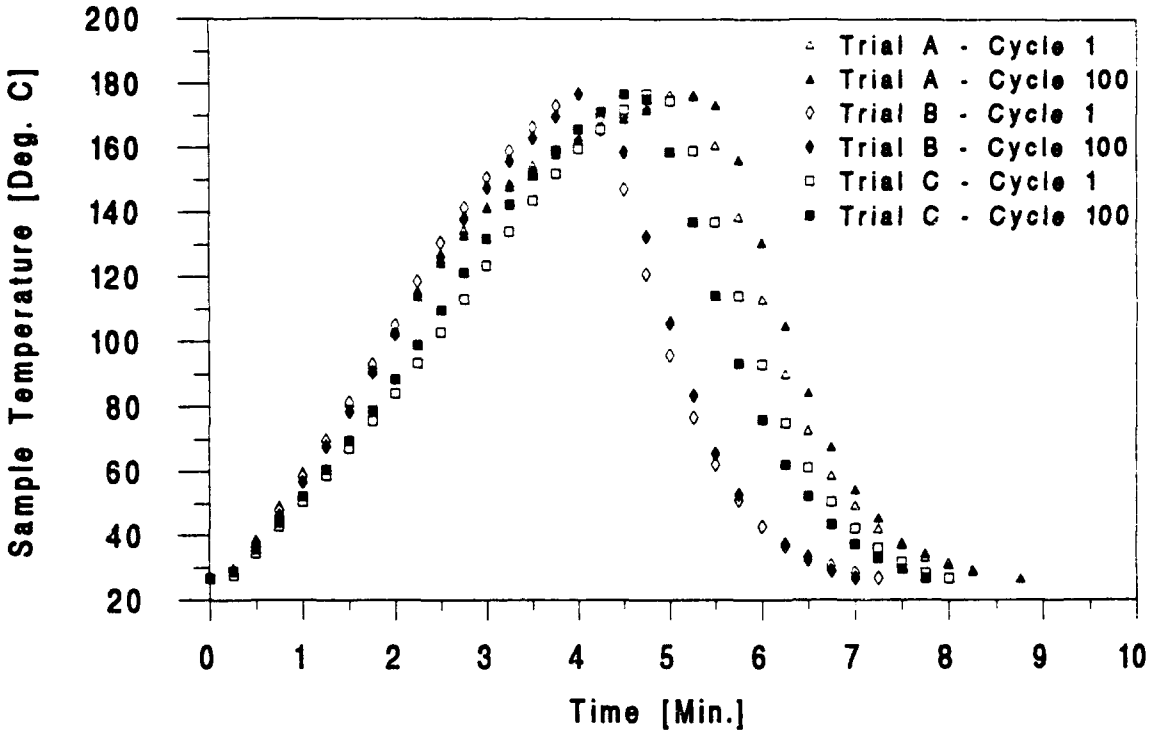

Figure 33. Sample temperature versus time for trials A, B and C (cycles 1 and 100).

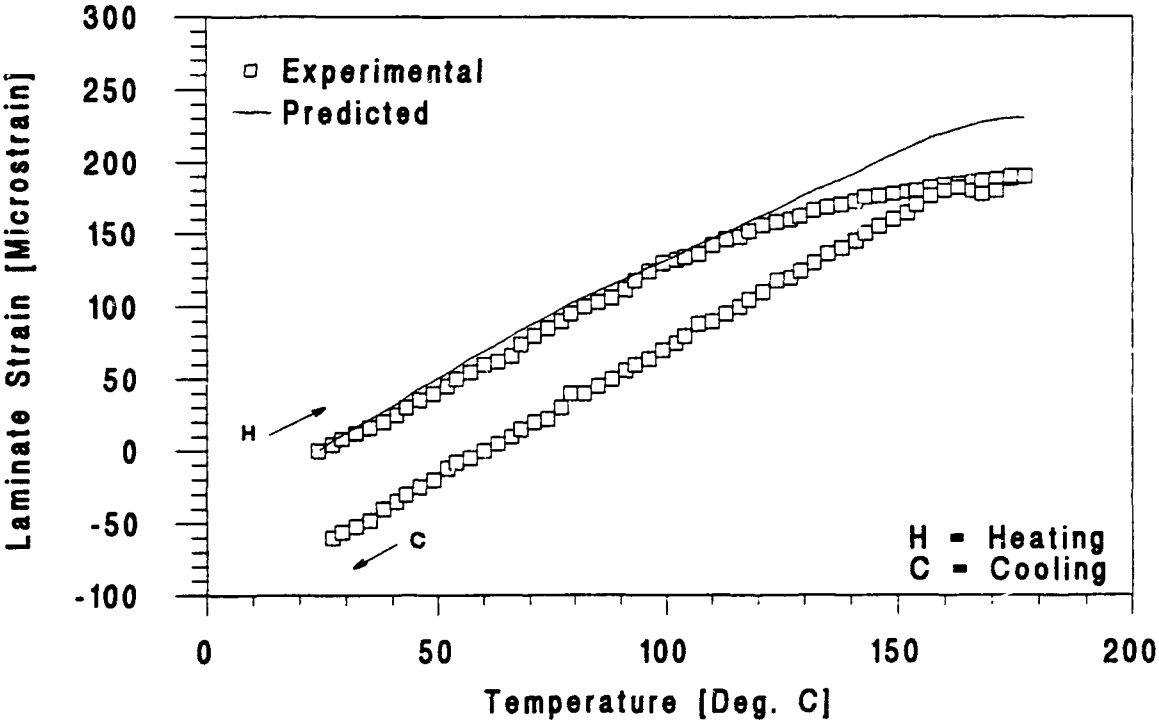

Figure 34. Predicted versus experimental laminate strain as a function of temperature (cycle 1) for IM6/BT3008 $[0/90]_{3S}$ in the unconstrained condition.

the strain-temperature response indicating the presence of permanent deformation in the sample. The hysteresis is attributed to time-dependent deformation in the 90° plies of the laminate. The effects of time-dependent deformation are more pronounced during heating due to the asymmetry in the heating and cooling rates at elevated temperature (Section 6.1.3). Time-dependent deformation was not accounted for in the analytical model which was used to predict the laminate response. Compressive stresses develop in the 90° plies when the laminate is heated above the stress free temperature (124 °C) due to the higher coefficient of thermal expansion of the 90° plies relative to the 0° plies (Section 5.2.1). Relaxation of the compressive stresses appears to occur over time at the higher temperatures, thereby releasing some of the constraint on the 0° plies and allowing them to contract. This results in a net decrease in laminate strain relative to that predicted without accounting for time-dependent deformation.

It is important to emphasize that the time-dependent deformation in the IM6/BT3008 laminate influences the ply stress distribution as well as the net laminate strain. Stress relaxation results in lower compressive stresses in the 90° plies at temperatures above 121 °C than those predicted in the baseline analysis (Section 5.2.1). As a result, the tensile stresses developed in the 90° plies during cooling will be higher than those predicted in the baseline analysis. The baseline analysis predicts a 90° ply stress of 17.2 MPa on cooling to 24 °C. This value corresponds to 44% of the transverse tensile strength of IM6/BT3008 at that temperature. For the sample shown in Figure 6-6, the hysteresis in cycle 1 resulted in a net decrease in laminate strain of approximately 60 μ at 24 °C. This corresponds to an increase of approximately 0.5 MPa in the 90° ply stress at 24 °C, bringing the value to approximately 17.7 MPa or 45% of the transverse tensile strength. This increase, while small, does represent an increase in the potential for microcracking in the 90° plies.

The progression of hysteresis in the laminate strain versus temperature response for the IM6/BT3008 sample in the unconstrained condition is shown in Figure 35 and 36. During cycles 2 through 40, the degree of hysteresis per cycle decreases but the net laminate strain

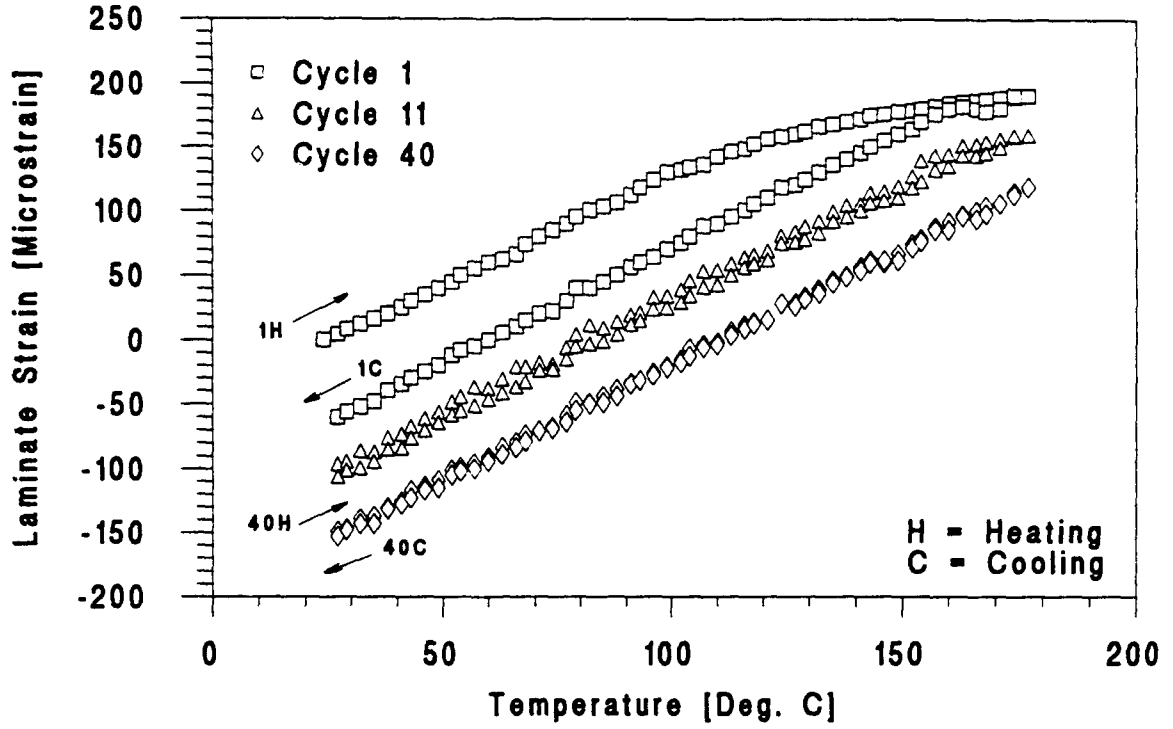

Figure 35. Experimental laminate strain as a function of temperature (cycles 1, 11 and 40) for IM6/BT3008 $[0/90]_{3S}$ in the unconstrained condition.

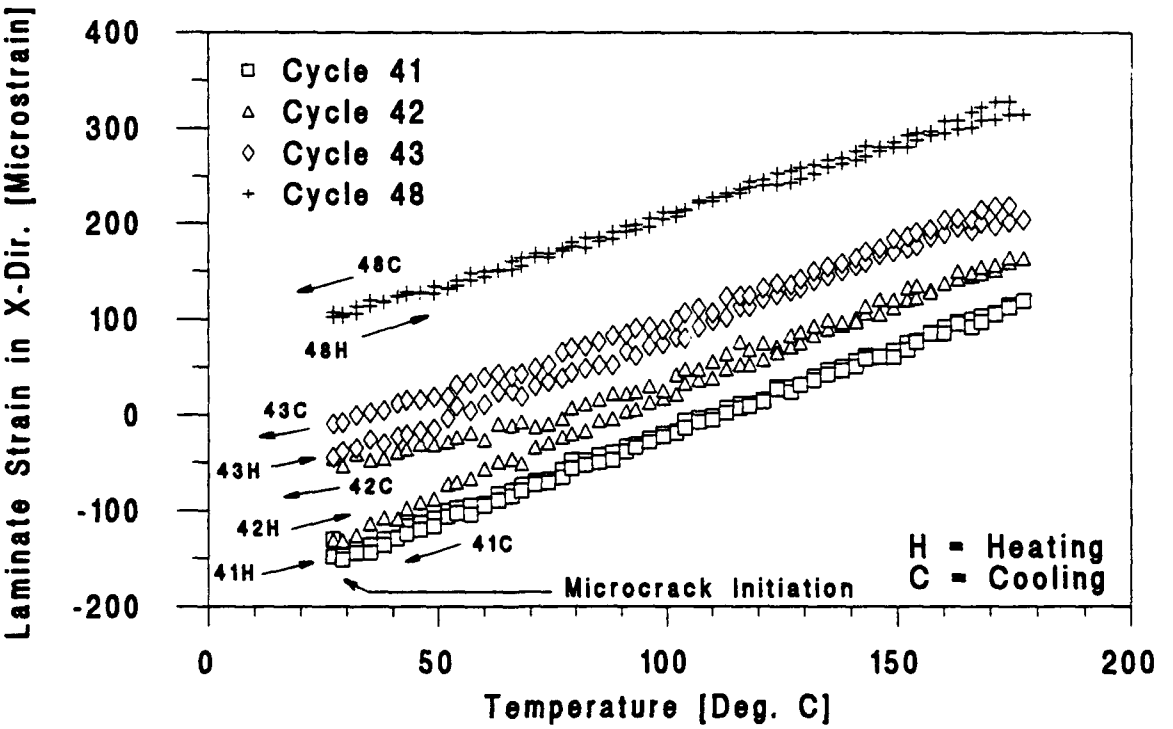

Figure 36. Experimental laminate strain as a function of temperature (cycles 41, 42, 43 and 48) for IM6/BT3008 $[0/90]_{3S}$ in the unconstrained condition.

at 24 °C continues to decrease. At the end of cycle 40, the progressive hysteresis has reduced the laminate strain by approximately 150 μ relative to the start of cycle 1. This corresponds to an increase of approximately 1.3 MPa in the 90° ply stress at 24 °C, bringing the value to approximately 18.5 MPa or 47% of the transverse tensile strength. At the end of cycle 41, there is a sharp increase in laminate strain of approximately 15 μ as the sample temperature approaches 24 °C. The increase in laminate strain is attributed to the initiation of microcracks in the 90° plies. Initiation of microcracks relieves some of the tensile stress in the 90° plies thereby reducing the constraint on the 0° plies and allowing them to expand. This, in turn, results in an increase in the laminate strain.

The data for cycle 42 shows a larger increase in laminate strain than expected for the initial heating portion of the cycle. This result suggests that the microcracks continue to propagate as long as a significant level of tensile stress is present in the 90° plies. As the temperature rises and the tensile stresses in the 90° plies are reduced, the microcracks arrest and the slope of the laminate strain versus temperature curve returns to the previous value. Microcrack propagation resumes during the latter portion of the cooling cycle as the tensile stresses in the 90° plies increase once again. The propagation of microcracks in cycle 42 produces an increase in laminate strain of approximately 85 μ. This process is repeated in cycles 43 through 48. With each cycle, the increase in laminate strain is reduced since the tensile stresses in the 90° plies are relieved by propagation of the microcracks. At the end of cycle 48, the laminate strain has been increased by approximately 260 μ relative to the end of cycle 40. This corresponds to a decrease of approximately 2.3 MPa in the 90° ply stress at 24 °C, bringing the value to approximately 16.2 MPa or 42% of the transverse tensile strength.

After cycle 48, the response of the laminate stabilizes for several cycles possibly due to the microcracks arresting at the adjacent 0° plies. Subsequently, signs of time-dependent deformation reappear at the upper end of the heating cycle and hysteresis becomes apparent on cooling. The degree of hysteresis per cycle is considerably less than the early cycles but

results in a steady decrease in laminate strain until the initiation of additional microcracks and the corresponding increase in laminate strain. This process is repeated throughout the test as shown in Figures 37 and 38. The maximum test duration for the present study was 1000 cycles. For the samples tested in the unconstrained condition, there were no signs of reaching a saturation crack density within 1000 cycles.

The observed changes in the laminate strain versus temperature response of the IM6/BT3008 samples during unconstrained thermal cycling have been attributed to time-dependent deformation in the 90° plies which leads to an increase in ply stress and ultimately to microcracking. This explanation is consistent with the damage observed in the IM6/BT3008 samples after cycling (Table 17). After 1000 cycles in the unconstrained condition, the samples exhibit an average transverse crack density of 29 ± 6 cracks/cm. No reduction in compressive modulus or strength is apparent relative to as-molded samples (Table 18). This is not surprising as the effects of microcracking on compressive properties are *minimized* by crack closure. Had the test duration been extended and delaminations initiated at junctions between microcracks in adjacent plies, it is likely that significant reductions in compressive properties would have been observed.

6.2.1.2 Fully-Constrained Thermal Cycling

Experimental values of constraining force as a function of sample temperature (cycle 1) are given in Figure 39 for a typical IM6/BT3008 sample in the fully-constrained condition. The data is compared with the prediction from the baseline analysis (Section 5.1.2). The prediction fits the data well up to approximately 110 °C. The slight difference in slope is attributed to overprediction of the laminate modulus by the analytical model which is based on classical laminate theory. Above 110 °C, the load begins to drop off from the predicted values. The deviation between the predicted and experimental load increases with temperature to the upper limit of the cycle (177 °C). On cooling, hysteresis is apparent in

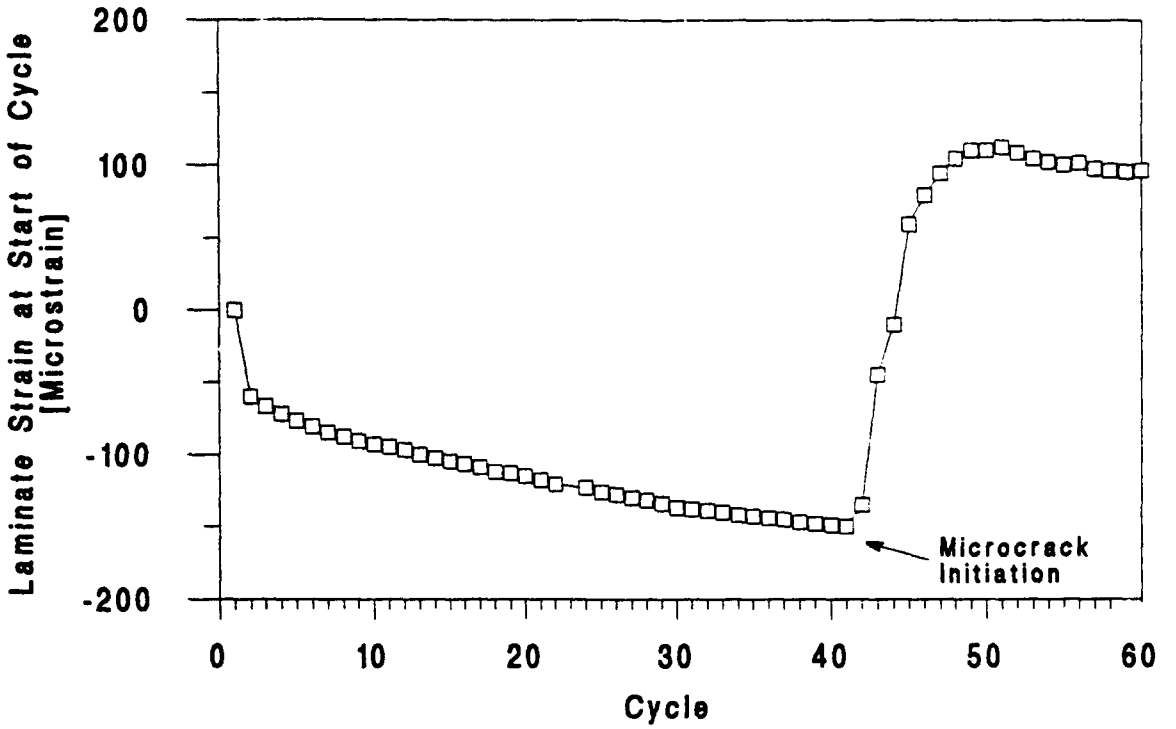

Figure 37. Experimental laminate strain at start of cycle (24 °C) for IM6/BT3008 $[0/90]_{3S}$ in the unconstrained condition (cycles 1 to 60).

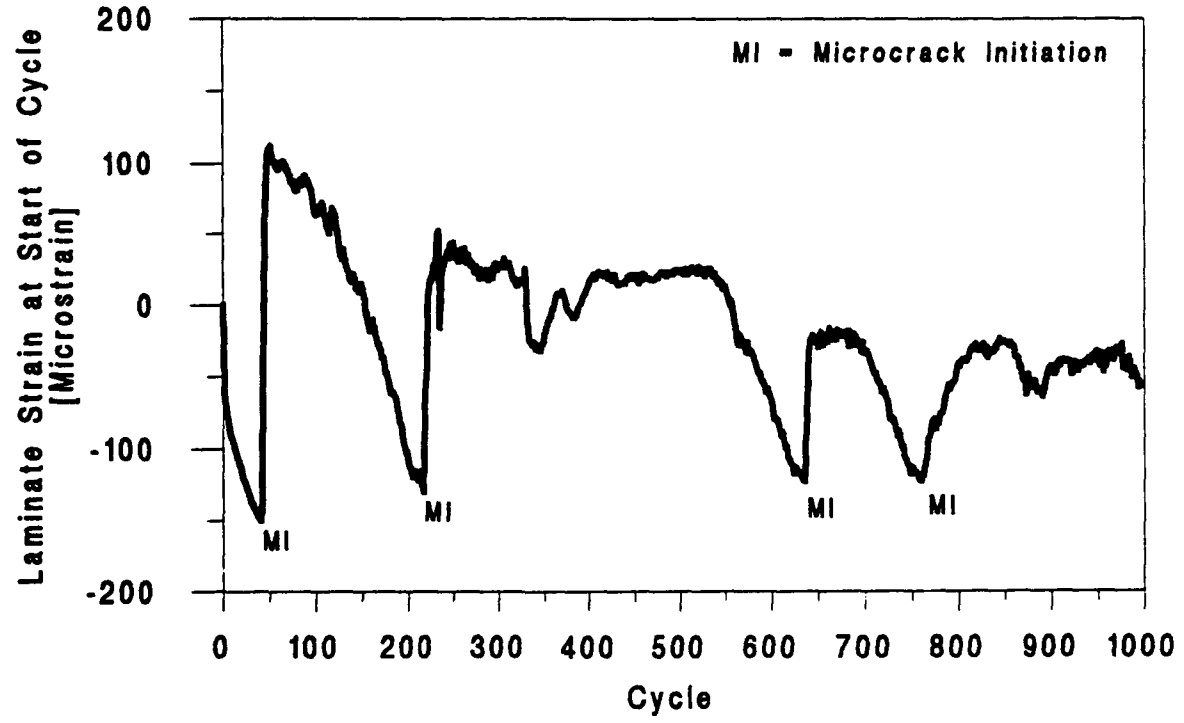

Figure 38. Experimental laminate strain at start of cycle (24 °C) for IM6/BT3008 $[0/90]_{3S}$ in the unconstrained condition (cycles 1 to 1000).

Table 17. Transverse crack density in IM6/BT3008 and IM7/5250-4 laminates.

Material	Transverse Crack Density [cracks/cm]			
	As-Molded	1000 Cycles From 24 to 177 °C		
		Unconstrained	Fully-Constrained	Over-Constrained
IM6/BT3008	0.0	23 ± 4	15 ± 4	20 ± 6[1]
IM7/5250-4	0.0	0.0	0.0	1 ± 0

[1]Significant fiber/matrix debonding observed in these coupons.

Table 18. Residual mechanical properties of IM6/BT3008 and IM7/5250-4 laminates.

Material	Compressive Modulus [GPa]			
	As-Molded	1000 Cycles From 24 to 177 °C		
		Unconstrained	Fully-Constrained	Over-Constrained
IM6/BT3008	74.5 ± 1.3	73.0 ± 2.7	73.6 ± 2.1	73.9 ± 11.3
IM7/5250-4	77.9 ± 8.6	73.8 ± 6.2	69.4 ± 0.9	81.9 ± 5.7

Material	Compressive Strength [MPa]			
	As-Molded	1000 Cycles From 24 to 177 °C		
		Unconstrained	Fully-Constrained	Over-Constrained
IM6/BT3008	820 ± 54	792 ± 40	798 ± 14	758 ± 11
IM7/5250-4	935 ± 99	930 ± 107	817 ± 7	873 ± 38

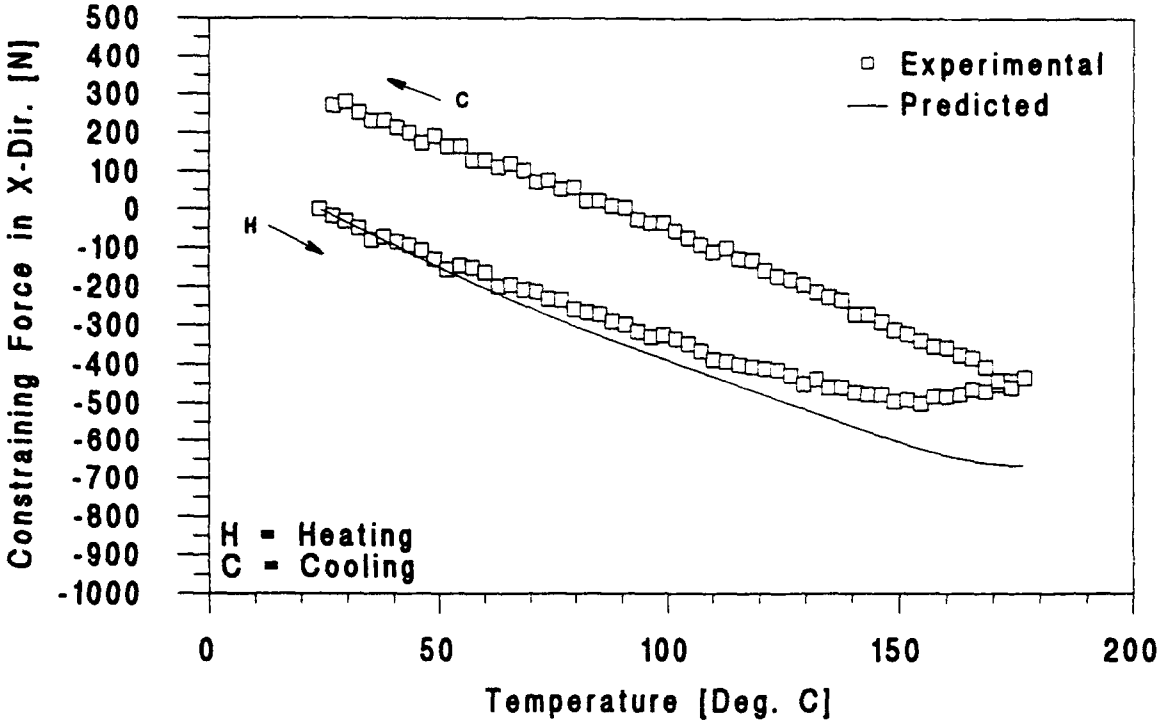

Figure 39. Predicted versus experimental constraining force as a function of temperature (cycle 1) for IM6/BT3008 $[0/90]_{3S}$ in the fully-constrained condition.

the load-temperature response indicating the presence of permanent deformation in the sample. As in the unconstrained case, the hysteresis is attributed to time-dependent deformation in the 90° plies of the laminate. The appearance of time-dependent deformation at lower temperature in the fully-constrained sample relative to the unconstrained sample is consistent with the 90° ply stress predictions from the baseline analysis (Section 5.2.1). Compressive stresses develop more rapidly in the 90° plies of the fully-constrained laminate relative to the unconstrained laminate. This is due to the application of a compressive constraining force which is applied to prevent expansion of the laminate and maintain the zero strain condition. As in the unconstrained laminate, relaxation of the compressive stresses appears to occur over time at the higher temperatures, thereby releasing some of the constraint on the 0° plies and allowing them to contract. This results in a net decrease in laminate strain. In order to maintain the zero strain condition, the compressive constraining force must be reduced to compensate for the decrease in laminate strain resulting from time-dependent deformation. As in the unconstrained case, the effects of time-dependent deformation are more pronounced during heating due to the asymmetry in the heating and cooling rates at elevated temperature.

The time-dependent deformation in the IM6/BT3008 laminate influences the ply stress distribution as well as the constraining force. Stress relaxation results in lower compressive stresses in the 90° plies during heating than those predicted in the baseline analysis (Section 5.2.1). As a result, the tensile stresses developed in the 90° plies during cooling will be higher than those predicted in the baseline analysis. The baseline analysis predicts a 90° ply stress of 17.2 MPa on cooling to 24 °C. This is the same value predicted for the unconstrained laminate since the constraining force is applied at 24 °C. It represents 44% of the transverse tensile strength of IM6/BT3008 at that temperature. For the fully-constrained sample shown in Figure 39, the hysteresis in cycle 1 resulted in a net increase in the constraining force of approximately 275 N at 24 °C. This corresponds to an increase of approximately 0.8 MPa in the 90° ply stress at 24 °C, bringing the value to approximately

18.0 MPa or 46% of the transverse tensile strength. Recall that for the unconstrained sample (Section 6.2.1.1) the 90° ply stress increased to approximately 17.7 MPa or 45% of the transverse tensile strength on cycle 1. This result suggests that the onset of microcracking should occur at a lower cycle count for the fully-constrained laminate relative to the unconstrained laminate.

The progression of hysteresis in the constraining force versus temperature response for the IM6/BT3008 sample in the fully-constrained condition is shown in Figures 40 and 41. During cycles 1 through 7, the degree of hysteresis per cycle decreases but the constraining force at 24 °C continues to increase. At the end of cycle 7, the progressive hysteresis has increased the constraining force by approximately 460 N relative to the start of cycle 1. This corresponds to an increase of approximately 1.4 MPa in the 90° ply stress at 24 °C, bringing the value to approximately 18.6 MPa or 48% of the transverse tensile strength. At the end of cycle 8, there is a sharp decrease in constraining force of approximately 70 N as the sample temperature approaches 24 °C. The decrease in constraining force is attributed to the initiation of microcracks in the 90° plies. Initiation of microcracks relieves some of the tensile stress in the 90° plies thereby reducing the constraint on the 0° plies and allowing them to expand. This, in turn, results in an increase in the laminate strain and a corresponding decrease in the tensile constraining force to maintain the zero strain condition. This explanation is supported by the fact that microcrack initiation appeared to occur at approximately the same level of 90° ply stress for both the unconstrained (18.5 MPa) and fully-constrained (18.6 MPa) samples. The more rapid initiation of microcracks in the fully-constrained sample (8 cycles) relative to the unconstrained sample (41 cycles) is expected considering the higher 90° ply stresses developed during heating which result in higher hysteresis per cycle.

During cycles 9 through 20, microcrack propagation occurs in the 90° plies of the fully-constrained sample in much the same manner as described previously for the unconstrained sample (Section 6.2.1.1). With each cycle, the decrease in constraining force

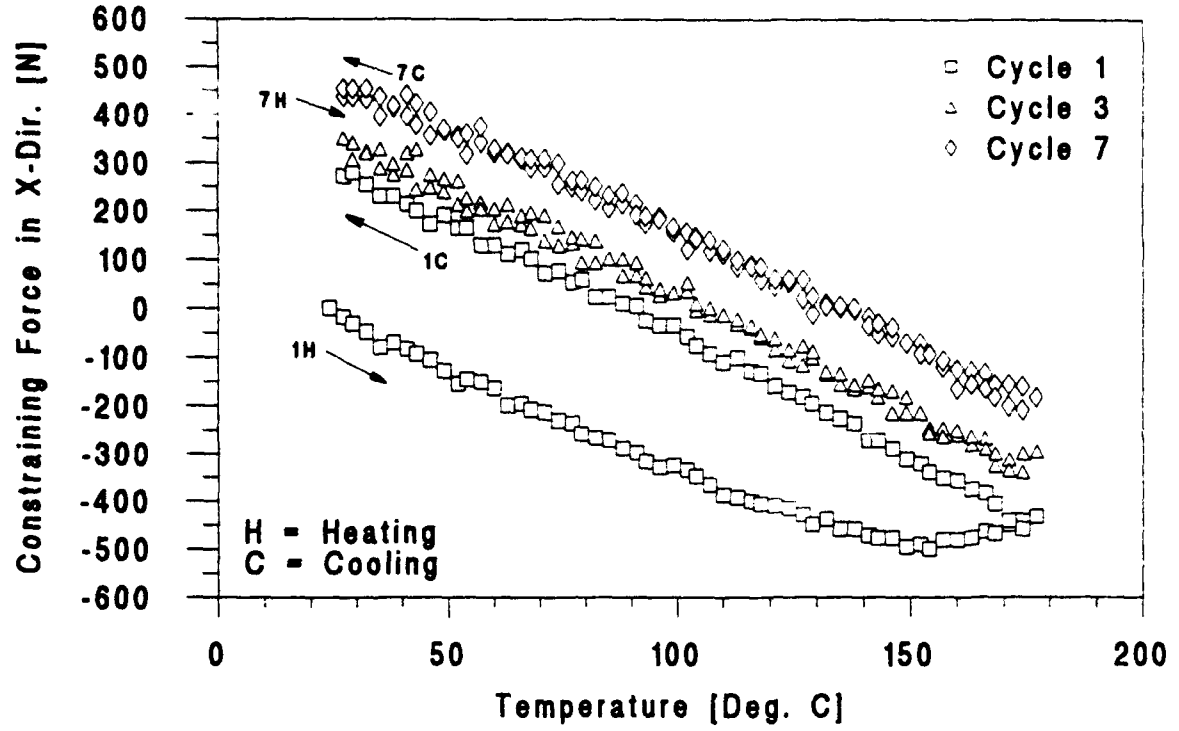

Figure 40. Experimental constraining force as a function of temperature (cycles 1, 3 and 7) for IM6/BT3008 $[0/90]_{3S}$ in the fully-constrained condition.

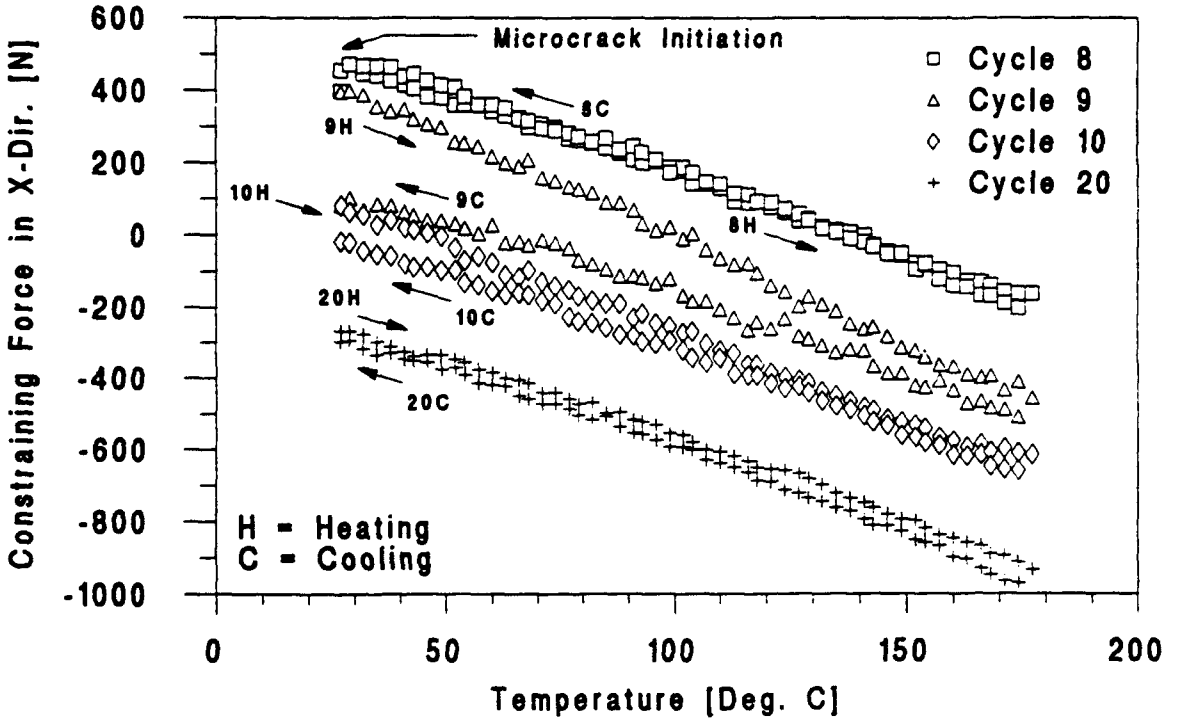

Figure 41. Experimental constraining force as a function of temperature (cycles 8, 9, 10 and 20) for IM6/BT3008 $[0/90]_{3S}$ in the fully-constrained condition.

is reduced since the tensile stresses in the 90° plies are relieved by propagation of the microcracks. At the end of cycle 20, the constraining force has been reduced by approximately 760 N relative to the end of cycle 7. This corresponds to a decrease of approximately 2.3 MPa in the 90° ply stress at 24 °C, bringing the value to approximately 16.3 MPa or 42% of the transverse tensile strength. After cycle 20, the response of the laminate stabilizes for several cycles possibly due to the microcracks arresting at the adjacent 0° plies. It is interesting to note that stabilization of the laminate response occurred at approximately the same level of 90° ply stress for both the unconstrained (16.2 MPa) and fully-constrained (16.3 MPa) laminates. As in the unconstrained case, signs of time-dependent deformation subsequently reappear at the upper end of the heating cycle and hysteresis becomes apparent on cooling. The degree of hysteresis per cycle is considerably less than the early cycles but results in a steady increase in constraining force until the initiation of additional microcracks and the corresponding decrease in constraining force. This process is repeated throughout the test as shown in Figures 42 and 43. The maximum test duration for the present study was 1000 cycles. For the samples tested in the fully-constrained condition, there were no signs of reaching a saturation crack density within 1000 cycles.

The observed changes in the constraining force versus temperature response of the IM6/BT3008 samples during fully-constrained thermal cycling have been attributed to time-dependent deformation in the 90° plies which leads to an increase in ply stress and ultimately to microcracking. Transverse ply cracking appears to initiate more rapidly for fully-constrained samples (8 cycles) relative to unconstrained samples (41 cycles) due to the higher 90° ply stresses developed during heating which result in more time-dependent deformation per cycle. However, crack density measurements performed on IM6/BT3008 samples indicate that the number of microcracks is statistically equivalent in the unconstrained and fully-constrained samples after 1000 cycles (Table 17). Residual compressive properties are also equivalent for the unconstrained and fully-constrained samples after 1000 cycles (Table 18).

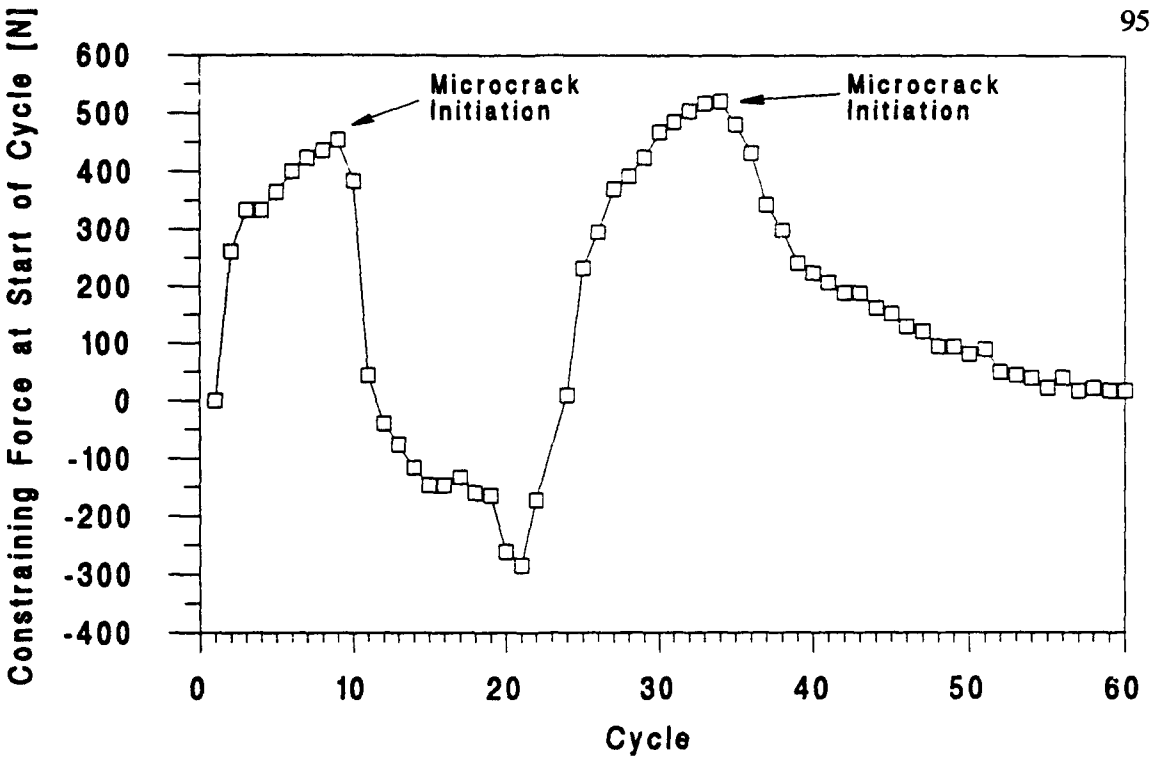

Figure 42. Experimental constraining force at start of cycle (24 °C) for IM6/BT3008 $[0/90]_{3S}$ in the fully-constrained condition (cycles 1 to 60).

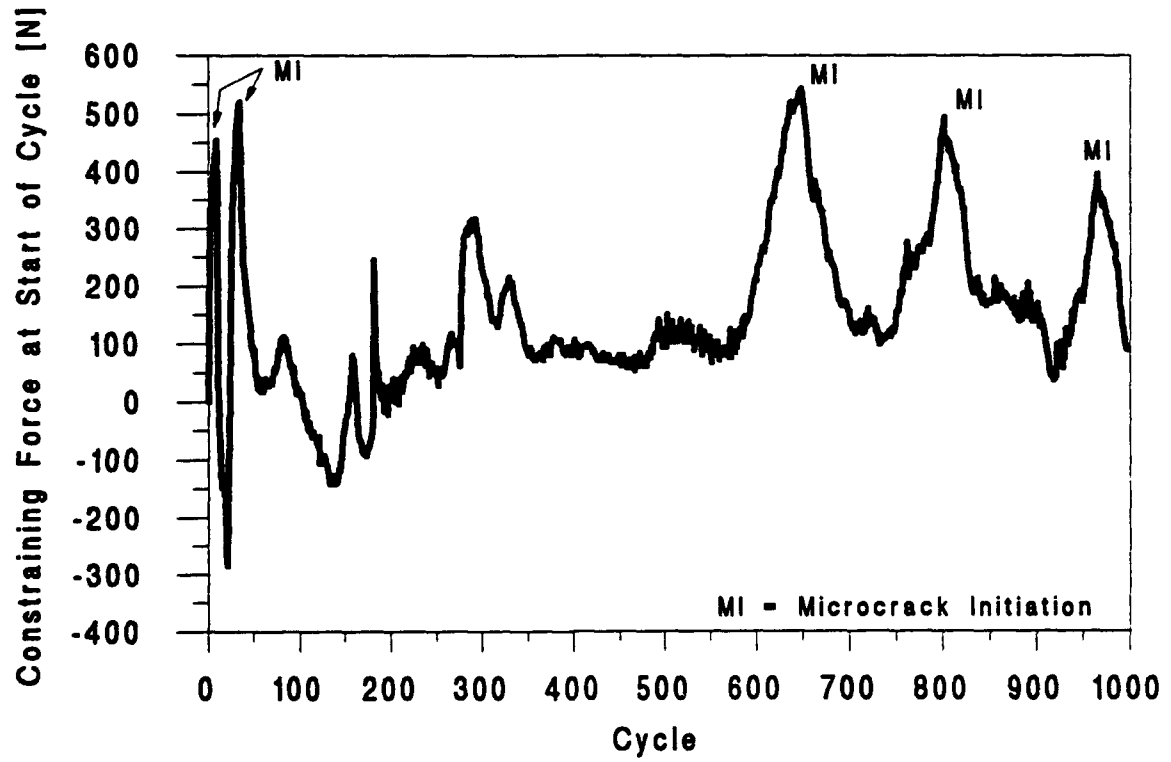

Figure 43. Experimental constraining force at start of cycle (24 °C) for IM6/BT3008 $[0/90]_{3S}$ in the fully-constrained condition (cycles 1 to 1000).

The compressive properties show no reduction relative to results for as-molded samples. This is likely the result of crack closure effects as discussed in Section 6.2.1.1.

6.2.1.3 Over-Constrained Thermal Cycling

Experimental values of constraining force as a function of sample temperature (cycle 1) are given in Figure 44 for a typical IM6/BT3008 sample in the over-constrained condition. In this case, the material applying the constraint is 6061-T6 aluminum (CTE = 23.6 μ/°C). The data is compared with the prediction from the over-constrained analysis (Section 5.1.4.2). The prediction fits the data to within 6% over the entire temperature interval. The small deviation between the predicted and experimental values is attributed to overprediction of the laminate modulus by the analytical model which is based on classical laminate theory. It is interesting to note that the over-constrained laminate exhibits no sign of hysteresis as observed in the unconstrained and fully-constrained laminates. However, time-dependent deformation is expected based on the ply stress predictions which indicate that the 90° ply stress is 77% of the transverse tensile strength at 177 °C. The lack of hysteresis in the constraining force versus temperature response can be explained in terms of the ply stress distribution. In the over-constrained samples, both the 0° and 90° plies are in tension once the temperature exceeds 30 °C (Section 5.2.1). Relaxation of the tensile stresses in the 90° plies over time at the higher temperatures may cause the 0° plies to carry additional tensile load but the increase in stress is very small relative to the longitudinal tensile strength of the material. Therefore, time-dependent deformation in the 90° plies is expected to result in little or no change in the net laminate strain for the over-constrained case. Since the net laminate strain is unaffected by the time-dependent deformation, no adjustment of the constraining force is required to maintain the over-constrained condition.

In Figure 45, constraining force versus temperature data for an over-constrained IM6/BT3008 sample during cycle 1 are compared with similar data for cycle 1000. Small but significant changes are apparent in the constraining force versus temperature response. The changes occur gradually throughout the test and are attributed to slight changes in laminate CTE and laminate modulus resulting from microcracking in the 90° plies. Crack initiation could not be traced to a specific cycle as in the unconstrained and fully-constrained samples. This was due to the ply stress distribution in the over-constrained laminate (see previous paragraph). Transverse crack density measurements performed on IM6/BT3008 samples indicate that the number of microcracks in the over-constrained samples is statistically equivalent to that in the unconstrained and fully-constrained samples after 1000 cycles (Table 17). However, extensive fiber/matrix debonding was observed in the over-constrained samples which was not apparent in the unconstrained or fully-constrained samples. This additional damage is accompanied by a small but significant reduction in laminate compressive strength (Table 18) which suggests that failure is initiated by matrix shear failure in the 90° plies. In cases involving transverse compressive loading, it has been suggested that matrix shear failure is precipitated by failure of the fiber/matrix interfacial bond [57]. Thus, the presence of fiber/matrix debonding in the 90° plies of the over-constrained samples would be expected to reduce the laminate compressive strength by initiating matrix shear failure in the 90° plies at lower stress levels. The laminate compressive strength for the over-constrained samples is 8% lower than that of the as-molded samples. No significant reduction was apparent for the unconstrained or fully-constrained samples where fiber/matrix debonding was not present. The residual compressive modulus for the over-constrained samples showed no reduction relative to the as-molded samples. This is probably due to crack closure effects as discussed in Section 6.2.1.1.

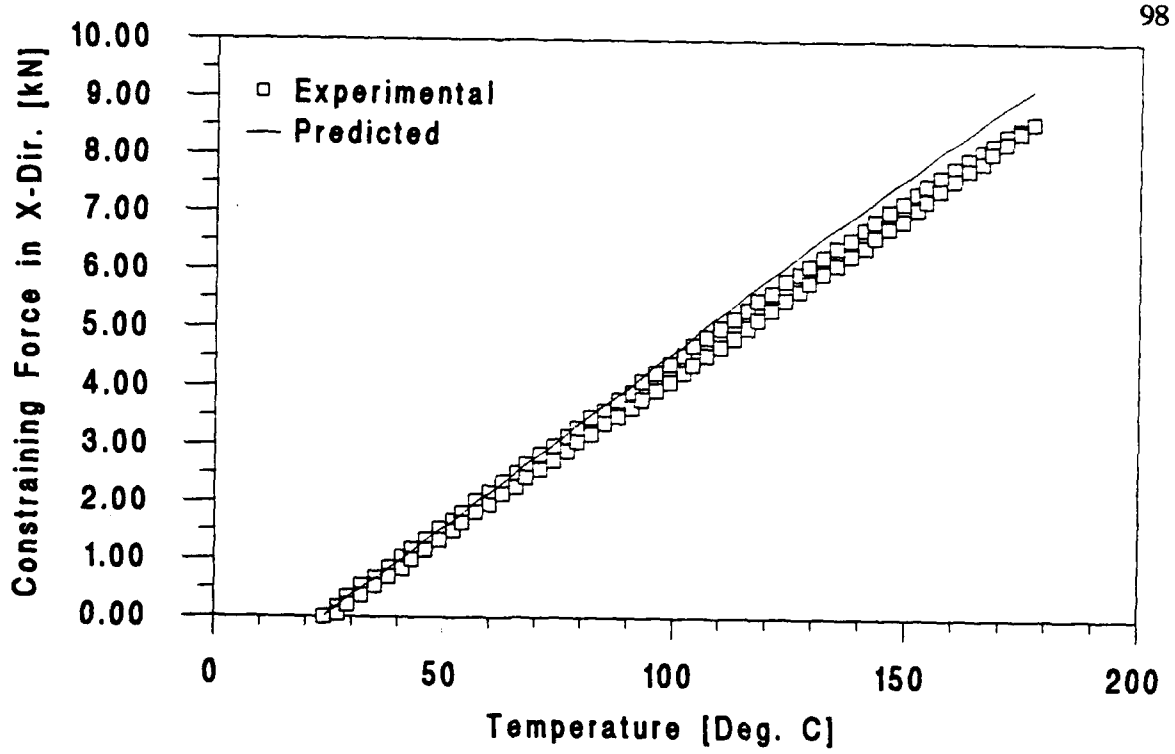

Figure 44. Predicted versus experimental constraining force as a function of temperature (cycle 1) for IM6/BT3008 $[0/90]_{3S}$ in the over-constrained condition.

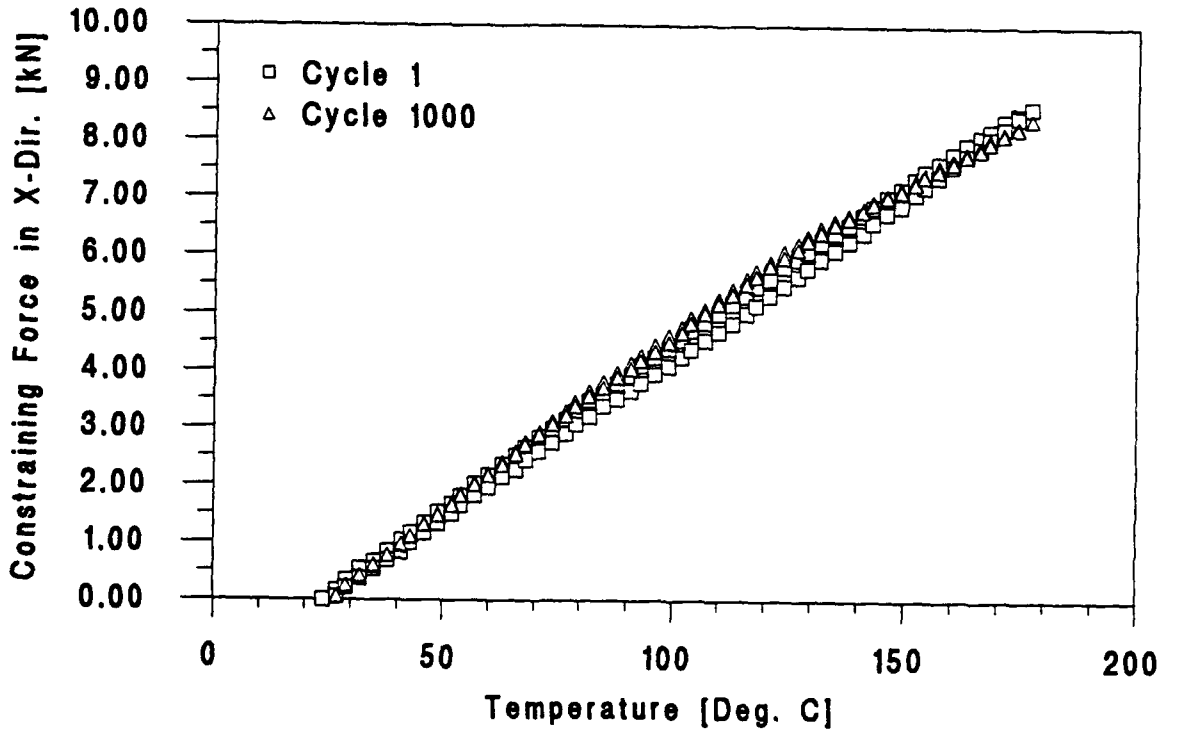

Figure 45. Experimental constraining force as a function of temperature (cycles 1 and 1000) for IM6/BT3008 $[0/90]_{3S}$ in the over-constrained condition.

6.2.2 IM7/5250-4

6.2.2.1 Unconstrained Thermal Cycling

Experimental values of laminate strain as a function of sample temperature (cycle 1) are given in Figure 46 for a typical IM7/5250-4 sample in the unconstrained condition. The data are compared with similar data for IM6/BT3008 discussed previously (Section 6.2.1.1). The IM7/5250-4 laminate exhibits significantly less thermal expansion over the temperature range from 24 to 177 °C. This result is consistent with the lamina coefficient of thermal expansion (CTE) data presented in Sections 4.3.1.3 and 4.3.2. Temperature-dependent CTE data were unavailable for IM7/5250-4. Single values were reported without specification of the temperature range over which they were measured. The longitudinal (0°) CTE reported for IM7/5250-4 was well below the range calculated for IM6/BT3008 over the 24 to 177 °C interval. The transverse (90°) CTE reported for IM7/5250-4 was at the lower end of the range calculated for IM6/BT3008. Based on this data, a significantly lower laminate CTE would be expected for IM7/5250-4.

In addition to its lower thermal expansion, the IM7/5250-4 laminate also differs from the IM6/BT3008 laminate in that it exhibits no signs of time-dependent deformation. In Figure 47, laminate strain versus temperature data for IM7/5250-4 during cycle 1 are compared with similar data for cycle 1000. No hysteresis is observed in the laminate strain versus temperature response for IM7/5250-4 at any point during the test. The lack of time-dependent deformation in the IM7/5250-4 laminate is attributed to the higher T_g of the 5250-4 bismaleimide resin (300 °C) relative to that of the BT3008 cyanate ester resin (221 °C).

The lack of hysteresis in the IM7/5250-4 samples subjected to unconstrained thermal cycling is consistent with the observed transverse crack densities (Table 17) and residual mechanical properties (Table 18). After 1000 cycles, no microcracking was observed in the samples and no change in compressive modulus or strength was apparent.

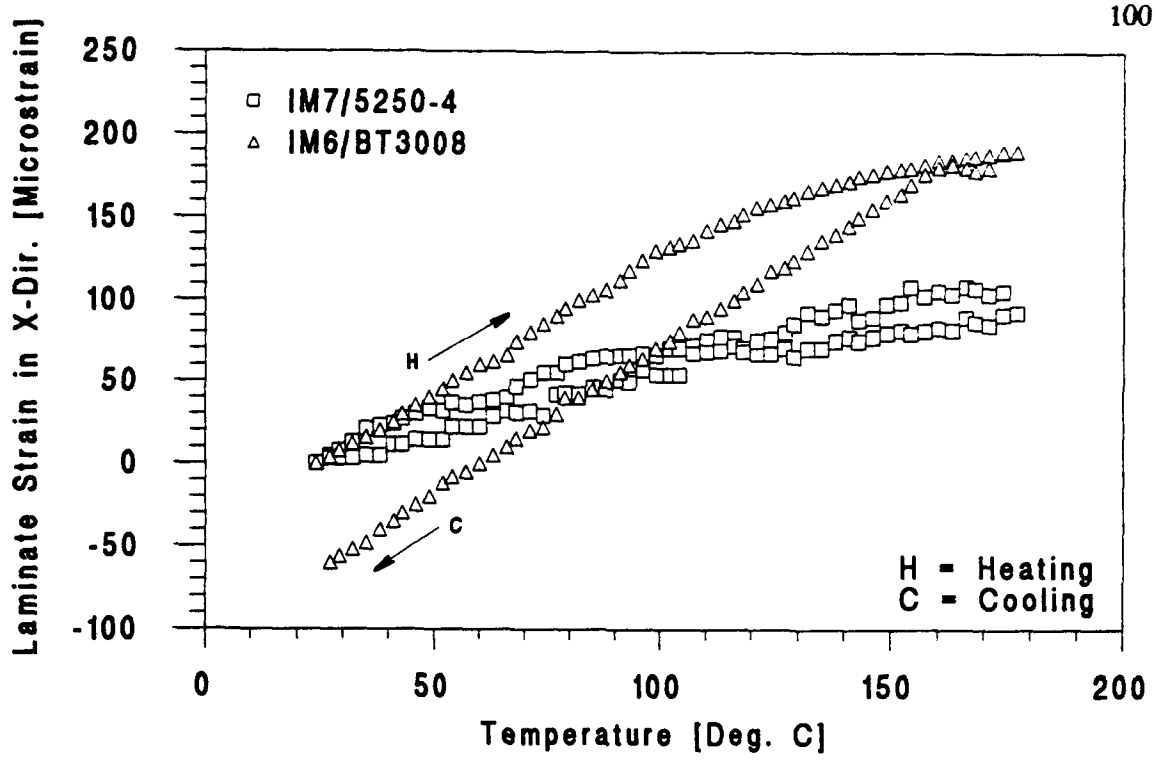

Figure 46. Experimental laminate strain as a function of temperature (cycle 1) for IM7/5250-4 $[0/90]_{5S}$ and IM6/BT3008 $[0/90]_{3S}$ in the unconstrained condition.

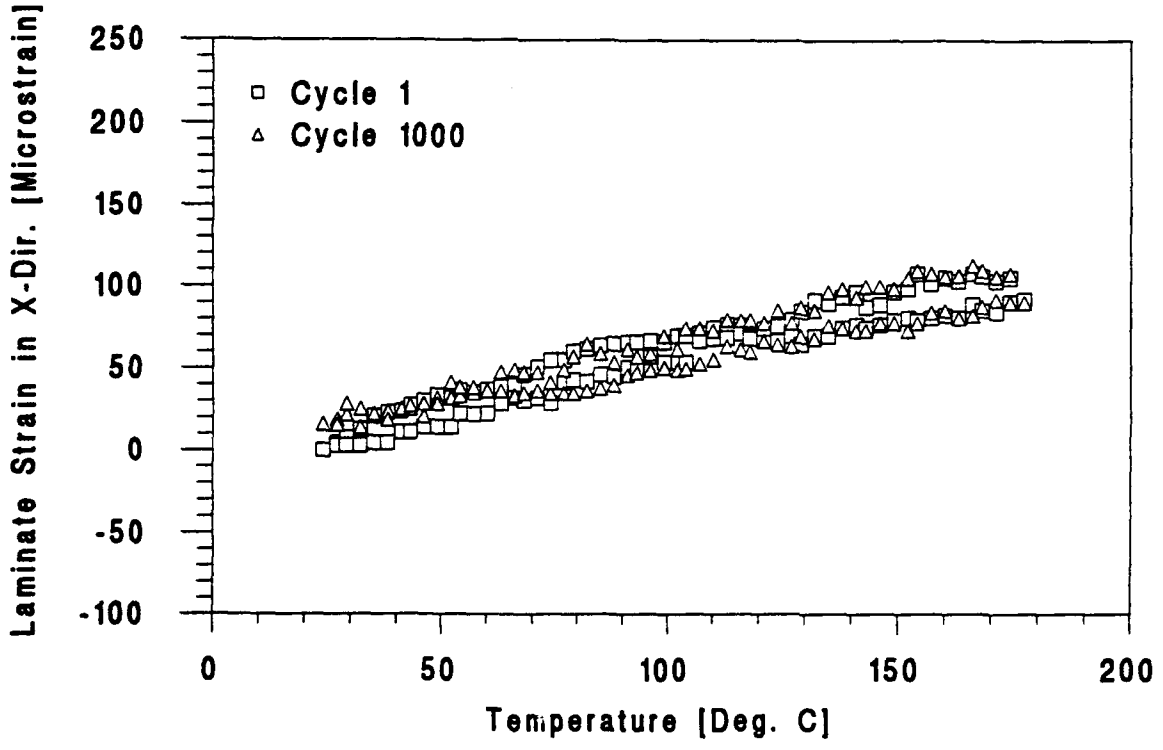

Figure 47. Experimental laminate strain as a function of temperature (cycles 1 and 1000) for IM7/5250-4 $[0/90]_{5S}$ in the unconstrained condition.

6.2.2.2 Fully-Constrained Thermal Cycling

Experimental values of constraining force as a function of sample temperature (cycle 1) are given in Figure 48 for a typical IM7/5250-4 sample in the fully-constrained condition. The data are compared with similar data for IM6/BT3008 discussed previously (Section 6.2.1.2). As discussed in Section 6.2.2.1, the IM7/5250-4 laminate exhibits significantly less thermal expansion over the temperature range from 24 to 177 °C which results in significantly lower values of constraining force. The IM7/5250-4 laminate also differs from the IM6/BT3008 laminate in that it exhibits no signs of time-dependent deformation. In Figure 49, constraining force versus temperature data for IM7/5250-4 during cycle 1 are compared with similar data for cycle 1000. As in the unconstrained case, no hysteresis is observed in the laminate response for IM7/5250-4 at any point during the test.

The lack of hysteresis in the IM7/5250-4 samples subjected to fully-constrained thermal cycling is consistent with the observed transverse crack densities (Table 17). After 1000 cycles in the fully-constrained condition, no microcracking was observed in the samples. A reduction in compressive modulus was noted but was within one standard deviation in the data (Table 18). However, a reduction in compressive strength was apparent which was significant to one standard deviation. This decrease may be due to the presence of damage not detectable using optical microscopy and not extensive enough to influence the laminate response during thermal cycling, or it may simply be an anomaly in the data. More testing will be required to make this determination.

6.2.2.3 Over-Constrained Thermal Cycling

Experimental values of constraining force as a function of sample temperature (cycle 1) are given in Figure 50 for a typical IM7/5250-4 sample in the over-constrained condition. In this case, the material applying the constraint is 6061-T6 aluminum (CTE = 23.6 μ/°C).

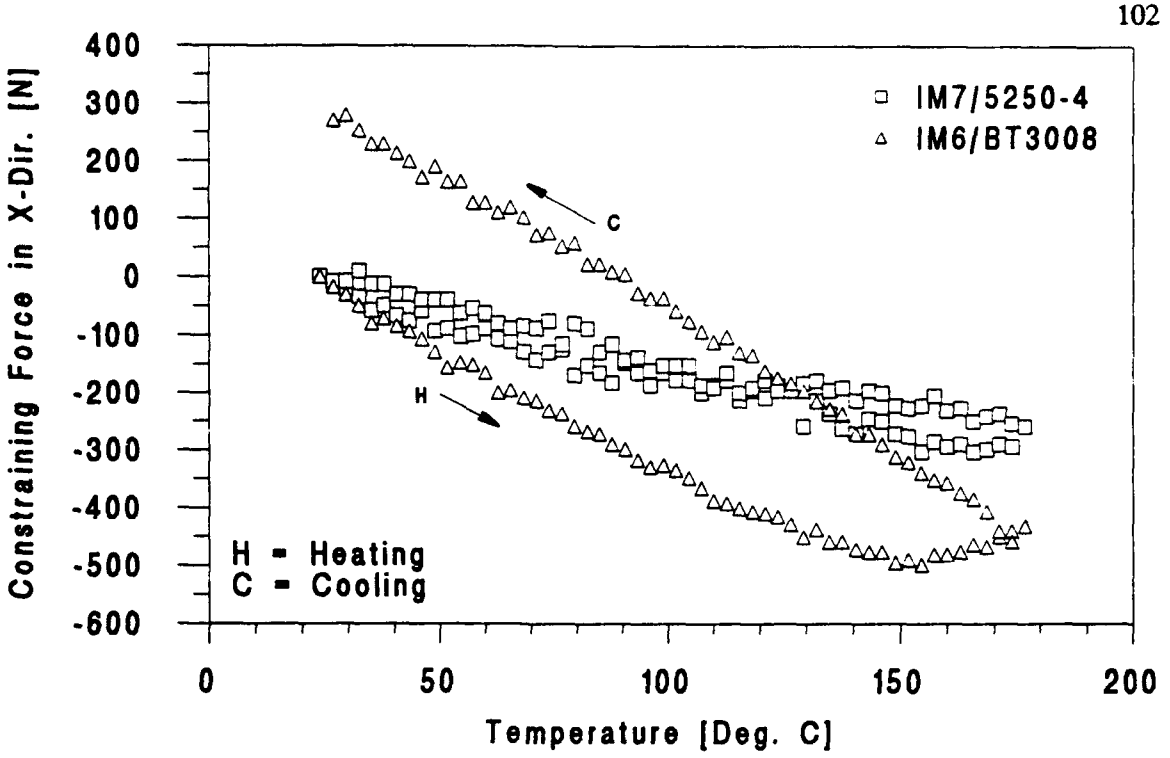

Figure 48. Experimental constraining force as a function of temperature (cycle 1) for IM7/5250-4 $[0/90]_{5S}$ and IM6/BT3008 $[0/90]_{3S}$ in the fully-constrained condition.

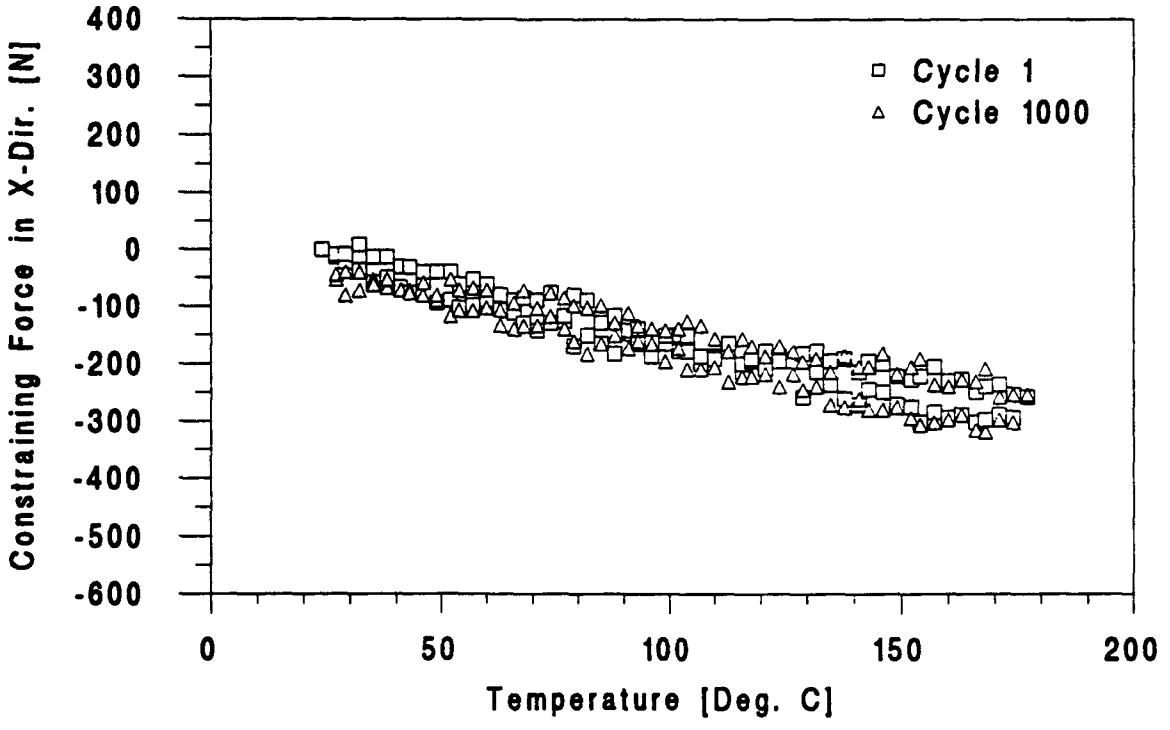

Figure 49. Experimental constraining force as a function of temperature (cycles 1 and 1000) for IM7/5250-4 $[0/90]_{5S}$ in the fully-constrained condition.

The data are compared with similar data for IM6/BT3008 discussed previously (Section 6.2.1.3). Although the IM7/5250-4 laminate exhibits significantly less thermal expansion than the IM6/BT3008 laminate (Section 6.2.2.1), its response in the over-constrained condition is nearly identical to that of the IM6/BT3008 laminate. This is attributed to the large mechanical strain applied to the laminates in the over-constrained condition which overshadows the differences in thermal strain. Since the cross-ply layups utilized in this study include a significant number of 0° plies, the large mechanical strain results in a fiber-dominated response for both the IM7/5250-4 and IM6/BT3008 laminates. Given the similar mechanical properties of IM6 and IM7 carbon fibers, a nearly equivalent response is expected for the two materials in the over-constrained condition. The slightly higher slope of the constraining force versus temperature curve for the IM7/5250-4 laminate above 150 °C is consistent with the higher T_g of the 5250-4 resin. Had the thermal cycle been extended above 177 °C, it is likely that this difference would have increased with temperature.

In Figure 51, constraining force versus temperature data for an over-constrained IM7/5250-4 sample during cycle 1 are compared with similar data for cycle 1000. Small but significant changes are apparent in the constraining force versus temperature response. The changes occur gradually throughout the test and are attributed to slight changes in laminate CTE and laminate modulus resulting from microcracking in the 90° plies. Crack initiation could not be traced to a specific cycle. This is thought to be due to the ply stress distribution (see discussion in Section 6.2.1.3). Transverse crack density measurements indicate that a small amount of microcracking did occur in the IM7/5250-4 samples cycled in the over-constrained condition (Table 17). However, this damage did not result in statistically significant reductions in compressive properties relative to as-molded material (Table 18). This is probably due to the low crack density as well as crack closure effects (Section 6.2.1.1).

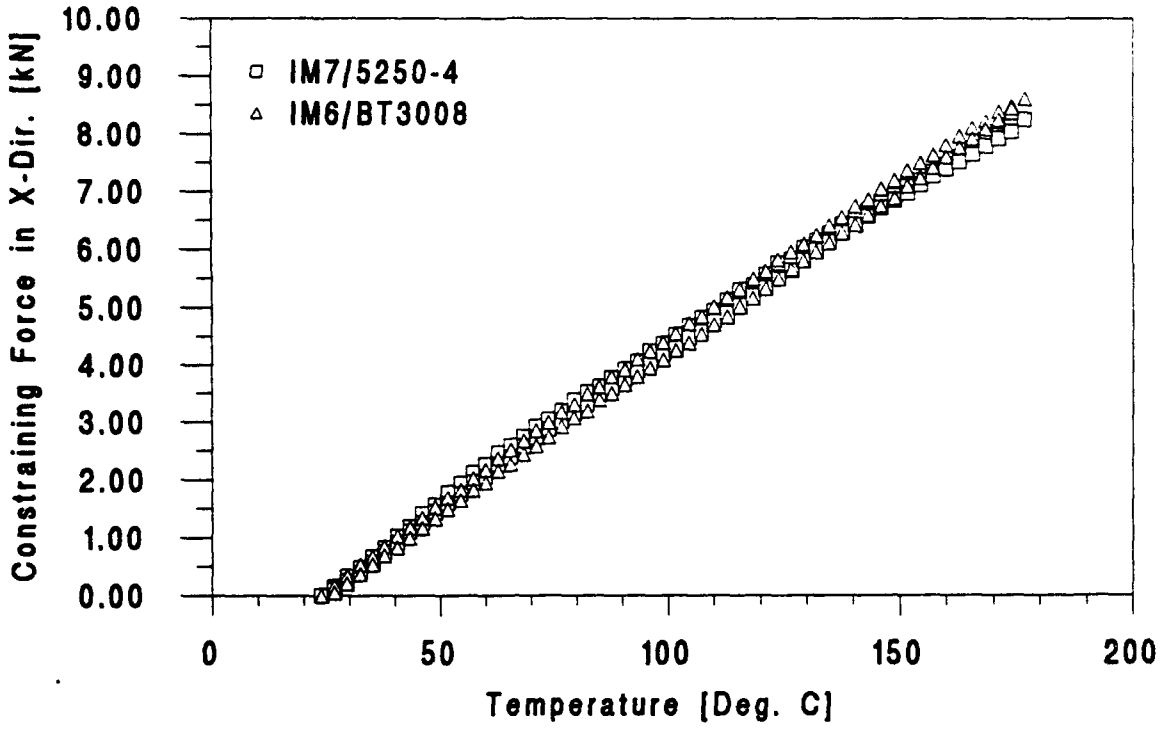

Figure 50. Experimental constraining force as a function of temperature (cycle 1) for IM7/5250-4 $[0/90]_{5S}$ and IM6/BT3008 $[0/90]_{3S}$ in the over-constrained condition.

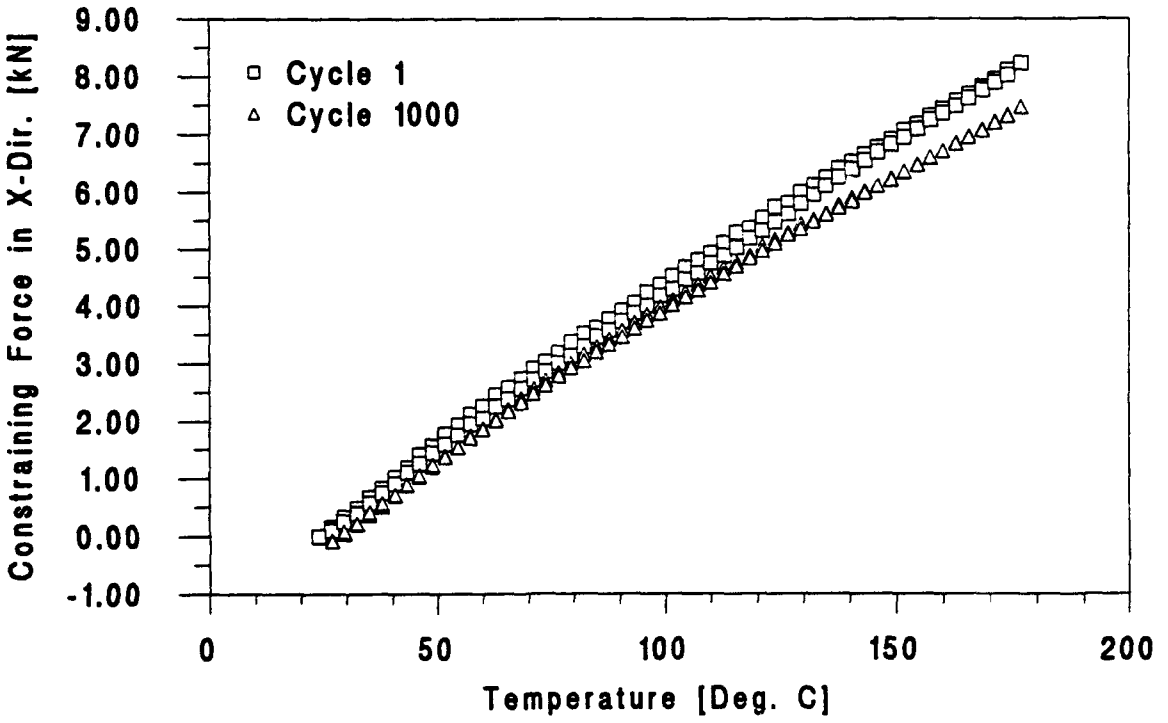

Figure 51. Experimental constraining force as a function of temperature (cycles 1 and 1000) for IM7/5250-4 $[0/90]_{5S}$ in the over-constrained condition.

7.0 SUMMARY AND CONCLUSIONS

The present thesis research program was undertaken to evaluate the effects of mechanical constraint on the response of polymer matrix composites during thermal cycling. Analytical and experimental techniques were used to characterize the response of a carbon fiber reinforced cyanate ester resin (IM6/BT3008). Additional experimental work was performed on a carbon fiber reinforced bismaleimide resin (IM7/5250-4). Cross-ply laminates of IM6/BT3008 and IM7/5250-4 were subjected to thermal cycles from 24 to 177 °C in the unconstrained, fully-constrained and over-constrained conditions. Laminate response, damage mechanisms and residual compressive properties were characterized for each material and degree of constraint.

For the IM6/BT3008 system, predicted ply stress distributions are significantly different for the various degrees of constraint. The predicted ply stress distributions are highly sensitive to the temperature-dependent lamina properties and the laminate stress free temperature. Predicted values of laminate strain (unconstrained condition) and constraining force (fully-constrained and over-constrained conditions) show good correlation with experimental results. However, some deviations are apparent at elevated temperature which are attributed to the effects of time-dependent deformation. Time-dependent deformation is not considered in the present analytical model.

Changes in the laminate strain versus temperature response are observed during thermal cycling of IM6/BT3008 laminates in the unconstrained condition. The changes are attributed to time-dependent deformation in the 90° plies which leads to changes in the ply stress distribution and ultimately to transverse microcracking. Similar changes in ply stress distribution occur for fully-constrained samples. However, microcracking initiates more rapidly for fully-constrained laminates due to higher 90° ply stresses which result in more time-dependent deformation per cycle. With continued cycling, microcrack densities for

unconstrained and fully-constrained laminates appear to converge and, in fact, become statistically equivalent after 1000 cycles.

The ply stress distribution in over-constrained laminates is substantially different from those in unconstrained and fully-constrained laminates. Time-dependent deformation in the 90° plies of fully-constrained laminates results in changes in the ply stress distribution but does not significantly alter the laminate response. Therefore, the initiation of microcracks is not traceable to a specific point in the test. The microcrack density in over-constrained laminates is statistically equivalent to that in unconstrained and fully-constrained laminates after 1000 cycles. However, extensive fiber/matrix debonding is observed in the over-constrained laminates which is not apparent in unconstrained and fully-constrained laminates. This additional damage is accompanied by a small but significant reduction in laminate compressive strength. No significant reduction was observed for unconstrained or fully-constrained laminates.

IM7/5250-4 laminates are unaffected by 1000 thermal cycles in the unconstrained and fully-constrained conditions. A small amount of transverse ply microcracking is observed in IM7/5250-4 laminates after 1000 thermal cycles in the over-constrained condition. However, this damage does not result in a statistically significant reduction in laminate compressive strength. The superior performance of the IM7/5250-4 system is attributed to the higher glass transition temperature (T_g) of 5250-4 resin relative to that of BT3008. The higher resin T_g reduces the amount of time-dependent deformation in the 90° plies of the laminate which, in turn, reduces the changes in ply stress distribution which ultimately lead to microcracking.

The results of this research indicate that the level of constraint can have a significant effect on the response of polymer matrix composites during thermal cycling. However, longer term testing is required to determine if the observed changes in response will ultimately affect the final failure mode and fatigue endurance of the materials.

8.0 FUTURE WORK

The present thesis research program provides some insight into the effects of mechanical constraint on the response of polymer matrix composites subject to thermal cycling. However, a considerable amount of additional work will be required to obtain a thorough understanding of this complex subject. This chapter indicates potential areas for future work based on lessons learned from the present study. The chapter is divided into three sections dealing with extensions of the current research program, modifications to the equipment and test methods, and advanced projects.

8.1 EXTENSIONS OF THE CURRENT RESEARCH

The results of the present study indicate that the effects of time-dependent deformation must be included in the analytical model. This will require modifications to the computer program as well as additional mechanical testing to characterize the time-dependent deformation at the lamina level for the IM6/BT3008 system. Specific plans for incorporating time-dependent deformation into the model are being formulated for implementation in a follow-on program.

The current research program examined the response of carbon fiber reinforced cyanate ester and bismaleimide composites subject to 1000 thermal cycles from 24 to 177 °C in the unconstrained, fully-constrained and over-constrained conditions. For the cyanate ester system, this duration was sufficient to initiate microcracks in the 90° plies for all degrees of constraint. However, for the bismaleimide system, microcrack initiation was observed only in the over-constrained condition. Furthermore, none of the laminates tested appeared to have reached a saturation crack density within 1000 cycles. Therefore, longer term testing would be expected to result in the formation of additional transverse ply cracking in the laminates. Delaminations may also initiate at intersections between transverse cracks in

adjacent plies. Such damage would certainly be expected to reduce the compressive properties of the laminates below the values observed in the present study. Given the expectation of further damage and the fact that 1000 thermal cycles is only a small percentage of life for most aircraft engine components, longer term testing is required to determine if the progression of damage will ultimately affect the final failure mode and fatigue endurance of the materials. With the current equipment, 1000 cycles is the maximum that can be achieved in a reasonable period of time (approximately 1 week). Modifications to the test equipment to achieve greater heating/cooling efficiency are under consideration.

8.2 MODIFICATIONS TO EQUIPMENT AND TEST METHODS

Lessons learned from the present research program suggest a number of modifications to the equipment and test methods. Equipment modifications under consideration include improved heating/cooling systems and improved strain measurement. Improvements under consideration for the heating system include the use of higher temperature capability heat tape, focused heat lamps or possibly a laser to increase heating efficiency. An upper temperature limit of at least 400 °C is desired to permit testing of polyimide-based composite systems. A liquid nitrogen based cooling system for subambient testing is also under consideration. Modifications to the computer program are underway which will provide more precise control of the thermal cycle and minimize the asymmetry in the heating and cooling rates. Non-contact, laser-based strain measurement systems are under consideration for use at higher temperatures. However, it remains to be seen if such systems can provide the required accuracy.

Test method modifications under consideration include the use of nondestructive inspection (NDI) techniques for damage characterization and the use of tensile tests for residual strength and modulus. NDI techniques under consideration include ultrasonic methods and penetrant enhanced X-ray radiography. These techniques will allow more

thorough characterization of damage development in the laminates. Tensile tests for residual strength and, in particular, modulus are required for short term tests due to the apparent insensitivity of compressive properties to moderate levels of transverse microcracking. For longer term tests in which crack densities are higher or in which delamination occurs, compressive tests will continue to be utilized.

8.3 ADVANCED PROJECTS

The current research program focused on carbon fiber reinforced cyanate ester and bismaleimide composites subject to thermal cycling from 24 to 177 °C in the unconstrained, fully-constrained and over-constrained conditions. Once the modifications to the equipment and test methods are complete, these and other materials can be subjected to thermal cycles which include excursions below ambient temperature. Such excursions will result in much larger transverse tensile stresses in the 90° plies. The larger transverse tensile stresses are expected to accelerate the formation of transverse microcracks. With the equipment modifications, the materials can also be exposed to thermal cycles which include excursions above 177 °C. Such excursions will result in greater time-dependent deformation which is expected to accelerate the formation of transverse microcracks. In addition to accelerating the formation of transverse microcracks, larger temperature excursions are expected to accelerate the formation of delaminations at intersections between transverse cracks in adjacent plies. Fiber breakage (tension) and/or fiber microbuckling (compression) may also occur due to the higher longitudinal stresses in the 0° plies. Given the expectation for increased damage and the current emphasis on extending the operational envelope for aircraft engine components, testing at higher/lower temperatures than considered in this study will ultimately be required to qualify materials for these applications.

The over-constrained testing performed in the current research program involved thermal cycles which were in-phase with the applied mechanical strain. The modifications to

the computer program currently underway to provide more precise control of the thermal cycle will allow over-constrained tests to be performed in which the thermal cycle is out-of-phase with the applied mechanical strain. This is often the case for large structures exposed to relatively rapid temperature fluctuations.

REFERENCES

[1] McConnell, V. P. "Tough Promises from Cyanate Esters," Advanced Composites. 7(3):28 (1992).

[2] Shimp, D. A. and Wentworth, J. E. "Cyanate Ester-Cured Epoxy Resin Structural Composites," Proc. 37th Intl. SAMPE Symposium. March (1992).

[3] Speak, S. C., Sitt, H. and Fuse, R. H. "Novel Cyanate Ester Based Products for High Performance Radome Applications," 36th Intl. SAMPE Symposium. April (1991).

[4] Shimp, D., Christenson, J. R. and Ising, S. J.. "AroCy Cyanate Ester Resins: Chemistry, Properties, and Applications," Technical Bulletin. Louisville, KY: Rhone-Poulenc Inc. (1990).

[5] Shimp, D. A. and Christenson, J. R. "Liquid Cyanate Ester Resins for Toughened Composites," Proc. 11th Intl. SAMPE Conference. May (1990).

[6] Saunders, K. J. Organic Polymer Chemistry. New York, NY: Chapman and Hall. pp. 216-223 (1988).

[7] Matsumoto, T., Mohri, M. and Nanjo, A. "On the Performance of High Modulus Pitch-Based Carbon Fiber/Toughened Polycyanate Ester Resin Composite," Proc. 37th Intl. SAMPE Symposium. March (1992).

[8] High Heat Resistant BT Resin (Fourth Edition). Technical Bulletin. Tokyo, Japan: Mitsubishi Gas Chemical Company, Inc. (1984).

[9] Donnellan, T. M. and Roylance, D. "Relationships in a Bismaleimide Resin System. Part I: Cure Mechanisms," Polymer Eng. and Sci. 32(6):409 (1992).

[10] Donnellan, T. M. and Roylance, D. "Relationships in a Bismaleimide Resin System. Part II: Thermomechanical Properties," Polymer Eng. and Sci. 32(6):415 (1992).

[11] Rankumar, R. L., Grimes, G. C. and Kong, S. J. "Characterization of T300/V-378A Graphite/Bismaleimide for Structural Applications," Composite Materials: Testing and Design (ASTM STP 893). Philadelphia, PA: ASTM (1986).

[12] Karasek, M. L., Sehitoglu, H. and Slavik, D. C. "Deformation and Fatigue Damage in 1070 Steel under Thermal Loading," Low Cycle Fatigue (ASTM STP 942). Philadelphia, PA: ASTM (1988).

[13] Adams, D. S. and Herakovich, C. T. "Influence of Damage on the Thermal Response of Graphite-Epoxy Laminates," J. Thermal Stresses. 7:91 (1984).

[14] Bowles, D. E. "Effects of Microcracks on the Thermal Expansion of Composite Laminates," J. Composite Materials. 17:273 (1984).

[15] Spain, R. G. "Thermal Microcracking of Carbon Fibre/Resin Composites," Composites. March (1971).

[16] Sykes, G. F., Funk, J. G. and Slemp, W. S. "Assessment of Space Environment Induced Microdamage in Toughened Composite Materials," Proc. 18th Intl. SAMPE Tech. Conf. October (1986).

[17] Adams, D. S., Bowles, D. E. and Herakovich, C. T. "Thermally Induced Transverse Cracking in Graphite-Epoxy Cross-Ply Laminates," J. Rein. Plastics and Composites. 5:152 (1986).

[18] Mazzio, V. F. and Mehan, R. L. "Effects of Thermal Cycling on the Properties of Graphite-Epoxy Composites," Composite Materials: Testing and Design (ASTM STP 617). Philadelphia, PA: ASTM (1977).

[19] Tomkins, S. S. and Williams, S. L. "Effects of Thermal Cycling on Mechanical Properties of Graphite Polyimide," J. Spacecraft. 21(3):274 (1984).

[20] Wilson, D., Wells, J. K., Hay, J. N., Lind, D., Owens, G. A. and Johnson, F. "Preliminary Investigations into the Microcracking of PMR-15/Graphite Composites - Part I: Effect of Cure Temperature," Proc. 18th Intl. SAMPE Tech. Conf. October (1986).

[21] Dutta, P. K. "Structural Fiber Composite Materials for Cold Regions," J. Cold Regions Engineering. 2(3):124 (1988).

[22] Bowles, D. E. and Shen, J. "Thermal Cycling Effects on the Dimensional Stability of P75 and P75-T300 (Fabric) Hybrid Graphite/Epoxy Laminates," Proc. 33rd Intl. SAMPE Symp. March (1988).

[23] Owens, G. A. and Schofield, S. E. "Thermal Cycling and Mechanical Property Assessment of Carbon Fibre Fabric Reinforced PMR-15 Polyimide Laminates," Comp. Science and Tech. 33:177 (1988).

[24] Camahort, J. L., Rennhack, E. H., and Coons, W. C. "Effects of Thermal Cycling Environment on Graphite/Epoxy Composites," Environmental Effects on Advanced Composite Materials (ASTM STP 602). Philadelphia, PA: ASTM (1976).

[25] Rosen, B. W., Nagarkar, A. P. and Hasin, Z. "Thermomechanical Response of GR/PI Composites," NASA-CR-165753. March (1981).

[26] Hahn, H. T. "Residual Stresses in Polymer Matrix Composite Laminates," J. Composite Materials. 10:266 (1976).

[27] Favre, J. P. "Residual Thermal Stresses in Fibre Reinforced Composite Materials - A Review," J. Mech. Behavior of Materials. 1(1-4):37 (1988).

[28] Chamis, C. C. Proc. 26th Annual Tech. Conf. - Society of the Plastics Industry. Section 17-D (1971).

[29] Griffin, O. H. J. Composite Materials. 17:449 (1983).

[30] Douglas, D. A. and Weitsman, Y. Proc. 3rd Intl. Conf. on Composite Materials (ICCM-III). Oxford: Pergamon Press (1980).

[31] Herrmann, K. and Mattheck, C. J. Thermal Stresses. 2:15 (1979).

[32] Tsai, S. and Hahn, H. T. Introduction to Composite Materials. Lancaster, Pa: Technomic (1980).

[33] Herakovich, C. T., Davis, Jr., J. G. and Mills, J. S. Thermal Stresses in Severe Environments. New York, NY: Plenum Press (1980).

[34] Scola, D. A., Bak, M. and Parker, D. J. SAMPE Journal. 22(2):47 (1986).

[35] Wilson, D., Wells, J. K., Hay, J. N., Lind, D., Owens, G. A. and Johnson, F. SAMPE Journal. 23(2):35 (1987).

[36] Pagano, N. J. and Hahn, H. T. Composite Materials: Testing and Design (ASTM STP 617). Philadelphia, PA: ASTM (1977).

[37] Jones, F. R., Wheatley, A. R. and Bailey, J. E. Composite Structures. London: Elsevier Applied Science (1980).

[38] Kim, R. Y. and Hahn, H. T. J. Composite Materials. 13:2 (1979).

[39] Wang, A. S. D. and Crossman, F. W. J. Composite Materials. 11:300 (1977).

[40] Law, G. E. Effects of Defects in Composite Materials (ASTM STP 836). Philadelphia, PA: ASTM (1984).

[41] Fiber Certification Report - IM6 Lot 685-3N. Hercules Inc., Wilmington, Delaware (29 November 1985).

[42] Neat Resin Test Data - BT3008. Mitsubishi Gas Chemical Company Inc., Tokyo, Japan (1993).

[43] Technical Data Sheet - 5250-4 Prepreg System. BASF Structural Materials Inc., Anaheim, California (17 February 1992).

[44] Technical Bulletin - Epon Resin 9405/Epon Curing Agent 9470. Shell Chemical Company, Oak Brook, Illinois (March 1986).

[45] Composite Test Data - IM6/9405-9470. Loral Defense Systems, Akron, Ohio.

[46] Soutis, C. "Measurement of the Static Compressive Strength of Carbon-Fibre/Epoxy Laminates", Composites Science and Technology, 42(4):373-392 (1991).

[47] Test Method for Shear Properties of Advanced Composite Materials by the V-Notched Beam Method (CEA TSP 00000999-005). Martin Marietta Electronic Systems Center, Orlando, Florida.

[48] Schapery, R. A. "Thermal Expansion Coefficients of Composite Materials Based on Energy Principles", Journal of Composite Materials, 2(3):380-404 (1968).

[49] Tsai, C. L. and Daniel, I. M. "Method for Thermomechanical Characterization of Single Fibers", Composites Science and Technology, In-Press.

[50] Adams, D. F. and Miller, A. K. "Hygrothermal Microstresses in a Unidirectional Composite Exhibiting Inelastic Material Behavior", Journal of Composite Materials, 11(7):285-299 (1977).

[51] Bowles, D. E. and Griffin, O. H. "Analysis of Thermal Stresses in Polymer Matrix Composites", Proc. 34th Intl. SAMPE Symposium, p. 575 (8-11 May 1989).

[52] Thompkins, S. S. and Funk, J. G. "Sensitivity of the Coefficient of Thermal Expansion of Selected Graphite Reinforced Composite Laminates to Lamina Thermoelastic Properties", SAMPE Quarterly, pp. 55-61 (April 1992).

[53] Camahort, J. L., Rennhack, E. H. and Coons, W. C. "Effects of Thermal Cycling Environment on Graphite/Epoxy Composites," Environmental Effects on Advanced Composite Materials (ASTM STP 602). Philadelphia, PA: ASTM (1976).

[54] Simpson, M., Jacobs, P. M. and Jones, F. R. "Generation of Thermal Strains in Carbon Fibre-Reinforced Bismaleimide (PMR-15) Composites - Part 1: The Determination of Residual Thermal Strains in Cross-Ply Laminates", Composites, 22(2):89-97 (1991).

[55] Tsai, S. W. Composites Design - 4th Edition. Dayton, Ohio: Think Composites Inc. (1988).

[56] Beer, F. P. and Johnston, E. R. Mechanics of Materials. New York, NY: McGraw-Hill Book Co. (1981).

[57] Collins, T. A. "Transverse Compressive Behavior of Unidirectional Carbon Fiber Reinforced Plastics", Composites, 5(3):108 (1974).

APPENDIX A - RHEOLOGY AND CURE CHARACTERISTICS OF BT3008

This appendix provides information on the rheology and cure characteristics of the BT3008 resin system with mix ratios (A:B) of 60:40 and 70:30. Based on this information, a mix ratio of 70:30 was selected for fabrication of composite laminates for physical/mechanical property characterization (Section 4.3.1) and thermo-mechanical fatigue testing (Section 6.2.1).

A.1 GEL TIME MEASUREMENTS

Gel times were measured for two 80-85 g samples of BT3008 resin (70:30 ratio) at 60 °C using standard laboratory gel point timers. The samples gelled after approximately 7.1 hr. These results were used to select the appropriate time interval for viscosity measurements (Section A.2).

A.2 VISCOSITY MEASUREMENTS

Resin samples of BT3008 weighing 180-200 g were prepared with 60:40 and 70:30 mix ratios. The resin components were heated to 50-60 °C prior to mixing. Immediately after mixing, the samples were brought to equilibrium at 60 °C and viscosity measurements were initiated. Viscosity measurements were made with a Brookfield Synchro-Lectric Viscometer (Model RVT). Spindle sizes and speeds were varied as necessary to achieve maximum accuracy in the measurements. The viscosity measurements for each mix ratio are summarized in Table A1.

A.3 CURE STUDY

Resin samples of BT3008 weighing approximately 100 g were prepared with 60:40 and 70:30 mix ratios. The samples were cured in an oven according to the following cycle:

- Heat at 1 °C/min. to 80 °C.
- Hold for 2 hr.
- Heat at 1 °C/min. to 120 °C.
- Hold for 2 hr.
- Heat at 1 °C/min. to 150 °C.
- Hold for 2 hr.
- Heat at 1 °C/min. to 180 °C.
- Hold for 2 hr.
- Heat at 1 °C/min. to 200 °C.
- Hold for 4 hr.
- Cool at 5 °C/min. to ambient.

All samples showed signs of oxidation on the surface following the cure. This material was removed and discarded. The remainder of each sample was ground into a coarse powder for evaluation by differential scanning calorimetry (DSC). DSC was performed using a Perkin Elmer 7 Series Thermal Analysis System calibrated with both indium (T_m = 156.6 °C) and lead (T_m = 327 °C) standards. The scan was performed over a temperature range of 150 to 250 °C at a heating rate of 20 °C/min. The glass transition temperature (T_g) was taken as the midpoint temperature of the heat capacity change. The T_g measurements are summarized in Table A2.

After the initial T_g measurements were completed, the remaining powder was postcured for 3 hr. at 200 °C to determine if any further increase in T_g was possible. The

T_g for each of the postcured samples is also given in Table A2. Note that the T_g was reduced for the 70:30 mix ratio following the postcure. The reduction was attributed to oxidative degradation similar to that observed on the surface of the resin samples after the initial cure but aggravated by the large surface area to volume ratio of the powder form.

Table A1. Viscosity vs time for BT3008 resin at 60 °C.

Time [hr.]	Viscosity [cP]	
	60:40 Mix Ratio	70:30 Mix Ratio
0.00	130	130
0.25	130	134
0.50	130	176
0.75	172	176
1.00	180	206
1.50	224	272
2.00	276	372
3.00	316	---
3.50	---	640
4.00	540	1010
5.50	1220	---

Table A2. T_g from DSC for BT3008 resin formulations.

Postcure	Glass Transition Temperature (T_g) [°C]		
	BT3008 Resin (60:40 Mix Ratio)	BT3008 Resin (70:30 Mix Ratio)	IM6/BT3008 Composite (70:30 Mix Ratio)
None	202	218	221
3 hr. at 200 °C	200	204	---